

DETECTION AND FUNCTION OF BIOGENIC MAGNETITE

Inaugural-Dissertation
zur Erlangung des Doktorgrades
der Fakultät für Geowissenschaften der
Ludwig Maximilians Universität
München, Deutschland

vorgelegt von

Alfonso F. Davila

6. September 2005

Dissertation eingereicht: 6 September 2005
Erster Berichterstatter: Prof. Dr. Nikolai Petersen
Zweiter Berichterstatter: Prof. Dr. Valerian Bachtadse
Tag der mündlichen Prüfung: 30 November 2005

Gerade Tatsachen gibt es nicht, nur Interpretationen.

Friedrich Nietzsche (1886-1887)

Table of Contents

| | |
|--|-----------|
| Table of Contents | vi |
| Zusammenfassung | i |
| Summary | iv |
| Introduction | 1 |
| 1 The magnetic properties of magnetite | 3 |
| 1.1 Introduction | 3 |
| 1.2 Magnetic properties of magnetite | 4 |
| 1.3 Instruments used in this study | 8 |
| 2 Magnetotactic bacteria | 9 |
| 2.1 Introduction | 9 |
| 2.2 Magnetotactic bacteria reviewed | 9 |
| 3 Magnetic properties of uncultured magnetotactic bacteria | 15 |
| 3.1 Introduction | 15 |
| 3.2 Sample preparation | 16 |
| 3.3 Rock magnetic properties of uncultured magnetotactic bacteria | 18 |
| 3.3.1 Isothermal remanent magnetization and anhysteretic remanent magnetization analysis | 18 |
| 3.3.2 Hysteresis and FORC analysis | 21 |
| 3.3.3 Low-temperature demagnetization of SIRM: The delta-delta test | 23 |
| 3.3.4 Cycling curves of SIRM (300 → 5 → 300 K) | 26 |
| 3.4 Interpretation | 27 |
| 3.5 Rock magnetic criteria for the identification of biogenic magnetite | 28 |
| 4 Detection of bacterial magnetite in lake sediments | 33 |
| 4.1 Introduction | 33 |
| 4.2 Optical identification of bacterial magnetite in lake sediments | 34 |
| 4.2.1 Acquisition and demagnetization of IRM and ARM | 36 |
| 4.2.2 Low temperature SIRM demagnetization: <i>The delta-delta test</i> | 37 |

| | | |
|-----------|---|------------|
| 5 | The magnetic sense of animals | 42 |
| 5.1 | Introduction | 42 |
| 5.2 | The geomagnetic field as a source of directional and positional information | 43 |
| 5.3 | The <i>inclination</i> compass and map sense of animals | 46 |
| 5.4 | Hypotheses of mechanisms of magnetic field perception | 46 |
| 6 | Biogenic magnetite and magnetic field perception | 50 |
| 6.1 | Introduction | 50 |
| 6.2 | SD and SP particles as components of the animal magnetic sense | 51 |
| 6.2.1 | The SD model | 51 |
| 6.2.2 | The SP model | 53 |
| 6.3 | A candidate magnetoreceptor structure in homing pigeons | 54 |
| 7 | Model experiments with ferrofluid spherules | 61 |
| 7.1 | Introduction | 61 |
| 7.2 | Ferrofluid spherules as technical analogues to the SP clusters | 62 |
| 7.3 | Response of individual ferrofluid spherules to weak magnetic fields | 63 |
| 7.4 | Response of groups of ferrofluid spherules to weak magnetic fields | 66 |
| 7.4.1 | The attraction-repulsion response of ferrofluid spherules | 69 |
| 7.4.2 | Pressure between two interacting ferrofluid spherules | 70 |
| 7.4.3 | The Pseudo-torque response of chains of ferrofluid spherules | 73 |
| 7.5 | Response of groups of ferrofluid spherules to strong, pulsed magnetic fields | 75 |
| 8 | Dynamics of SP clusters in a liquid medium | 80 |
| 8.1 | Introduction | 80 |
| 8.2 | Interacting clusters of SP magnetite particles | 81 |
| 8.2.1 | Dynamics of SP clusters in a weak magnetic field | 84 |
| 8.2.2 | Characteristic time response of interacting SP clusters | 85 |
| 8.2.3 | Dynamics of SP clusters in a strong pulsed field | 87 |
| 9 | Magnetoreceptor mechanisms based on interacting clusters of SP magnetite | 91 |
| 9.1 | Introduction | 91 |
| 9.2 | The Attraction-Repulsion model | 92 |
| 9.3 | The Pressure Model | 94 |
| 9.4 | The Pseudo-Torque Transducer Model | 96 |
| 10 | Testing the SP models with behavioral experiments | 99 |
| 10.1 | Introduction | 99 |
| 10.2 | Pulse experiments in birds | 100 |
| 10.3 | Interpretation of the pulse experiments | 100 |
| 10.3.1 | Chain recovery process | 102 |
| 10.3.2 | Effects of a bias field | 104 |
| | Conclusions | 107 |
| | Acknowledgements | 110 |
| | Bibliography | 111 |
| | Lebenslauf | 123 |

Zusammenfassung

Magnetit ist ein in Gesteinen und Böden häufig vorkommendes Begleitmineral. Wie Lowenstam (1962) als erster erkannt hatte, wird Magnetit auch häufig durch biochemische Prozesse gebildet, wobei dieser Bildungsprozess je nach Organismus unterschiedlich gesteuert werden kann. Lowenstam (1981) unterscheidet zwei grundsätzlich unterschiedliche Bildungsprozesse, einen biologisch induzierten (BIM - biologically induced mineralization) und einen biologisch kontrollierten (BCM - biologically controlled mineralization) Prozess. Im ersten Fall ist der Organismus nur indirekt an der Magnetitproduktion beteiligt, indem ein intrazellulär ablaufender Prozess eine magnetitbildende Reaktion außerhalb des Zellkörpers zur Folge hat. Im zweiten Prozess nehmen genetisch bedingte Vorgänge direkt an der Magnetitbildung teil.

In der vorliegenden Arbeit werden zwei Beispiele von biogenem Magnetit mit sehr unterschiedlich magnetischen Eigenschaften studiert. Im ersten Beispiel handelt es sich um Magnetit, wie er in den sogenannten magnetotaktischen Bakterien gebildet wird, im zweiten Beispiel um Magnetit im Gewebe des Kopfes von Brieftauben.

Für den ersten Teil der Arbeit wurden reine Konzentrate magnetotaktischer Bakterien hergestellt und diese dann mit Methoden des Gesteinsmagnetismus gemessen. Hinsichtlich der Bildungsprozesse der BCM stellen diese Bakterien ein einzigartiges Studienobjekt dar, da sie intrazellulär wohl definierte und in Ketten angeordnete Kristallite von Magnetit synthetisieren. Diese Kettenanordnung gibt den Bakterien die Eigenschaft einer schwimmenden Kompassnadel. Die magnetischen Kristalle, sogenannte Magnetosome, sind bezüglich ihrer magnetischen Eigenschaften stabile Einbereichsteilchen (single domain particles, SD), die großen und formbedingt ein maximales, permanentes magnetisches Moment besitzen. Der

Größenbereich liegt zwischen 30 und 130 nm.

Die untersuchten Bakterien stammen aus Sedimenten des Chiemsees. Mit Hilfe des sogenannten Bakteriodroms wurden ca. 10^7 Zellen extrahiert und damit so weit angereichert, dass eine detaillierte Untersuchung mittels makroskopischer Magnetisierung möglich war.

Ein erstes Ziel der magnetischen Untersuchungen war es, Kriterien zur Identifizierung von bakteriell gebildetem Magnetit zu entwickeln. Dazu wurden folgende Methoden angewandt: 1) Erwerb einer isothermalen remanenten Magnetisierung (IRM) mit anschließender Entmagnetisierung, 2) Erwerb einer anhysteretischen remanenten Magnetisierung und 3) Messung der Temperaturabhängigkeit einer SIRM (saturation isothermal remanent magnetisation), wobei die Probe im Null-Feld (ZFC - zero field cooling) bzw. im 2.5 T-Feld (FC - field cooling) von 300 auf 5 K abgekühlt wird. Die beste Aussagefähigkeit hatte dabei der sogenannte *delta – delta* Test ($\delta\text{FC}/\delta\text{ZFC}$), der von Moskowitz et al. (1993) eingeführt worden war. Diese Methode basiert auf dem Verlust der remanenten Magnetisierung der Magnetosomenketten beim Verwey-Übergang bei ca. 120 K, dem sogenannte δ -Wert. Aus diesem Wert einer jeden FC-Kurve und dem entsprechenden Wert der ZFC-Kurve wird das δ -Verhältnis ($\delta\text{FC}/\delta\text{ZFC}$) berechnet. Nach Moskowitz et al. (1993) sind Verhältnisse über 2 ein deutlicher Hinweis auf die Anwesenheit von biologisch bedingten Ketten aus Magnetit Einbereichsteilchen. Alle hier untersuchten Proben lieferten δ -Verhältnisse von über 2 und belegen damit die Nützlichkeit dieser Untersuchungsmethode zum Nachweis von SD-Ketten magnetischer Partikel.

Es wird ferner aber auch gezeigt, dass die Anwendbarkeit von gesteinsmagnetischen Untersuchungsmethoden zum Nachweis und zur Charakterisierung biogenen Magnetits in natürlichen Proben wie Seesedimenten begrenzt ist, da diagenetische Prozesse und das Vorhandensein anderer, nicht-biogener Magnetitpartikel die magnetischen Eigenschaften der untersuchten Proben stark beeinflussen. Es zeigt sich somit, dass die zuverlässigste Methode zum Nachweis von Magnetosomen im Sediment eine optische Identifizierung mit Hilfe des Transmissions Elektronenmikroskops ist. Diese Methode ist allerdings mühsam und sehr zeitaufwendig.

Die Magnetiteinlagerungen in den Schnäbeln von Tauben unterscheiden sich hinsichtlich

ihrer magnetischen Eigenschaften deutlich von dem oben beschriebenen biogenen Magnetit magnetotaktischer Bakterien.

Schon früh wurden Magnetiteinlagerungen im Gewebe unterschiedlicher Tiergruppen mit der Fähigkeit der Orientierung im Magnetfeld der Erde in Zusammenhang gebracht. Die Magnetitpartikel in Taubenschnäbeln sind wesentlich kleiner, als die bakteriellen Magnetosome (2 bis 10 nm) und besitzen somit ganz unterschiedliche magnetische Eigenschaften. Aufgrund ihrer kleinen Größe werden diese Partikel als superparamagnetisch bezeichnet. Sie sind durch eine starke induzierte Magnetisierung und das absolute Fehlen einer remanenten Magnetisierung charakterisiert. Die Magnetitpartikel in den untersuchten Tauben bilden kugelförmige Cluster mit einem durchschnittlichen Durchmesser von 1 bis 3 μm vor.

Das Verhalten dieser Cluster in Magnetfeldern wurde mit Mikrokügelchen eines Ferrofluids simuliert. Diese Mikrokügelchen bilden ein Analog zu SP-Clustern in den Brieftauben. Es zeigte sich, dass die magnetischen Eigenschaften der Mikrokügelchen stark von der geometrischen Anordnung dieser Kügelchen abhängig ist. Der wichtigste Unterschied zu den bakteriellen Magnetitteilchen besteht darin, dass diese Kügelchen ein polaritätsunabhängiges Verhalten im Magnetfeld zeigen. D. h. sie reagieren nicht als Vektor (wie ein technischer Kompass), sondern als magnetische Achse. Der wechselseitige Einfluß der Kügelchen untereinander hängt von der Stärke des magnetischen Feldes ab. Aufbauend auf diesen Erkenntnissen wurden 3 Modelle experimentell und theoretisch entwickelt und auf ihre Anwendbarkeit als biologischer Magnetfeldsensor getestet: 1) das Anziehungs-Abstoßungs-Modell, 2) das Druck-Modell (Druck zwischen zwei benachbarten Kügelchen) und 3) das Pseudo-Drehmoment-Modell.

Die magnetischen Eigenschaften dieser Modelle wurden schließlich dem Verhalten von Brieftauben und Zugvögeln gegenübergestellt, wie es aus Verhaltensversuchen im künstlichen Magnetfeld bekannt ist. Es zeigte sich, dass sich die meisten Verhaltensmuster lebender Vögel sehr gut mit Hilfe der hier entwickelten Modelle erklären lassen.

Summary

Magnetite is a widespread accessory mineral in rocks and soils. As was first shown by Lowenstam (1962), magnetite frequently forms also by biochemical processes, with varying degrees of control of the organisms over the mineralization process. Lowenstam distinguishes between biologically induced (BIM) and biologically controlled mineralization (BCM). The former refers to processes with no biological control, and the latter to processes with strict metabolic and genetic control.

In this thesis, two examples of biogenic magnetite with eminently different magnetic properties are studied. One is magnetite as found in so-called magnetotactic bacteria; the second example is magnetite as identified in tissue of pigeon's heads.

In the first part of this work, the results of a series of rock magnetic measurements on concentrated samples of pure magnetotactic bacteria will be presented. These bacteria offer a unique opportunity to study the process of biologically controlled mineralization, since these organisms synthesize intracellular particles of magnetite or greigite arranged in chains, that give the bacterium the characteristic property of a swimming compass needle. The magnetic crystals, so-called magnetosomes, are magnetically speaking stable single-domain particles, characterized by a size such that the particles have minimum induced magnetization and maximum permanent magnetic moment (i.e. particle size between 30 and 130 nm).

The bacteria studied here have been harvested in sediments from lake Chiemsee. They were extracted from the sediments and concentrated to an extent that enabled a detailed characterization by macroscopic magnetic measurements. The so-called Bacteriodrome was used to concentrate samples of approximately 10^7 cells.

Different magnetic criteria, aiming to specifically identify bacterial magnetite in sediments, have been tested, including: (1) acquisition and demagnetization of isothermal remanent magnetization (IRM); (2) acquisition of anhysteretic remanent magnetization and (3) thermal dependence of low temperature saturation IRM, after cooling in zero field (ZFC) or in a 2.5 T field (FC) from 300 to 5 K. The best method turns out to be the so-called *delta – delta* test ($\delta\text{FC}/\delta\text{ZFC}$), first proposed by Moskowitz et al. (1993), and based on the low temperature variation of the SIRM, measured both in a strong field (FC) and in zero field (ZFC). At the Verwey transition (~ 120 K) the δ -value for each curve is determined and the δ -ratio ($\delta\text{FC}/\delta\text{ZFC}$) calculated. Values exceeding 2, are indicators for the presence of chains of stable single-domain particles, which form only under strict biological control.

However, it is shown that the suitability of rock magnetic techniques to detect and characterize biogenic magnetite in bulk, natural samples such as lake sediments is still limited, due to diagenetic processes and the occurrence of other non-biogenic magnetic minerals, which blur the distinct magnetic properties of the former. The only certain proof for bacterial magnetite is the optical identification -although time consuming and tedious- by Transmission Electron Microscopy.

The magnetite inclusions found in pigeon tissue are very different in their magnetic properties with respect to bacterial magnetite. With their small grain size (between 2 and 10 nm), these particles fall within the superparamagnetic size range and are characterized by a large induced magnetization and no permanent magnetic moment. The pigeon magnetite is concentrated in spherical clusters of approximately 1-3 μm in diameter.

The response of these clusters to magnetic fields has been simulated by spherules of ferrofluid. Depending on their geometrical arrangement these spherules show peculiar magnetic properties. Based on these properties, three models have been developed experimentally and theoretically with respect to a possible application as biological sensory elements. The magnetic properties of the sensory models are tested in the light of behavioral experiments conducted in the past on homing pigeons and migratory birds. In these experiments, the birds were exposed to defined magnetic fields to specifically affect a magnetite-based magnetoreceptor. As will be seen, most of the responses of the birds

observed in the behavioral experiments can be explained by simulating the effects of these magnetic treatment on ferrofluid spherules.

Introduction

Magnetite is the most important magnetic mineral on Earth and occurs in continental and oceanic crust as a primary or secondary mineral in igneous, sedimentary and low- and high-grade metamorphic rocks (Roesler, 1979). Magnetite commonly forms at relatively high temperatures, although it also crystalizes at ambient temperatures in slightly reducing environments. In 1962, Lowenstam was the first to identify magnetite in the radula (tongue plate) teeth of chitons, showing that also life had devised mechanisms to synthesize magnetite by means of biochemical processes. Indeed, biogenic magnetite can be generated by a wide spectrum of mechanisms, which differ in the degree of control the organism has over the mineralization process.

Lowenstam (1981) distinguishes between biologically induced (BIM) and biologically controlled (BCM) mineralization. He describes BIM as the process with least biological control. In the case of magnetite, BIM is often related to dissimilatory iron-reducing bacteria. During respiration, these absorb ferric ions (Fe^{3+}) in the form of amorphous ferric oxy-hydroxide and export ferrous ions (Fe^{2+}) into the environment, where they interact with excess ferric oxy-hydroxide resulting in extracellular magnetite precipitates that usually resemble those formed inorganically (Frankel and Blakemore, 1991). Thus BIM of magnetite occurs through chemical changes in the environment due to biological activity. The mechanisms governing the formation of such particles are seemingly altered by evolution and natural selection to a low extent, hence BIM of magnetite has likely remained practically invariant throughout geological time.

BCM of magnetite, on the other hand, occurs both in prokaryote and eukaryote cells with a remarkable level of control of the particle size, shape, composition and structure. Contrary to what occurs in BIM processes, the degree of control that organisms exhibit in BCM processes is only achievable as a result of millions of years of evolution of the biological functions in which these particles are involved.

Biogenic magnetite is nowadays found widespread in organisms and as fossil remnants

in sedimentary deposits and soils.

Aims of this work:

1.-To work out criteria to distinguish between biogenic and inorganically formed magnetite. Interestingly, biogenic magnetite particles synthesized through strict biological control, often have distinct magnetic properties, which distinguish them from their inorganic counterparts. For that reason, classic rock magnetic techniques have proved a useful tool for the detection and characterization of biogenic magnetite. Magnetic measurements are relatively fast and non-invasive, allowing for a quick screening of the magnetic properties of bulk samples without altering their original physical and chemical properties.

2.-To investigate the possible functional role of biogenic magnetite in organisms. Up to this day, biogenic magnetite has been linked to bacterial magnetotaxis, hardening of the radula in chitons and animal magnetoreception. While the role of biogenic magnetite in magnetotaxis and as hardening structure has been clearly established, the involvement of these particles in animal magnetoreception is still a working hypothesis.

This will be studied on **two aspects**:

1.-Magnetite formed in magnetotactic bacteria. Here the work is concentrated on developing methods and criteria to discriminate biogenic magnetite and inorganically formed magnetite in sedimentary deposits (chapters 3 and 4).

2.-Magnetite found in tissue of the head of homing pigeons. Here the focus is on developing and testing models of possible magnetoreceptor mechanisms based on the interaction of biogenic magnetite with the Earth's magnetic field (chapters 6 to 10).

Chapter 1

The magnetic properties of magnetite

"[...]when the nature of the lodestone shall have been by our labours and experiments tested, then will the hidden and recondite but real causes of this great effect be brought forward, proven, demonstrated... and the foundations of a grand magnetic science being laid will appear anew, so that high intellect may no more be deluded by vain opinions"

William Gilbert. *De Magnete* (1600)

1.1 Introduction

As a result of biologically controlled synthesis, biogenic magnetite particles often have properties that make them intrinsically distinct from their inorganic counterparts. In this respect, magnetic measurements, which can provide information on the size, concentration, spatial arrangement and composition of the particles, have proven a resourceful tool for the detection and characterization of biogenic magnetite particles. Therefore, in order to establish effective rock magnetic criteria for the identification of biogenic magnetite in natural samples, it is necessary to understand the fundamental magnetic properties of this mineral.

The effectiveness of magnetic measurements is, however, limited for a number of reasons. Biogenic magnetite normally appears at very low volume concentrations in bulk samples, often at the lower level of instrument sensitivity. Furthermore, the size of biogenic

magnetite particles generally falls in the magnetically stable single-domain to superparamagnetic range [see figure 2.3]. At these sizes, magnetite particles are easily altered by the chemical conditions of the surrounding environment, which results in changes of their magnetic properties. It is for this reason that the study of biogenic magnetite ought to be undertaken from a multidisciplinary approach, in which both magnetic and non-magnetic techniques are used.

1.2 Magnetic properties of magnetite

Magnetite has the structural formula $Fe^{3+}(Fe^{2+}Fe^{3+})O_4$ and is the most important magnetic mineral on Earth. Crystallographically, it is a cubic mineral with inverse spinel structure, and ferrimagnetic properties. The unit cell has eight tetrahedral sites filled with Fe^{3+} cations and sixteen octahedral sites, half of which are filled with Fe^{2+} cations and the other half with Fe^{3+} cations.

Saturation magnetization (J_s), or spontaneous magnetization, is a fundamental property of a ferromagnetic material, independent of particle size. For magnetite $J_s \sim 90$ emu/g. J_s is a function of temperature and pressure. The maximum value of J_s occurs at 0° K. As the sample is heated, the observed magnetization decreases and goes to zero at the Curie point (T_c), when the thermal energy (kT_c , where k is Boltzmann's constant) equals the ferrimagnetic coupling energy. T_c is another intrinsic parameter of a ferrimagnetic material and in the case of magnetite $T_c \sim 850$ K ($\sim 580^\circ$ C). The dependence of J_s with temperature is a diagnostic property for identifying minerals, since each ferrimagnetic material has a different Curie temperature.

At a temperature (T_v) of ~ 120 K, magnetite undergoes an ordered arrangement of Fe^{2+} and Fe^{3+} ions on the octahedral sublattice, resulting in a slight distortion of the unit cell from cubic to monoclinic or triclinic (Miyamoto and Chikazumi, 1988). At this transition, referred to as the Verwey transition after the pioneering work of its discoverer (Verwey, 1939), the electrical conductivity of magnetite drops sharply by a factor of 100, due to a reduction of electron mobility on the B-sublattice (Gleitzer, 1997). Above T_v , electrons from the 3d shells move or "hop" between the Fe^{3+} and Fe^{2+} cations on the B-sublattice, and magnetite behaves as a moderate electric conductor. This crystallographic transition also affects the saturation magnetization, and is often used to identify magnetite in bulk samples (Néel, 1949).

When studying biogenic magnetite, it is paramount to establish the size of the particles synthesized by the organism. The main subdivisions, multi-domain (MD), pseudo-single-domain (PSD), magnetically stable single-domain (SD), and superparamagnetic (SP), are determined by the number of magnetic domains contained within the particle (the domain state). The domain state determines the magnetic properties which will, in turn, be selected according to physiological requirements and the role the magnetite particles play in the organism. Magnetic domains are regions within a magnetic particle where the direction of spontaneous magnetization is uniform, although different domains within a single particle may have different directions. Consequently, a MD particle can have zero remanence if the magnetization directions cancel each other; a magnetically stable SD, on the other hand, is always magnetized to saturation and shows a remanent magnetization at room temperature; finally, due to their small volume, SP particles lose their remanence in time spans of seconds to nano-seconds, and can be considered, for practical reasons, to acquire only an induced magnetization in the presence of a magnetic field [Figure 1.1] (Banerjee and Moskowitz, 1985).

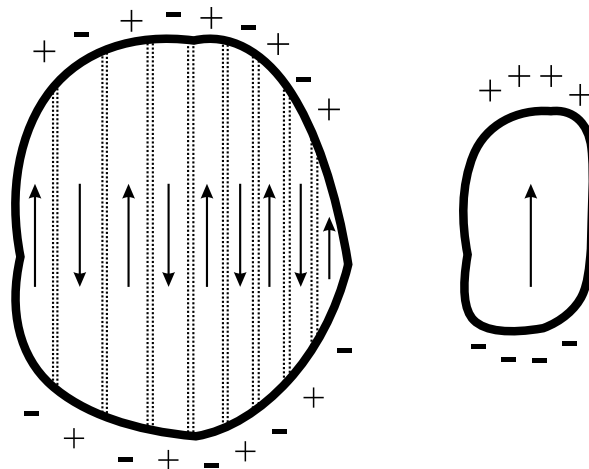


Figure 1.1: Magnetic domains of a MD particle (*left*) and a SD particle (*right*). As a result of domains magnetized in opposite directions, MD particles have a net magnetization close to 0, while stable SD particles are always magnetized to saturation and show a remanent magnetization at room temperature. The plus and minus signs represent magnetic surface charges. Dotted lines represent domain walls.

A useful magnetic parameter to distinguish different magnetic mineralogies in bulk samples, as well as their domain states, is the saturation isothermal remanent magnetization (SIRM). SIRM is the remanence left in a sample after a strong steady field has

been applied. Typical values of SIRM fields for magnetite are ~ 100 mT. IRM acquisition and demagnetization curves are also useful for studying the effects of interactions between magnetic particles, since non-interacting SD grains produce symmetrical curves whereas interacting SD or MD grains produce asymmetrical curves. Finally, SIRM is temperature dependent and the study of the variations of SIRM both at high- and low temperatures can be used as a diagnostic parameter of domain state and mineralogy (Banerjee and Moskowitz, 1985).

Some magnetic parameters, such as the saturation magnetization, M_s , remanent magnetization after saturation, M_{rs} , coercive force, H_c and coercivity of remanence, H_{cr} , and their ratios (M_{rs}/M_s and H_{cr}/H_c) serve to define domain states, although the limits between SD, PSD and MD behavior are not well defined, and often the interpretation of these parameters is not straightforward. For the case of uniaxial SD crystals of magnetite, the theoretical values of the remanence ratio and the coercivity ratio are $M_{rs}/M_s \sim 0.5$ and $H_{cr}/H_c \sim 1.0$, respectively (Wohlfarth, 1958). For SD magnetite, these ratios are essentially temperature invariant, except in the blocking range just below T_c , where M_{rs}/M_s falls and H_{cr}/H_c rises steeply (Dunlop and Özdemir, 1997). In the case of MD particles, $M_{rs}/M_s \leq 0.05$ and $H_{cr}/H_c \geq 4$ (Day et al., 1977). By definition, SP particles have both M_{rs} and $H_{cr}=0$; but particle interactions or small mixtures of SP and SD particles often occur, giving finite, albeit low, values for M_{rs} and H_{cr} (Wasilewski, 1973; Banerjee and Moskowitz, 1985; Evans and Heller, 2003).

The ratios M_{rs}/χ_0 and χ_0/M_s (where χ_0 is the low field magnetic susceptibility) are also useful in distinguishing SP from non-SP behavior. In SD and MD particles of magnetite, M_s/χ_0 will vary from ~ 2 to 70 mT, whereas for SP particles $M_s/\chi_0 < 0.01$ mT (Thompson et al., 1980). Table 1.1 shows characteristic values and behavior for some magnetic parameters for the different domain states of magnetite particles.

The coercive force (H_c), strongly depends on particle interactions. Single SD particles show a maximum H_c whereas for SP particles H_c is zero. However, interacting SP particles behave differently (Radhakrishnamurthy et al., 1973) yielding relatively large values of H_c and interacting SD particles can collectively act as MD particles, and thus act to diminish H_c values (Kneller, 1969; Banerjee and Moskowitz, 1985). This fact has important consequences in biomagnetism studies, since magnetic measurements of biological tissue can incorrectly identify the presence of, for example, individual SD particles instead of interacting SP particles.

A useful technique in determining the domain state of the magnetite particles is the

| Parameter | SP | SD | MD |
|-----------------|--------------------------------|-----------------------------------|-----------------------------------|
| M_{rs}/M_s | $\ll 0.01$ | ~ 0.5 | ≤ 0.05 |
| H_{cr}/H_c | $\gg 10$ | ~ 1.5 | ≥ 4 |
| M_{rs}/χ_0 | < 0.01 mT | 2-70 mT | 2-70 mT |
| χ_0/J_s | $> 7 \cdot 10^{-4}$ mT $^{-1}$ | $\sim 7 \cdot 10^{-4}$ mT $^{-1}$ | $\sim 7 \cdot 10^{-4}$ mT $^{-1}$ |
| $\chi_0 - T$ | large decrease | small decrease | peak at ~ 118 K |
| H_c/T | large increase | small increase | decrease at ~ 118 K |
| $J_r - T$ | large increase | small increase | decrease at ~ 118 K |

Table 1.1: Characteristic values and behavior for some magnetic parameters for magnetite depending on the domain state. From Banerjee and Moskowitz (1985)

low-temperature measurement of coercivity, remanence, and low field susceptibility (χ_0). The susceptibility of MD particles is practically invariant between T_c and T_v (Stacey and Banerjee, 1974); however near T_v , χ_0 increases and produces a characteristic peak. Elongated SD particles show a slight decrease of χ_0 with temperature and the peak at 120 K is suppressed. SP particles have the most drastic changes in susceptibility with temperature. Between 300 K and 4 K, χ_0 can vary by as much as a factor of 200 (Banerjee and Moskowitz, 1985).

SP grains of magnetite are also characterized by a steep increase of M_{rs} and H_c while cooling from 30 K to 5 K. In this temperature range, SP particles behave as stable single domains and are able to acquire relatively large remanences. In contrast, in SD and MD grains, M_{rs} and H_c do not display significant variations as temperature decreases. For MD magnetite, as it cools through T_v , both M_{rs} and H_c decrease. In SD particles controlled by shape anisotropy or interacting strongly, both M_{rs} and H_c show slight increases associated with the increase in J_s .

Despite these well established rock magnetic properties, the identification and characterization of biogenic magnetite in natural samples is often a challenging enterprise. The volume concentration of biogenic magnetite particles in natural environments is typically very low, often at the level of detection of the instruments, and many instruments used in rock magnetism fail to detect biogenic magnetite particles in the samples. A possible solution to this problem is to prepare magnetic extracts, where only the magnetic fraction of the sample is analyzed, however, in organic samples, even magnetic extracts often do not yield sufficient concentrations of material for analysis.

Magnetotactic bacteria (MTB) offer a unique opportunity to study the physical and chemical properties of biogenic magnetite. These bacteria synthesize, within their body,

chains of biogenic SD particles. A few strains of MTB have been cultured in laboratory, allowing for their concentration in amounts that suffice for magnetic characterization. MTB can also be extracted from natural samples in large amounts for later analysis. For their important role in the studies of biogenic magnetite, the next three chapters will be focused on the study of MTB.

1.3 Instruments used in this study

As will be seen, the study of biogenic magnetite particles ought to be undertaken from a multidisciplinary approach, in which both magnetic as well as non-magnetic instruments are used.

The observation and concentration of live MTB (chapter 3) and the manipulation of ferrofluid microdroplets (chapter 7) were carried out in the Bacteriodrome (Petersen et al., 1989), which consists of a light microscope equipped with coils to generate controlled magnetic fields around the sample (see figure 3.3).

Scanning electron microscopy (SEM) and transmission electron microscopy (TEM) on MTB and sediment samples were performed with a JEOL JSM5900 SEM and a JEOL JEM100CX TEM, at the Dept. of Electron Microscopy of the Technical University in Munich.

Isothermal and anhysteretic remanence magnetization measurements were carried out on a Princeton Measurements Alternating Gradient Magnetometer AGM (Model MicroMag 2900) and a 2G Enterprises cryogenic magnetometer (SQUID). The hysteresis curves and FORC analysis were obtained using a Variable Field Transmission Balance (VFTB) and a AGM MicrMag 2900, respectively. Low temperature magnetic measurements were carried out using a Quantum Design Magnetic Property Measurement System (MPMS-7XL), a low-temperature SQUID magnetometer, at the University of Bremen.

Chapter 2

Magnetotactic bacteria

”It became apparent, however, that light was not the stimulus directing the migration of these organisms [...]. It was experimentally confirmed that the migration of the bacteria was, indeed, directed by the earth’s magnetic field”

Richard P. Blakemore. *Science* (1975)

2.1 Introduction

In 1975, Richard P. Blakemore discovered a new type of bacterium with an unusual preference to move along the local geomagnetic field lines (Blakemore, 1975). These magnetotactic bacteria (MTB) have since then been thoroughly studied and the nature of their magnetotactic behavior is now fairly well understood, and linked to the presence of intracellular chains of SD magnetic crystals. MTB offer a unique opportunity to understand the processes involved in the biologically controlled mineralization of magnetite, as well as a source to study the physical and chemical properties of these particles. MTB have also been used to develop techniques that allow for the detection and characterization of biogenic magnetite particles in both organic and inorganic samples.

2.2 Magnetotactic bacteria reviewed

Magnetotactic bacteria are characterized by the presence, within their cellular body, of one or more chains of magnetically stable SD crystals of magnetite (iron-oxide type) or

greigite (iron-sulfide type), the so-called magnetosomes, which often appear enveloped by a phospholipid membrane, [Figure 2.1].¹

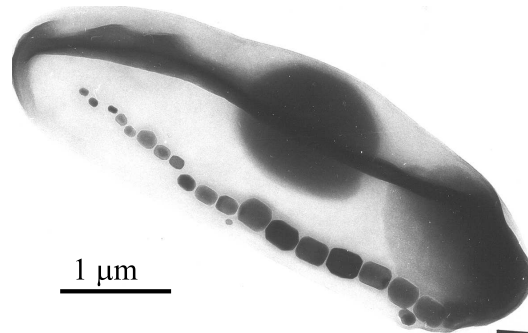


Figure 2.1: Magnetotactic vibrio with a chain of SD magnetosomes. Growing magnetosomes can be seen on the left part of the chain.

The phylogeny of a number of species of MTB has been determined by sequencing their 16S rRNA genes. Interestingly, with the exception of a distinct large rod-shaped bacterium located in the *Nitrospira* phylum (Spring et al., 1993), all known iron-oxide type species of MTB belong to the α -subdivision of the Proteobacteria, while all the iron-sulfide type species are related to the dissimilatory sulfate-reducing bacteria within the δ -subdivision of the Proteobacteria. Each subdivision of the Proteobacteria forms a distinct phylogenetic lineage, hence magnetotaxis based on iron-oxides and iron-sulfides has separate evolutionary origins (DeLong et al., 1993). Far from being a rarity, MTB are ubiquitous in aquatic environments, suggesting that magnetotaxis may be a common trait among prokaryote organisms inhabiting localized chemical gradients.

Being microaerophilic organisms that inhabit the oxic-anoxic transition zone (OATZ) of marine and fresh-water sediments or water columns, the evolutionary advantage of magnetotaxis is, perhaps, not difficult to understand. When a MTB is released outside of the OATZ, due for example to a turbulence in the water column, it finds itself suddenly in a high, potentially toxic oxygen-rich environment. The bacterium needs then to move towards a more appropriate environment as quickly as possible. It is in this situation when the intracellular chains of magnetic particles play their evolutionary role: the geomagnetic field lines, inclined with respect to the surface of the Earth (except in the equator, where they run parallel to the surface), will exert a torque on the intracellular chain until it

¹For the sake of clarity, in this work the term *magnetosome* is used in a rather generic way, to refer to the intracellular particles synthesized by MTB for magnetotaxis purposes, independently of their occurrence (i.e. within the bacterial cell or in the environment after the cell's death).

is oriented parallel to them. This magnetic torque is in turn transferred to the cellular body; then, the bacterium needs only to swim along the field lines until it reaches the OATZ of the sediment or the water column [Figure 2.2]. It is necessary to note that the orientation itself is passive and only due to the magnetic torque exerted on the chain of magnetic particles. The movement of the bacterium is due to the use of its flagellum, and it is not magnetically driven, hence the term passive magnetotactic orientation, or magnetotaxis.² Nature has also elegantly solved the problem of antipodal geomagnetic field lines in the southern and northern hemispheres. While in the south hemisphere the field lines run upwards, pointing towards the water surface, in the north hemisphere they run downwards, pointing towards the sediment surface. Therefore, MTB from the south hemisphere are adapted to swim in a direction antiparallel to that of the geomagnetic field lines (south seeking MTB), whereas MTB in the north hemisphere swim parallel to the magnetic field lines (north seeking MTB) [Figure 2.2].

Magnetotaxis provides an alternative orientation mechanism to chemotaxis, the response of cells to chemical stimuli by directed movement, where the bacteria display a so-called tumble-and-run motion consisting of relatively large displacements followed by localized, short range excursions, during which the bacteria sample different chemicals until they reach the appropriate environment [Figure 2.2].

To understand the origin, nature and magnetic properties of MTB and bacterial magnetosomes, is of interest for a number of reasons. Bacterial magnetosomes and their fossils, (magnetofossils), can significantly contribute to the bulk magnetic properties and the remanent magnetization recorded in marine and lake sediments and terrestrial soils [e.g. Petersen et al. (1986); Fassbinder et al. (1990); Paasche et al. (2004); Pan et al. (2005)]. Furthermore, bacterial magnetosomes are a novel source for fundamental studies in nanomagnetism, magnetic materials and medicine [e.g. Mann (2001)], and the investigation of magnetosome formation in MTB may provide a new avenue to understand biomineralization processes in higher organisms (Frankel et al., 1983). Finally, chains of magnetofossils may represent a biomarker to prove the past existence of life in other planets (McKay et al., 1996; Friedmann et al., 2001; Thomas-Keprta et al., 2002).

Thomas-Keprta et al. (2002) proposed six distinct properties for magnetosomes that could be used to distinguish them from their inorganic counterparts:

²The magnetosome chains will respond to the geomagnetic field both when the bacterium is in the water column and in the sediment. Yet, the role of magnetotaxis within the sediment, if existent, remains unclear. MTB have, nevertheless, a certain degree of freedom in their magnetotactic behavior and are often found swimming in a direction antiparallel or perpendicular to the expected direction.

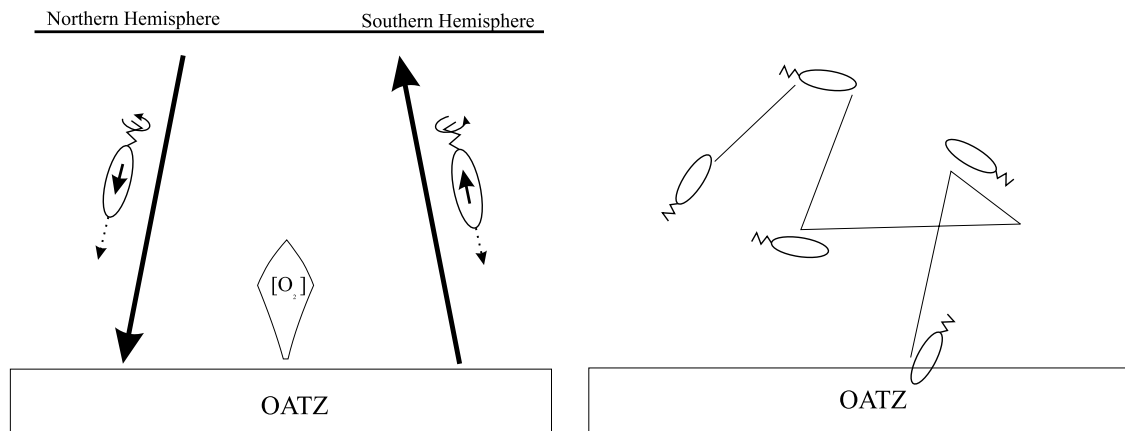


Figure 2.2: *Left* Bacterial magnetotaxis. The chain of SD particles provides the bacterium with a net magnetic moment (small arrows), that aligns the bacterium with the geomagnetic field lines (large arrows). In both hemispheres, cells at high oxygen concentrations swim towards the optimal OATZ. While MTB from the Northern hemisphere swim parallel to the field lines, those from the Southern hemisphere swim antiparallel to them. *Right* Bacterial chemotaxis. The bacterium displays a tumble-and-run behavior, consisting of relatively long displacements followed by random, localized movements (stars), during which the bacterium samples the chemical conditions of the environment.

Narrow size-range (stable single-domains), characteristic shape (restricted width-to-length ratios) and alignment in chains within cells

Magnetosomes always fall within the SD size range for both magnetite and greigite, which, as mentioned, is theoretically the most suitable size for orientation [Figure 2.3]. The use of chains of stable SD crystals is not fortuitous, since these particles are uniformly magnetized, with the maximum magnetic dipole moment per unit volume, and have a high, stable magnetic remanence. This magnetization is blocked in a given direction determined by the crystal's shape and lattice structure, giving the particle a north and a south magnetic pole. As already mentioned above, SD particles will always try to align their magnetic moment with the ambient magnetic field lines, giving rise to torque responses when the direction of the magnetization of the particle differs from the direction of the magnetic field. When arranged in chains, adjacent SD particles interact strongly due to their relatively large magnetization, and spontaneously align their magnetic moments along the chain direction, when a new magnetosome is forming at the end of a chain (see figure 2.1). This results in a net, stable magnetic moment for the whole chain. The chain will then behave as a biological compass needle orienting parallel to the geomagnetic field. As explained above, larger MD particles would have relatively low magnetic remanence,

impeding a torque response. SP particles, on the other hand, cannot acquire a stable magnetic remanence at all. Generally speaking a chain structure is not energetically the most favorable arrangement, which would correspond to a cluster arrangement with zero magnetic remanence. Hence, chains of SD particles are rare in nature and are considered inherent to the presence of MTB.

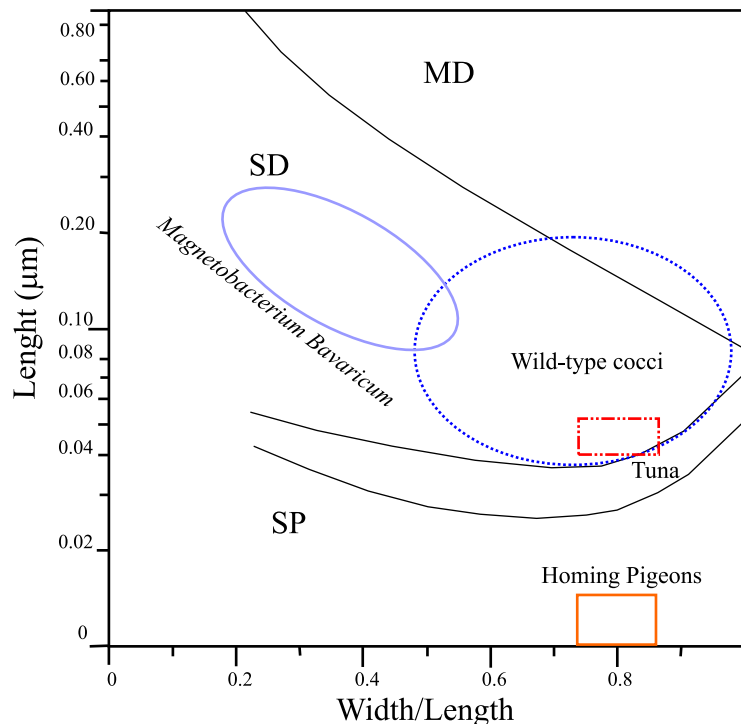


Figure 2.3: Grain-size range of the biogenic magnetite particles found in MTB (*Magnetobacterium bavaricum*, and wild-type cocci), tuna and homing pigeons [data from Hanzlik et al. (2000)]. Modified from Kirschvink et al. (1985) and Petersen et al. (1989).

Chemical purity and few crystallographic defects

The almost total absence of chemical impurities in the composition of magnetosomes and of imperfections in crystal structure, is highly desirable from the point of view of magnetic optimization, since such impurities and imperfections reduce the saturation magnetization of the particles, and thus the degree of efficiency when aligning with the geomagnetic field lines. Evolution and natural selection have probably favored those biomineralization mechanisms that yield chemically pure and crystallographically perfect magnetosomes, by preferentially selecting the organisms according to their (passive)-orientation capabilities.

An unusual truncated hexa-octahedral morphology and elongation along the [111] or [100] axis

Within the chains of magnetosomes, the magnetite crystals orient their [111] direction parallel to the chain axis, while greigite crystals are oriented with the [100] direction along the axis³. These six properties reflect the extent to which organisms can control biological mineralization processes.

Electron microscopy is the best technique yet available to identify biogenic magnetite, since it allows for direct morphological, crystallographical and chemical characterization of minerals. However, to prepare samples for electron microscopy and to analyze them is time consuming. Furthermore, the sample preparation can potentially alter the physical and chemical properties of the particles, thus blurring their biological characteristics and making them indistinguishable from their inorganic counterparts.

In the next chapter, results from a series of rock magnetic measurements performed on pure samples of MTB are described. Apart from providing important information on the physical and chemical properties of bacterial magnetite, these measurements are used as a guide to the detection of biogenic magnetite in natural samples. Magnetic measurements allow for a fast screening of bulk samples without altering their physical and chemical properties, thus offering a good complement to electron microscopy.

³Greigite magnetosomes also show a lower degree of perfection in the crystal structure when compared to magnetite magnetosomes. This fact has been attributed to differences in the demineralization mechanisms (Posfai et al., 1998)

Chapter 3

Magnetic properties of uncultured magnetotactic bacteria

"All life is an experiment."

Ralph Waldo Emerson. (1803-1882)

3.1 Introduction

In previous rock-magnetic studies on freeze-dried cells of cultured *Magnetospirillum magnetotacticum*, Moskowitz et al. (1988) and Moskowitz et al. (1993) reported magnetic properties of bacterial magnetosomes significantly different from those of synthetic, dispersed powders of magnetite particles of comparable grain size. Moskowitz et al. (1993) proposed a combination of room temperature coercivity analysis and low temperature remanence measurements to detect intact chains of SD particles of magnetite. In these studies, the authors found that the different ratio of remanence loss at the Verwey transition (T_v) between low temperature zero-field cooling (δ_{ZFC}) and field cooling (δ_{FC}) of the SIRM (saturation isothermal remanent magnetization) can be used as a parameter for the detection of magnetosome chains, which show unusually high δ -ratios: $\delta_{FC}/\delta_{ZFC} > 2$ (see Figure 3.8).

In this chapter a rock magnetic study on pure samples of wild-type MTB will be presented. Apart from magnetically characterizing uncultured MTB, this work also serves

as a test for the rock magnetic criteria proposed by Moskowitz et al. (1993).

3.2 Sample preparation

The Alpine foreland lake Chiemsee (southern Germany) is a natural laboratory for the study of MTB. The uppermost sediments of this lake host abundant MTB, distributed in the OATZ [Figure 3.1]. The predominant species are a wild-type round coccoid and the rod-shape giant "*Magnetobacterium bavaricum*" [Figure 3.2A,C]. Interestingly, these species can survive and reproduce under laboratory conditions for a period of 15-20 months; which allows for the concentration of natural populations in amounts that suffice for their magnetic characterization. "*Magnetobacterium bavaricum*" has a length of up to 12 μm , and individual cells may contain more than 600 bullet-shaped magnetosomes, arranged in 3-5 bundles of chains within the cellular body. Round-shaped magnetotactic cocci, have a diameter of approximately 1 μm , and contain two chains of truncated hexahedral magnetosomes. The magnetosomes of both "*Magnetobacterium bavaricum*" and magnetotactic cocci are 30-130 nm in size [Figure 3.2B,D], which falls into the stable SD particle size range for magnetite, as shown in figure 2.3.

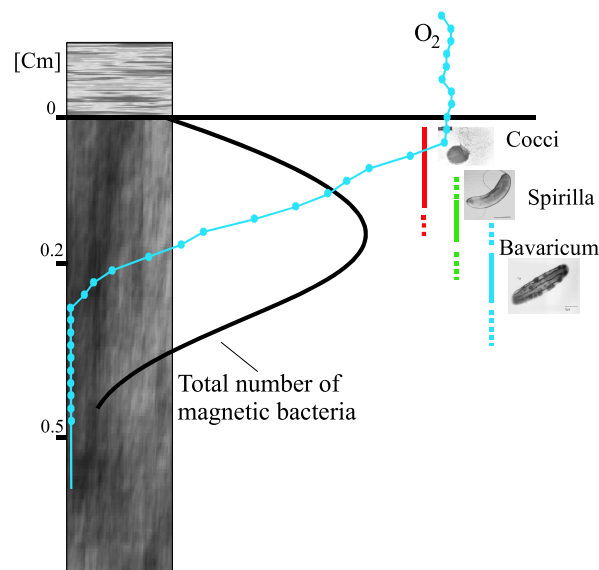


Figure 3.1: MTB in sediments from Lake Chiemsee. The higher densities occur in the uppermost millimeters of the sediment, at the OATZ, where several species of bacteria are often found distributed at different depths.

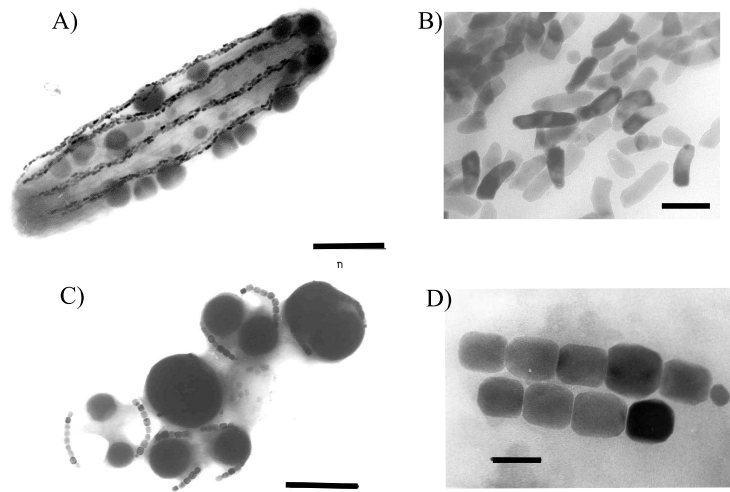


Figure 3.2: Uncultured MTB collected to analyze their magnetic properties. (A) "*Magnetobacterium bavaricum*" with bullet shaped magnetosomes (B); and (C) magnetotactic cocci with truncated hexahedral magnetosomes (D). Scale bar in (A-C)= $1\mu\text{m}$; in (B-D)= $0.1\mu\text{m}$. From Hanzlik (1999)

The concentration of MTB from bulk sediment samples was done in the so-called "Bacteriodrome" (Petersen et al., 1989) [Figure 3.3], which consists of a Leitz Laborlux D light microscope (stripped of all magnetic parts) surrounded by two set of rectangular coils (40 cm diameter) orientated perpendicular to each other in the horizontal plane. The Bacteriodrome allows the manipulation of magnetotactic bacteria in the field of view of a light microscope.

To concentrate the MTB, a drop of fresh sediment was first dripped onto a clean microscope glass-slide. A drop of distilled water was then carefully added at the side and connected with the mud drop. By controlling the horizontal magnetic field produced by the coils, living MTB were forced to swim away from the mud and towards the distilled water, were they concentrated in the waterfront [Figure 3.4A]. Finally, the mud was carefully removed from the section after 30 minutes and the same procedure repeated with a new, fresh drop of sediment, until sufficient MTB cells had accumulated for later magnetic measurements. As can be seen in Figure 3.4B-D, MTB cells were purposely concentrated at a very high density, by controlling the position of the waterfront. The fast swimming cocci and slow swimming "*Magnetobacterium bavaricum*" were dominant in the samples. Although this procedure is effective for obtaining a pure sample of MTB, it is also time consuming and non selective with the different species of MTB living in the sediment. By this technique several million cells per sample were collected. Two samples (named P2



Figure 3.3: The Bacteriodrome used to study the swimming behavior of MTB and to concentrate cells. The light microscope is surrounded by two pairs of coils which allow for a control of the ambient field both in intensity and horizontal direction.

and P3) were prepared. The concentrated MTB were air-dried at ambient temperature and stored in a sealed closure to avoid dust contamination. Magnetic measurements were immediately carried out after the collection process was finished.

3.3 Rock magnetic properties of uncultured magnetotactic bacteria

All results of the rock-magnetic measurements are summarized in Table 3.1 and Table 3.2, at the end of the chapter.

3.3.1 Isothermal remanent magnetization and anhysteretic remanent magnetization analysis

Stepwise IRM acquisition up to a maximum field of 150 mT (saturation field) and demagnetization of saturation IRM (SIRM) were measured following two approaches: (1) static (DC) field IRM acquisition and back-field demagnetization of SIRM; and (2) pulsed-field IRM acquisition and alternating field (AF) demagnetization of SIRM. The IRM curves

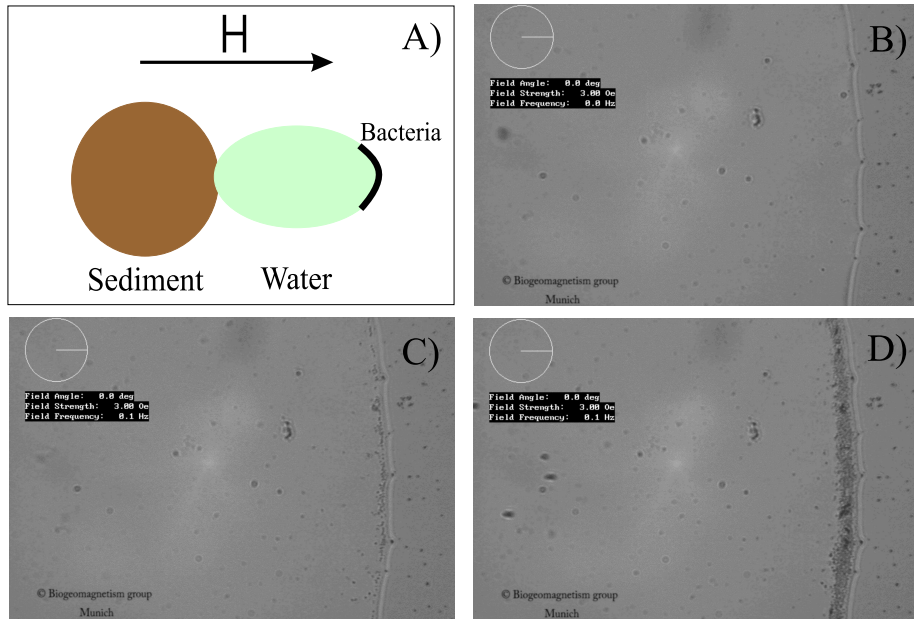


Figure 3.4: (A) Extraction and accumulation of MTB from sediments (H =magnetic field). (B-D) different stages of the concentration process. By means of controlled magnetic fields, the cells were forced to swim out of the sediment and towards the edge of a water drop.

were normalized to the maximum value of the SIRM and the reversed static field demagnetization was transformed as $(1 + IRM(-H)/SIRM)/2$ to simplify comparison with AF result.

ARM acquisition and demagnetization was measured by combining a weak steady bias field and a decaying AF field in two steps: First the sample was placed in a weak, steady DC field ($50 \mu\text{T}$) and an AF field was superimposed increasing stepwise from 5 to 120 mT. The remanence was measured after each AF step. The acquired ARM was later removed with an AF field. Finally, an ARM was imparted by applying an increasing weak DC field (from 0.01 to 0.1 mT) in a constant AF peak field of 80 mT.

The IRM coercivity spectra for sample P2 are plotted in Figure 3.5A. This sample yielded a value for the median destructive field, H_{mdf}^1 of 41 mT and 43 mT for the DC and for the AF demagnetization treatments, respectively. The R-values² of the Wohlfarth-Cisowski test (Cisowski, 1981), are $R_{df}=0.45$ and $R_{af}=0.41$ for the DC field and the AF field treatments, respectively. As can be seen in Figure 3.5A, the pulsed-field treatment

¹The H_{mdf} is defined as the field required to reduce the initial remanence of the sample by 50%

²The R-value is obtained as the intersection value of the SIRM acquisition and demagnetization curves

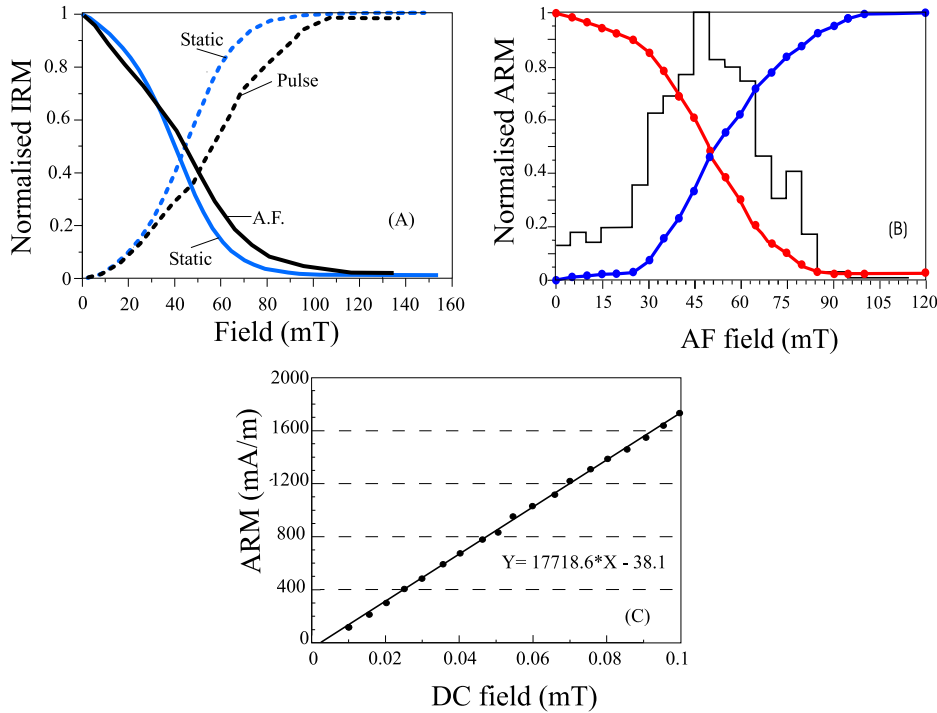


Figure 3.5: (A) Saturation remanent magnetization (SIRM) acquisitions by static and pulse fields (dashed lines), and demagnetization by AF and static fields (solid lines). (B) Anhyseretic remanent magnetization (ARM) acquisition in an increasing peak alternating field (blue line), AF demagnetization (red line) and the corresponding coercivity spectrum (line). (C) ARM acquisition as a function of an increasing DC-field.

shifts significantly the IRM acquisition to higher fields compared with the DC field treatment. This phenomenon is related to the characteristic response time of the magnetite particles to the different magnetic treatments (Moskowitz et al., 1993). Because there is less time for the magnetosomes to respond to a short pulse treatment, higher pulse fields are required to achieve the same remagnetisation state obtained with the static fields. Figure 3.5B shows the ARM acquisition and demagnetization of sample P2. The demagnetization curve shows a distinct shoulder, typical of SD behavior. The median destructive field is 49 mT and the R-value is 0.47. The field dependence of the ARM of sample P2, presented in Figure 3.5C, shows a linear relationship. The measured susceptibility of ARM (χ_{ARM}) is $177.2 \cdot 10^{-5}$ SI. Similar values were obtained for sample P3.

3.3.2 Hysteresis and FORC analysis

Room temperature hysteresis loops were measured for the P2 and P3 samples up to a maximum field of 1 T. To examine the domain state, the initial magnetization curves $M_{si}(B)$ were measured before measuring the full hysteresis loop, following the procedure proposed by Fabian (2003). First, the sample was given a saturation remanence, M_{rs} , by applying a maximum field; the ambient field was then set to zero in 2 or 3 steps in order to avoid overshooting to negative fields. Next, the initial magnetization curve plus hysteresis loop starting from this state was measured. The FORC analysis (First Order Reversal Curves, see Mayergoyz (1986)) was carried out following Roberts et al. (2000) [Figure 3.6]. For comparison, the FORC diagram of a powder of inorganic SD magnetite particles was also measured.

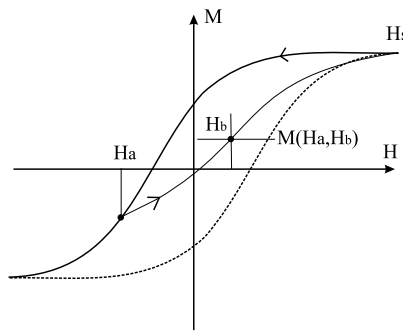


Figure 3.6: Procedure followed to obtain the FORC diagrams. Each FORC was measured by saturating the sample at H_s , decreasing the field to a value of $H_a < H_s$, and reversing the field sweep to the saturated state in a series of steps (H_b). This sequence was repeated for several values of H_a . The magnetization $M(H_a, H_b)$ was measured at each step and the mixed second derivative was calculated to obtain the FORC distribution

The hysteresis loops of both samples show a potbellied-shape with a coercive force (H_c) ranging from 31 (P2) to 35 mT (P3), and a coercivity of remanence (H_{cr}) of ~ 45 mT [Figure 3.7]. The ratio of saturation remanence to saturation magnetization (M_{rs}/M_s) is 0.47 (P2) and 0.51 (P3), while the ratio of coercive force to coercivity of remanence, H_{cr}/H_c is 1.36 (P2) and 1.5 (P3). Both samples are saturated at 100 mT. The value for the saturation magnetic moment of sample P2 is $6.7 \cdot 10^{-8} \text{ Am}^2$ and $2.8 \cdot 10^{-8} \text{ Am}^2$ for P3. No significant orientation-dependency changes of the hysteresis parameters are observed. The number of cells accumulated in samples P2 and P3 was determined from the values of saturation magnetization³ as $\sim 67 \cdot 10^6$ and $\sim 28 \cdot 10^6$ cells, respectively.

³Assuming a magnetic moment for a single MTB of 10^{-15} Am^2 (Hanzlik, 1999)

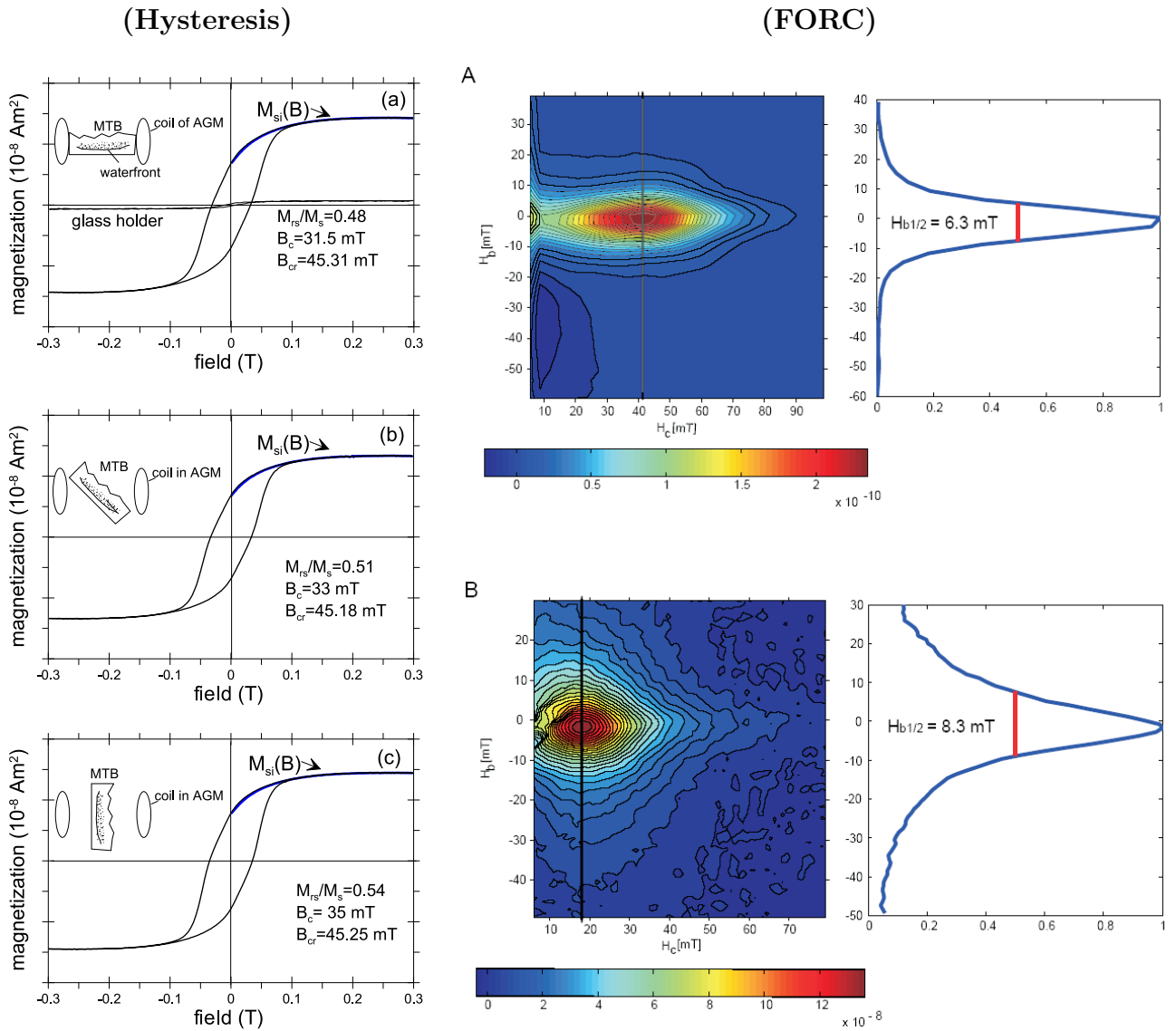


Figure 3.7: *Left* Room-temperature hysteresis loops measured at different orientations (a, b, c). The hysteresis of the glass holder is presented in (a), indicating a negligible influence. *Right* FORC diagram of sample P3 (Top) and a powder sample containing SD magnetite particles (Bottom). The characteristic interaction strength ($H_{b1/2}$) diagrams are also presented (cross section of the FORC diagram). See text for further details.

Figure 3.7 presents the FORC diagram obtained from sample P2, which shows features typical for SD grain size, as well as of the SD powder sample. The FORC distribution of the MTB sample has relatively small vertical spread along the H_b axis. Along the H_c axis, it is nearly closed and peaks at $H_c=42$ mT. On the other hand, the FORC distribution of the SD powder sample shows a far greater vertical spread. To estimate the range of the magnetic interactions in the MTB sample (i.e. particle-particle, chain-chain or cell-cell interaction), the characteristic interaction strength ($H_{b1/2}$) is determined from the vertical profile through the high-coercivity peak of the distribution. The characteristic interaction strength is defined as the value of the interaction field where the FORC distribution is reduced to half of its maximum value, and its value depends on the distance between the interacting particles. Hence, relatively large values of interaction strength correspond to small range interactions (i.e. particle-particle); whereas relatively low values of interaction strength correspond to large range interactions (i.e. chain-chain or cell-cell). For the MTB sample, $H_{b1/2}=6.3$ mT; whereas for the SD powder sample $H_{b1/2}=8.3$ mT [Figure 3.7].

Figure 3.8a and b, shows the Day plot⁴ for sample P2 and for the sediments from which they were extracted. As can be seen, the Day plot parameters for the MTB sample fall well within the SD range ($M_{rs}/M_s \sim 0.5$, $H_{cr}/H_c \sim 1.4$). On the other hand, for the sediment samples they fall in the PSD range. This is due to the presence, within the sediments, of other non-biogenic magnetic components which blur the magnetic properties of the bacterial magnetite, thus reducing the effectiveness of rock magnetic techniques to detect biogenic magnetite in bulk samples. As can be seen, however, sediments from the uppermost 5 cm, where most of the MTB occur, plot closer to the value of the pure MTB samples.

3.3.3 Low-temperature demagnetization of SIRM: The delta-delta test

The *delta – delta* test (Moskowitz et al., 1993) is based on two facts: 1) the monoclinic phase of magnetite at temperatures below the Verwey transition (T_v) has a larger magneto-crystalline anisotropy than the cubic phase and 2) magnetosome chains have a

⁴Day plots (Day et al., 1977) consist of a two-dimensional space divided into regions (SD, PSD and MD behavior) using theoretical bounds as guides. The two dimensions represented in the Day plot are the ratios of the hysteresis parameters M_{rs} , M_s , B_{cr} and B_c , which are sensitive to domain state, hence provide information about the grain size and shape of the magnetic particles.

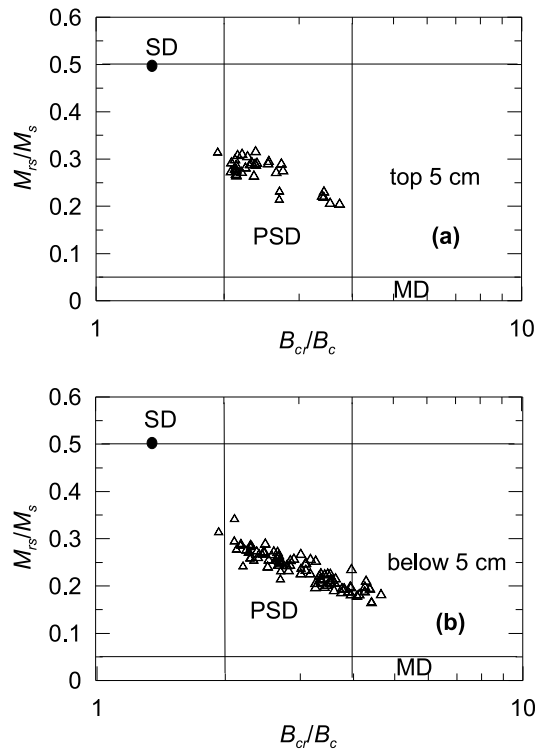


Figure 3.8: (A) Comparison of the Day plot for the MTB sample (black dot) and for samples from the uppermost 5 cm and (B) for samples below 5 cm in the sediment column (triangles). Due to the presence of non-biogenic magnetic phases in the sediments, the Day plot parameters are shifted towards the PSD range in the bulk samples. This shift is more pronounced in samples below 5 cm, where the density of MTB is significantly lower.

pronounced shape anisotropy that favors the magnetization along the chain axis. As a result of 1), the magnetization of individual magnetosomes will be stable in one of the monoclinic c -axes at $T < T_v$; as a consequence of 2), the c -axes nearest to the chain axis will be preferentially occupied. A strong magnetic field applied during cooling between 300 K and 5 K, however, will outweigh the anisotropy due to the chain structure, such that those c -axes nearest to the field axis will be preferentially occupied. When the field is switched off at $T < T_v$ after cooling in the strong field (FC), the magnetization will be blocked in a metastable thermoremanence state, which is energetically less favorable than the remanence state induced during zero field cooling (ZFC). After heating through T_v , the magneto-crystalline anisotropy tensor undergoes a symmetry change and the thermoremanence can be unblocked. Therefore, the presence of chains of magnetosomes in the samples will be revealed by the different thermal dependence of the magnetic remanence

acquired after ZFC and FC [Figure 3.9].

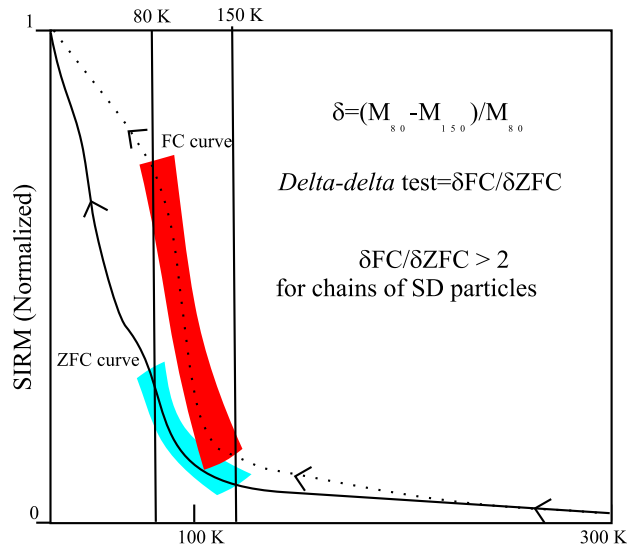


Figure 3.9: Scheme showing the principles of the delta-delta test. The low temperature variation of the SIRM is measured both in a strong field (FC) and in zero field (ZFC). Between 80 and 150 K the δ -value for each curve is determined and the δ -ratio ($\delta_{FC} / \delta_{ZFC}$) calculated. Chains of SD particles yield distinctly large values.

To study the variation of the SIRM with temperature, the samples were cooled from 300 to 5 K through the Verwey transition either in zero field (ZFC) or in a strong field of 5 T (FC). At 5 K a SIRM was imparted using a strong field of 5 T, and the variation of the SIRM was monitored in zero field at intervals of 2-5 K during the warming process (5-300 K).

The thermal decay of the SIRM obtained at 5 K after FC and ZFC treatments for samples P2 and P3 is shown in Figure 3.10A,B. As can be seen, the SIRM of both samples after FC treatment, rapidly decay between 5-30 K and 90-110 K. The latter drop closely matches the value for the temperature of the Verwey transition measured in cultured MTB ($T_v \sim 100$ K) (Moskowitz et al., 1993). The δ -ratios ($\delta_{FC} / \delta_{ZFC}$)⁵ are 2.6 and 3.9 for samples P2 and P3, respectively. Both values are greater than 2, the threshold value for chains of bacterial magnetite proposed by Moskowitz et al. (1993). The reasons for the decay in the SIRM between 5-30 K are unclear, and several interpretations will be proposed in the discussion below.

⁵Following Moskowitz et al. (1993), $\delta = (M_{irm}(80) - M_{irm}(150)) / M_{irm}(80)$

3.3.4 Cycling curves of SIRM (300 \rightarrow 5 \rightarrow 300 K)

The cycling of SIRM was measured following a standard procedure. The SIRM was given in a field of 5 T at 300 K, then cooled in zero field to 5 K and then warmed up to 300 K. Remanence values were measured at intervals of 5 K.

As can be seen in Figure 3.10C,D, during the cooling cycle (300 \rightarrow 5 K), the remanence of the samples increases steadily down to a temperature of 130-100 K. This increase is followed by a gradual decrease at 80-70 K, and then a constant level until 5 K. Compared with the initial value, the gain in remanence during cooling approaches $\sim 4\%$. During the warming cycle (300 \rightarrow 5 K), the remanence shows a reversible behavior with respect to the cooling cycle until 70-80 K, followed by an increase between 100-150 K, and a decrease between 150-300 K. The loss of remanence at 300 K with respect to the initial value at this temperature averages $\sim 4 - 6\%$.

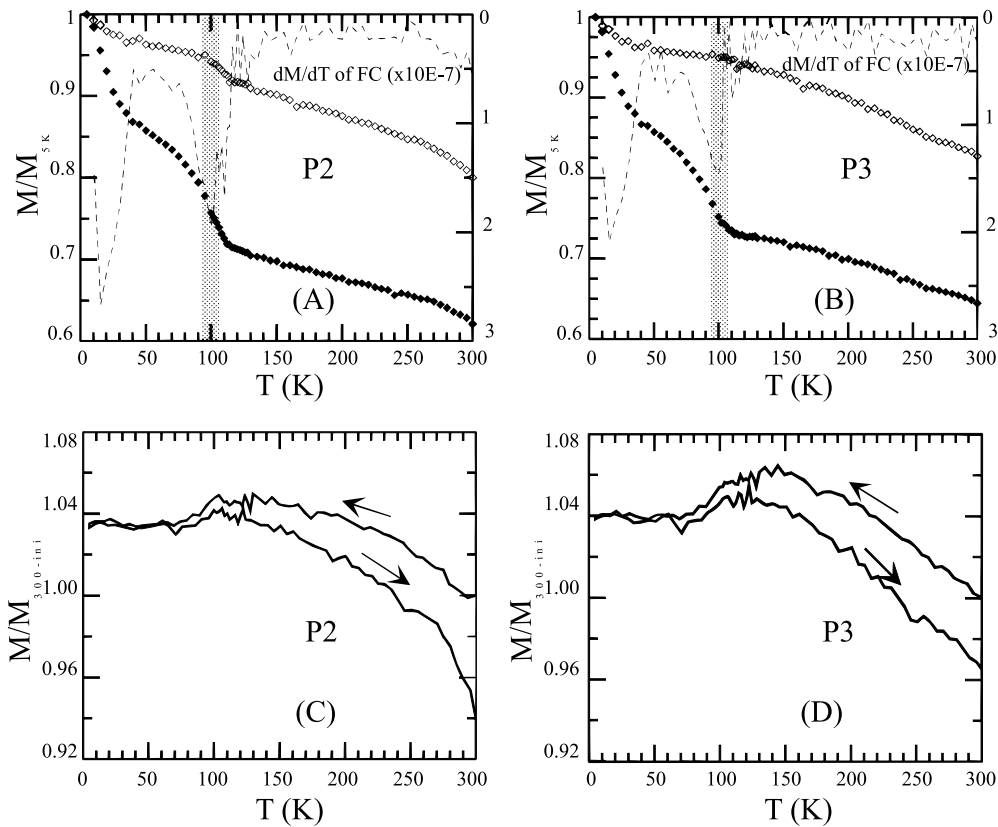


Figure 3.10: Low-temperature magnetic measurements of samples P2 and P3. (A) and (B), normalized SIRM warming curves after FC (filled diamond) and ZFC (outlined diamond) treatments, and the first derivatives of curves after FC (dashed line). (C) and (D), cycling curves of $SIRM_{300K}$.

3.4 Interpretation

Results of the room-temperature magnetic measurements demonstrate that the magnetosomes consist of SD magnetite. The relevant observations are (1) the shoulder seen in the demagnetization curve of ARM [Figure 3.6b]; (2) a relative high coercive force (~ 33 mT) and coercivity of the remanence (~ 45 mT); (3) the low saturation field (< 100 mT) and the broad pot-bellied shaped of hysteresis loops [Figure 3.7a-c]; and (4) the closed pattern of FORC diagram [Figure 3.7A].

Magnetic interactions in bulk samples strongly affect their magnetic properties. Because the samples contain millions of dehydrated cells ($\sim 10^7 - 10^8$ magnetosomes), magnetostatic interactions of magnetite particles may be significant. Agglomeration of cells and shrinkage of the cell membrane and cytoplasm (thereby decreasing the distances between magnetosomes and magnetosome chains) could substantially enhance the particle and chain interactions. For non-interacting, uniaxial SD particles, the R-value should be 0.5. With increasing interactions, the R-value decreases. The R-values for the samples are 0.39 and 0.45, indicating moderate magnetostatic interactions.

The FORC diagrams provide another useful technique to understand the nature of the magnetic interactions in our samples. Recently, Muxworthy et al. (2004) systematically investigated the effects of magnetostatic interactions on the FORC behavior using micromagnetic modelling. These studies revealed that interacting assemblages of SD grains show more PSD-like behavior if the particle distance is small, resulting in a decrease of the coercivity and greater spread off the H_c axis. As can be seen in Figure 3.7, the coercivity value of the SD powder sample as determined in the FORC diagram is distinctly lower than that of the MTB sample (~ 18 mT vs ~ 42 mT), suggesting a shorter distance between the interacting powder particles. This idea is supported by the fact that the MTB sample shows a lower characteristic interaction strength, compared to that of the SD powder (6.3 vs 8.3 mT), and hence a larger distance of the interacting particles. This results for the SD powder sample are interpreted as due to the dominant particle-particle magnetic interactions, while for the MTB sample the dominant interactions are interpreted as due to chain-chain and/or cell-cell interactions. Hence, the FORC diagram is sensitive enough to resolve the different nature of the magnetic interactions in both samples.

The FORC diagram of the MTB sample also shows a very elongated shape along the H_c -axis, a feature that can be attributed to a Gaussian distribution of coercivity values. The high coercivity values of up to ~ 100 mT could be due to the elongated magnetosomes

of "*Magnetobacterium bavaricum*".

With regard to the low-temperature measurements, the *delta – delta* test (δ_{FC}/δ_{ZFC}) of both P2 and P3 shows values greater than 2. As mentioned above, due to air-drying at room temperature, oxidation may affect the behavior of the sample at the Verwey transition, and therefore also the δ -ratio. The samples also show that the intensity drops at T_v are diminished for the ZFC curves [Figure 3.9A,B], indicating that the samples might have suffered oxidation to some extent during the concentration process. On the other hand, the apparent Verwey transition at ~ 100 K for the FC curves suggest that this oxidation is only partial, probably leading to the formation of a maghemite rim around a magnetite core in some grains (Smirnov and Tarduno, 2000). The relatively low values of T_v (~ 100 K instead of ~ 120 K) may also be an intrinsic feature of magnetosomes.

Causes for the remanence drop between 5-30 K in the curves after FC cooling are unclear. We propose several explanations: (1) SP behavior of growing magnetosomes just below the threshold of SD/SP (see figure 2.1); (2) partial oxidation that decreases the effective SD grain size; (3) the presence of siderite (transition at ~ 35 K) (Housen et al., 1996) or pyrrhotite (transition at 34 K) (Dekkers et al., 1993). However, it is difficult to determine the oxidation state of magnetite magnetosomes in the samples and its effect on the δ -ratio. It is still an open question as to whether chains of oxidized magnetosomes yield enhanced δ -ratios as predicted from numerical modelling. While the δ -ratio of an MV-1 sample increased strongly from 1.55 to 4.8 after three years of aging (Carter-Stiglitz et al., 2004), an MS-1 sample after four years of exposure to air had a δ -ratios of only 1.1 (Weiss et al., 2004a). The difference in storage in these studies and the magnetosomes of different species may cause the discrepancies. It is clear that more experimental data are needed to identify short-term and long-term effects of oxidation on the δ -ratio.

3.5 Rock magnetic criteria for the identification of biogenic magnetite

The establishment of effective rock magnetic criteria for identification of bacterial magnetite in sediments depends heavily on understanding the specific properties of bacterial magnetite. It is therefore interesting to compare the results presented here for isolated bacteria with literature data. As can be seen in Table 1, the samples have larger values of H_{cr}

(P2=40 mT; P3=45.5 mT) than those for freeze-dried whole cells (M-1=27.6 mT) and isolated magnetosomes (M-2=16.6 mT) of "*Magnetospirillum magnetotacticum*" (Moskowitz et al., 1988); the same can be observed for the MDF values [Table 3.1]. These parameters do not exhibit clear consistencies among biogenic SD particles, while they are indistinguishable from that of a synthetic SD magnetite sample, suggesting that those parameters alone cannot pinpoint the biogenic origin of the magnetite particles.

On the other hand, whole cell samples of both uncultured (wild-type cocci and "*Magnetobacterium bavaricum*") and cultured bacteria (strain MV, *M. magnetotacticum* MS-1, and *M. magneticum* AMB-1) have δ -ratios greater than 2 [Table 2], regardless of the preparation method. This confirms the assumption that intact chain arrangements lead to high δ -ratios (Moskowitz et al., 1993). The extracted magnetosomes (disrupted chains) and SD magnetite induced by GS-15 (non-chain arrangement), on the other hand, have δ -ratios less than 1.6 [Table 3.2]. These results, therefore, serve as a calibration of the *delta – delta* test with naturally occurring populations of MTB with positive results.

The average δ_{ZFC} and δ_{FC} values for whole cell samples, extracted magnetosomes samples and extracellular magnetite produced by GS-15 cultured in a reducing environment with low- CO_2 concentrations, fall between ~ 0.1 and 0.3 , which are distinctly lower than that of inorganic stoichiometric magnetite (including SD magnetite) and extracellularly-produced magnetite produced by GS-15 cultured in high- CO_2 concentrations, but higher than δ_{FC} of greigite and maghemite (Vali et al., 2004). This suggests that the δ_{FC} can be used as a first indicator of magnetosome chains. However, caution should be taken because δ_{FC} of non-stoichiometric (oxidized) inorganic magnetite may fall into the same range (Özdemir et al., 1993).⁶

Another significant feature in Table 3.2 is that all samples (regardless of species and preparation methods) show the low T_v at $(102.9 \pm 5.0$ K). This implies that the low transition temperature of magnetosomes may be one of the important evidences of biogenic magnetite. The lowered T_v can be attributed to a bulk non-stoichiometry of magnetosomes because surface effects due to cation deficient terminations are negligible in magnetite crystals as large as 50 nm. An alternative cause for a lowered T_v would be chemical impurity, as often observed in inorganic magnetite, where titanium or manganese substitute iron. If so, the tenet that bacteria produce stoichiometric, pure magnetite should be reconsidered.

⁶Except for the case of the MV2 strain, the values of δ_{ZFC} reported for MTB samples are also clearly different from that reported for both isolated magnetosomes and synthetic magnetite, although similar to the values obtained for maghemite and greigite.

MTB are ubiquitous in a broad diversity of natural environments from marine to continental fresh water habitats. As a result, these particles are often found as part of mixtures with different non-biological minerals, which also contribute to the bulk magnetic properties of the samples. Due to their small grain size, these particles are also prone to undergo chemical alterations, which ultimately affect their magnetic properties. For that reason, it is necessary to test the suitability of rock magnetic techniques to identify bacterial magnetite in bulk natural samples. This will be the subject of the next chapter.

| Sample | M_s (Am^2) | H_c (mT) | H_{cr} (mT) | M_{rs}/M_s | H_{cr}/H_c | R_{AF} | $[\text{IRM}(\text{ARM})]$ | MDF | $[\text{IRM}(\text{ARM})]$ | ARM/SIRM |
|------------------------------------|-------------------------|------------|---------------|--------------|--------------|----------|----------------------------|-----|----------------------------|----------|
| Strain M-1 (a) | - | 26.7 | 27.6 | 0.53 | 1.02 | - | 0.62 | - | 32 | 0.11 |
| Strain M-2n (a) | - | 3.7 | 16.6 | 0.41 | 4.49 | - | 0.21 | - | 9 | 0.005 |
| Strain MV1 (b) | - | - | - | 0.49 | 1.1 | - | - | - | - | - |
| Strain MS1 (b) | - | - | - | 0.44 | 1.1 | - | - | - | - | - |
| P2 (c) | $6.7 \cdot 10^{-8}$ | 6.7 | 40 | 0.47 | 1.50 | - | 0.41(0.47) | - | 43(49) | 0.03 |
| P3 (c) | $2.8 \cdot 10^{-8}$ | 3.4 | 45.5 | 0.51 | 1.36 | - | 0.39(0.44) | - | 45(51) | 0.02 |
| Synthetic magnetite (d) (cubic) | - | 21.3 | 30-40 | 0.28 | 1-2 | - | - | - | 28 | - |
| Synthetic magnetite (d) (acicular) | - | 38.4 | 50-60 | 0.4 | 1-2 | - | - | - | 43 | - |

Table 3.1: Comparison of the magnetic parameters (room-temperature experiments) between the uncultured and cultured MTB cells and synthetic magnetite. a-Moskowitz et al. (1988); M-2, extracted magnetosome chains; b-Moskowitz et al. (1993); c-this study; d-Dunlop (1986), cubic magnetite (42 nm) and acicular magnetite ($30 \times 200 \text{ nm}^2$)

| Sample | T_v (K) | LTD_{FC} | LTD_{ZFC} | δ_{ZFC} | δ_{FC} | δ_{FC}/δ_{ZFC} |
|----------------------------------|--------------|-------------|-------------|----------------|---------------|----------------------------|
| <i>Whole Cells</i> | | | | | | |
| MV1 (a) | 110 | 34 | 15 | 0.06 | 0.24 | 4.0 |
| MV1 (a) | 101 | 36 | - | 0.04 | 0.19 | 4.8 |
| MV2 (a) | 110 | 34 | 0.10 | 0.24 | 2.4 | - |
| MS1 (a) | 101 | 35 | 15 | 0.06 | 0.16 | 2.7 |
| AMB-1 (b) | 98 | 40 | 16 | 0.04 | 0.23 | 5.6 |
| P2 (c) | 100 | 36 | 19 | 0.06 | 0.14 | 2.3 |
| P3 (c) | 100 | 37 | 19 | 0.03 | 0.11 | 3.7 |
| Mean | 102.9 | 36.0 | 16.8 | 0.06 | 0.19 | 3.7 |
| \pms.d. | 5.0 | 2.1 | 2.0 | 0.02 | 0.05 | 1.3 |
| <i>Isolated magnetosomes (a)</i> | | | | | | |
| | | 46 | - | 0.18 | 0.19 | 1.1 |
| | | - | - | 0.21 | 0.22 | 1.0 |
| | | - | - | 0.26 | 0.26 | 1.0 |
| <i>Extracellular magnetite</i> | | | | | | |
| GS-15 (a) | - | - | 0.56 | 0.53 | 0.9 | - |
| GS-15 (e) 668h | - | - | 0.09 | 0.15 | 1.6 | - |
| GS-15 (e) 34d | - | - | 0.09 | 0.1 | 1.1 | - |
| <i>Synthetic particles</i> | | | | | | |
| magnetite (a) 37 nm | 120 | 68 | - | 0.38 | 0.48 | 1.3 |
| magnetite (a) 100 nm | 120 | 80 | - | 0.52 | 0.67 | 1.3 |
| magnetite (a) 210 nm | 120 | 90 | - | 0.82 | 0.86 | 1.0 |
| magnetite (a) 1000 nm | 120 | 93 | - | 0.88 | 0.90 | 1.0 |
| maghemite (a) | - | 15 | - | 0.02 | 0.03 | 1.1 |
| greigite (a) | - | 19 | - | 0.05 | 0.05 | 0.9 |

Table 3.2: Comparison of the low-temperature demagnetization of SIRM acquired at 20 K for the uncultured and cultured MTB cells. a-Moskowitz et al. (1993); b-Weiss et al. (2004b); c-this study; d-Weiss et al. (2004a); e-Vali et al. (2004). $LTD_{FC(ZFC)} = (M_{rm20K} - M_{300K})/M_{20K} \cdot 100$. See text for description

Chapter 4

Detection of bacterial magnetite in lake sediments

"The great tragedy of science - the slaying of a beautiful hypothesis by an ugly fact."

Thomas H. Huxley. (1825-1895)

4.1 Introduction

In the previous chapter the magnetic properties of uncultured MTB were characterized, and the rock magnetic criteria for the identification of bacterial magnetosome chains, as proposed by Moskowitz et al. (1993) was also tested, with positive results. However, bacterial magnetite often occur in sediments, soils or rocks as part of a mixture of different magnetic components, including authigenic, anthropogenic and diagenetic phases, which can potentially blur the magnetic signal of the biogenic component. Furthermore, owing to their small particle size, biogenic magnetite particles are also prone to be dissolved under reducing conditions [e.g. Hilgenfeldt (2000)] or to undergo low temperature oxidation. Both processes will affect the magnetic properties of the particles. It is therefore of interest to understand how chemical alteration, and the mixing of different mineralogical phases affect the rock magnetic criteria for the detection of biogenic magnetite.

As outlined in chapter 3, the most useful magnetic property measurements are: (1) acquisition and demagnetization of isothermal remanent magnetization (IRM) using static,

pulse and alternating field; (2) acquisition of anhysteretic remanent magnetization and (3) thermal dependence of low temperature saturation IRM after cooling in zero field (ZFC) or in a 2.5 T field (FC) from 300 to 5 K. Here, these rock magnetic measurements are applied to bulk sediments samples containing MTB and bacterial magnetosomes, to clearly establish the suitability of the rock magnetic criteria for the identification of biogenic magnetite.

4.2 Optical identification of bacterial magnetite in lake sediments

Surface sediment samples were collected from Lake Chiemsee (Southern Germany), in a site where a high abundance of various MTB were reported (Petersen et al., 1989). For comparison, surface sediments in a site with low concentrations of MTB were also collected. This material approximately corresponds to the upper 5 centimeters of the sediment column and was kept in 120 cm^3 aquariums. Examination of the freshly collected sediment samples in the Bacteriodrome confirmed the presence of live MTB in high concentrations in the MTB-rich sediments, and their almost total absence in the MTB-poor sediments.

Electron microscopic examinations were conducted on magnetic extracts from the sediments to characterize the different magnetic components. Fine-grained bacterial magnetite was observed, in coexistence with coarser-grained detrital magnetite crystals [Figure 4.1 A-C]. Figure 4.1D,E shows magnetosomes from the studied surface-sediment samples. A dead intact cell of "*Magnetobacterium bavaricum*" with hundreds of magnetite magnetosomes was also observed [Figure 4.1F].

The originally linear chains of magnetosomes were found disrupted, probably as a consequence of cell shrinkage during dehydration (Shcherbakov et al., 1997). These magnetite magnetosomes are bullet-shaped [Figure 4.1E], with typical dimensions of 35 nm and 120 nm for the short and long axis, respectively, and fall well in the stable Single-Domain (SD) magnetite range (Fabian et al., 1996; Winklhofer et al., 1997) [see also Figure 2.3]. Figure 4.1D shows magnetosomes which resemble that observed in cocci or spirilla (Shcherbakov et al., 1997; Hanzlik, 1999). Once the presence of living MTB and also of bacterial magnetosomes was confirmed in the sediments, the suitability of the rock magnetic criteria introduced in chapter 3, to detect bacterial magnetite in bulk sediment samples, was tested.

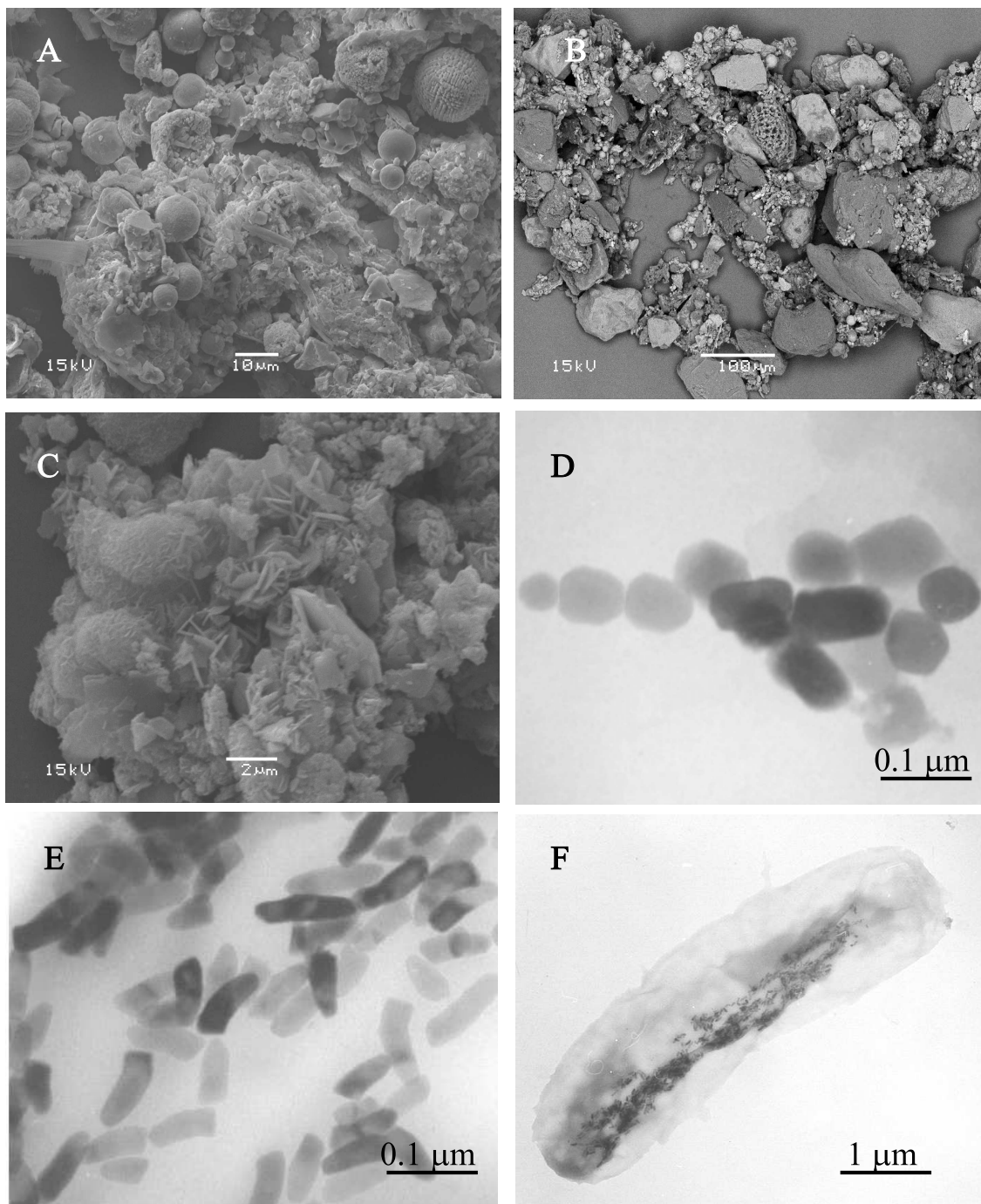


Figure 4.1: Micrographs of electron microscope observations on magnetic extracts from lake Chiemsee. (A) iron spherules from industrial pollution; (B) detrital coarse-grained magnetite particles; (C) needle-like iron oxyhydroxide grains; (D) prismatic shape magnetosomes (from cocci or spirilla) in a short chain; (E) bullet-shaped magnetosomes of "*Magnetobacterium Bavaricum*"; (F) a whole cell of "*Magnetobacterium Bavaricum*".

4.2.1 Acquisition and demagnetization of IRM and ARM

The analysis of remanence coercivity was used to distinguish between high-coercivity and low-coercivity phases. Stepwise IRM acquisition, static field and alternating field (AF) demagnetization were conducted on representative bulk sediment samples from MTB-rich and from MTB-poor sediments. All remanence measurements were made along a single axis of remanence acquisition.

Figure 4.2a shows that the IRM remanence coercivity of the MTB-rich sample is very similar to that of the pure MTB sample, with $H_{cr} \sim 50$ mT, while the MTB-poor sample yields the lower value of ~ 43 mT. The demagnetization curve of both MTB-rich and MTB-poor samples decay faster than the MTB sample and have median destructive field (MDF) values between 30-35 mT, $\sim 2/3$ of the pure MTB sample (chapter 3)[Figure 4.2a]. The intersection (R-value) of IRM acquisition and AF demagnetization is distinctly less than 0.5, suggesting magnetic interactions of magnetic particles in the bulk sediment samples (Wohlfarth, 1958; Cisowski, 1981). Contrary to what is expected, the curve corresponding to the MTB-poor sediments lies closer to that of the pure MTB sample than does the curve of the MTB-rich sediments.

ARM acquisition (peak alternating field 100mT), static field and AF demagnetization were also performed on sister samples. Figure 4.2b shows a comparison of ARM acquisition and demagnetization of the pure MTB sample, the MTB-rich and MTB-poor sediment samples. The remanent coercivities are 51, 46, and 40 mT, respectively. In that case, the coercivity of the MTB-rich sample and its curve lie closer to that of the MTB-sample. The R-values of the samples are close to 0.5. Moreover, we obtained a positive difference of the MDFs of ARM and IRM, i.e. ($MDF_a - MDF_i$), for both MTB-rich and MTB-poor samples, indicating very fine-grained SD magnetite in the sediments [according to Lowrie and Fuller (1971) and Johnson et al. (1975)].

Comparisons of remanence demagnetization spectra of the ARM and the IRM between the pure MTB sample and the two type sediments of Lake Chiemsee, MTB-rich and MTB-poor, by AF and static fields are presented in Figure 4.3. The spectra of the MTB-rich samples highly resemble that of the pure MTB sample, confirming the optical analysis that biogenic SD magnetite is the main magnetic component in the lake Chiemsee surface sediments. Moreover, as seen from Figure 4.2 and Figure 4.3, these results indicate that remanent coercivity spectra of ARMs are more suitable for discriminating the biogenic SD fraction. However, it must be kept in mind that the coercivity of remanence may also be affected by magnetic mineral phases like iron-sulphides, and caution should be

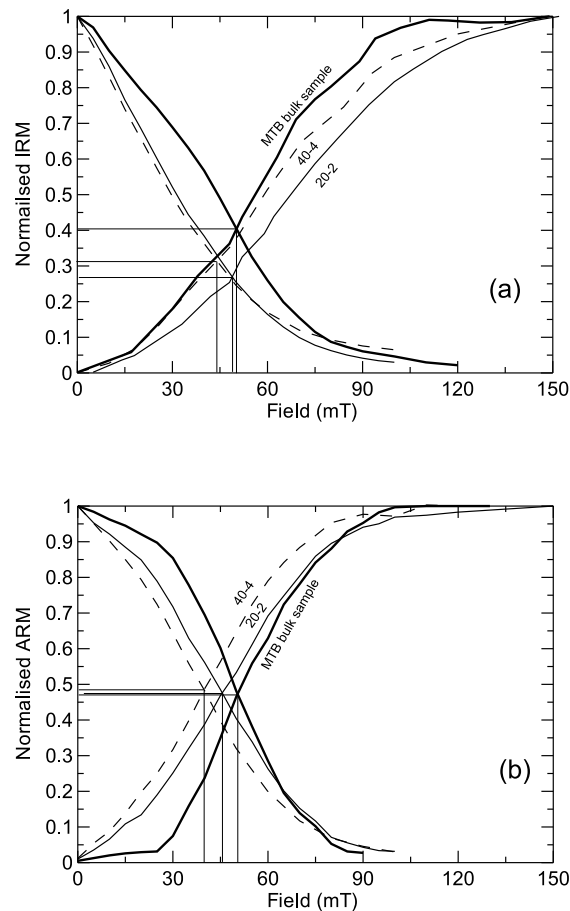


Figure 4.2: Comparison of representative remanent coercivity spectra analysis of bulk sediment samples. Sample MTB-rich (thin solid line), sample MTB-poor (dashed line) and pure MTB sample (thick solid line). (a) IRM acquisition and AF demagnetization. (b) ARM acquisition and AF demagnetization. Horizontal lines show the R-values and the vertical lines show the median remanent coercivities.

taken when using the coercivity as domain-state indicator. A mixture of magnetically hard components such as greigite, hematite and goethite with magnetically soft magnetite particles can compromise the coercivity of remanence to some extent.

4.2.2 Low temperature SIRM demagnetization: *The delta-delta test*

The loss of SIRM during warming in zero-field after samples were cooled both in zero-field (ZFC) and in a strong field of 5 T (FC) is shown in Figure 4.4. Two fresh bulk aquarium

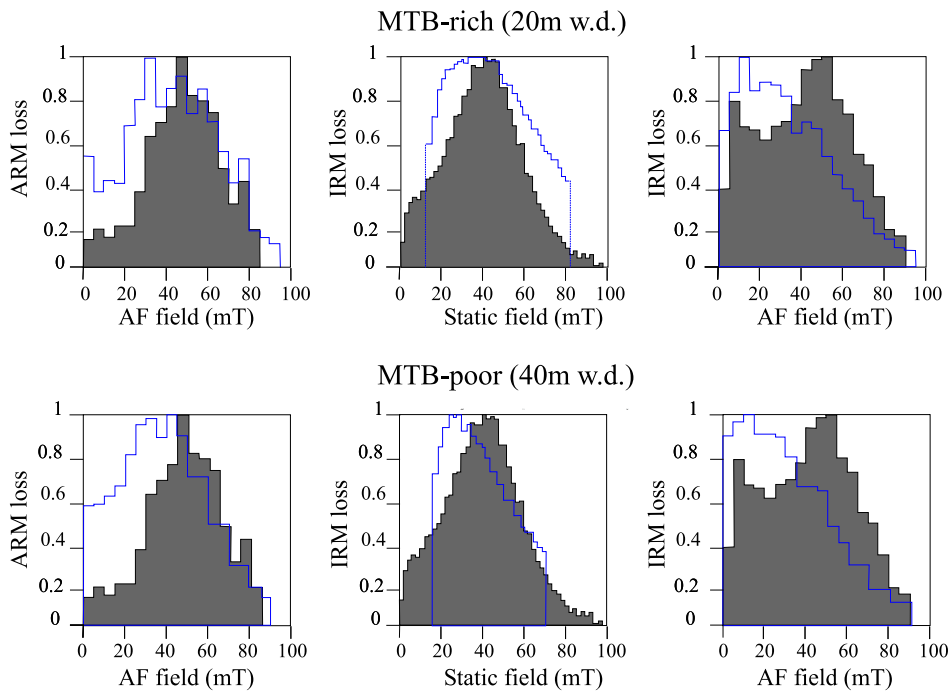


Figure 4.3: Comparisons between the remanence coercivity spectra analysis of a representative MTB-rich sample (upper row) and a MTB-poor sample (lower row) with a pure MTB sample (filled). The loss of remanence was normalized to the maximum value of the corresponding spectrum.

sediment samples containing MTB were selected for the measurements. One sample was freeze-dried and the other was air-dried before the measurements. The remanence after exposure to 5 T at 5 K was measured at intervals of 2-5 K during warming in zero field from 5 to 300 K. The actual field of the sample during warming up was less than 0.2 mT.

Both ZFC and FC warming curves show a distinct drop of remanence below 40 K (not shown in figure 4.4), which may relate to some contribution from siderite (Pan et al., 2002; Frederichs et al., 2003) and/or superparamagnetic components in the samples. A distinct remanence drop around 100-115 K [Figure 4.3A,B] indicates the Verwey transition of magnetite. Interestingly, the two samples have a different Verwey transition temperature (T_v)¹. Compared to T_v of the freeze-dried sample [Figure 4.4A], T_v of the air-dried sample is shifted to lower temperatures [Figure 4.4B], suggesting some extent of oxidation. Above 130 K, the remanence decreases gradually with temperature.

The δ -ratios ($\delta FC / \delta ZFC$) obtained for the freeze-dried and air-dried samples are 1.47 and 1.25, respectively. Both values are greater than 1.2, which according to Moskowitz

¹Here defined as the temperature at which the derivative $\delta J / \delta T$ is at maximum

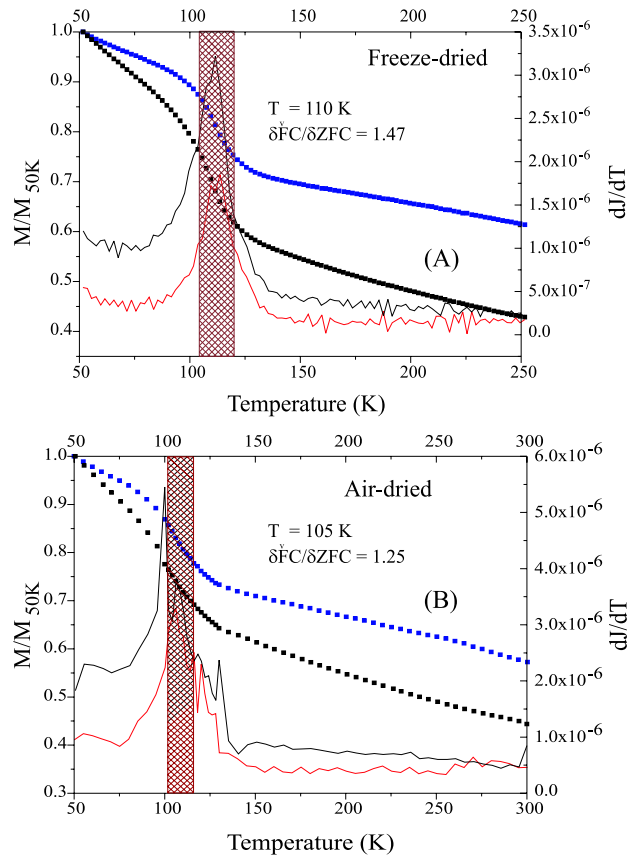


Figure 4.4: Low-temperature SIRM demagnetization curves after samples were cooled in FC (solid circles) and in ZFC (open circles) of freeze-dried (A) and air-dried (B) bulk sediments containing MTB. Solid (dashed) lines refer to the first derivative, $\delta J/\delta T$, of warming curve after FC (ZFC) cooling, respectively. T_v is the temperature at the Verwey transition, here defined as the temperature at which $\delta J/\delta T$ is maximum (grey shading)

et al. (1993) is the upper value for the purely inorganic end member, but lower than the minimum value of 2 for the end member representing solely SD magnetite arranged in chains. These δ -ratios are also slightly lower than the threshold (1.5) for a positive chain response in mixtures of chains and inorganic magnetite [see case 3 in Moskowitz et al. (1993)].

Limitations of the rock magnetic criteria for the identification of biogenic magnetite in bulk samples

Moskowitz et al. (1993) introduced the δ -ratio as a diagnostic magnetic parameter for

identification of magnetosome chains. As shown in the previous chapter, samples consisting purely of MTB with intact chains of magnetite magnetosomes have δ -ratios, $\delta_{FC}/\delta_{ZFC} > 2$. The δ -ratios obtained here for the sediment samples, with abundant MTB and fossil magnetosomes, however are less than 1.5 [Figure 4.3A,B]. This might be caused by a number of reasons:

1.- A disruption of magnetosome chains, as seen by the TEM observations [Figure 4.1] may reduce the ratio δ_{FC}/δ_{ZFC} . So far it is unclear to which extent the linear magnetosome chains are preserved intact in lake or marine sediments. Most likely only a fraction of them will be preserved.

2.- The low-temperature oxidation of bacterial magnetite could also lower the δ -ratio because the Verwey transition is highly sensitive to the degree of oxidation (Aragon et al., 1985). For fully oxidized magnetite, the Verwey transitions will be suppressed for both ZFC and FC curves, and one can expect the δ -ratio to approach 1. This may be the case for three carbonate samples that contained magnetofossils (Weiss et al., 2004a) with δ -ratios of only 0.9-1.2. It has been shown by Petersen et al. (1986) that the fossil magnetosomes in deep-sea sediments from the South Atlantic (Oligocene) are almost pure maghemite, perfectly retaining their original shape. However, for a slight degree of oxidation, Carter-Stiglitz et al. (2004) proposed that the δ -ratio could be enhanced, because the Verwey transition of the ZFC curve is more affected by oxidation than that of the corresponding FC curve. This contradicts however the results of the air-dried sediment samples studied here, which suffered low-temperature oxidation with a corresponding shift of the Verwey transition to lower temperatures [Figure 4.3A,B].

Also, the mixture of detrital magnetite particles [Figure 4.1E,F] could significantly reduce the δ -ratio. For example, previous studies on inorganic magnetite of different grain sizes showed that their delta values are between 1.0 and 1.2 (Moskowitz et al., 1993). Generally, the mixture of magnetosome chains with inorganic magnetite, maghemite, hematite and greigite leads to a decrease of the δ -ratio. An unambiguous identification of magnetosomes (δ -ratio > 1.5) requires that the chain fraction exceed 40 – 50% of the MD/PSD magnetic mineral fraction and 75% of the SD fraction in a sample (Moskowitz et al., 1993). This means that the chain fraction in both MTB-containing samples is not exceeding 60% of the total magnetic mineral content and that the samples are a mixture of magnetosome chains and other detrital magnetite fraction.

In summary, the investigations presented here confirm that the measurement of the δ -ratio of a sample is a useful tool to help discriminating bacterial SD magnetite particles

and other non-biogenic magnetic contributions. However the mixture of detrital PSD/MD magnetite together with the disruption of magnetosome chains in the bulk samples and the possible effects of low-temperature oxidation probably causes the decrease of the δ -ratio. This may be the common case in most environments where bacterial magnetite are preserved. These results suggest that ambiguities remain when only using the δ -ratio criteria for the detection of bacterial magnetite in bulk sediments.

Chapter 5

The magnetic sense of animals

”All our knowledge has its origins in our perceptions.”

Leonardo da Vinci. (1452-1519)

5.1 Introduction

The magnetic sense of animals has generally been related to orientation and navigation purposes, therefore this chapter starts with an introduction of the magnetic field parameters most likely to be used by organisms to gather directional and positional information. Second the two most common orientation mechanisms observed in animals, based on magnetic field parameters, are described: The inclination compass for directional information and the navigational map for positional information. With few exceptions, the biological mechanism underlying magnetic field perception in animals is still unknown. As will be seen, it has been suggested that inclusions of biogenic magnetite particles connected to nerve structures can provide a suitable transducer mechanism of the geomagnetic field.

5.2 The geomagnetic field as a source of directional and positional information

In 1961 Kramer suggested that animals transported to an unfamiliar site need both a map sense to determine the direction of the displacement from home, and a compass to find that direction. The *Map-and-Compass* model involves a two-step process for orientation: in the first step, the animal establishes its position relative to the loft with the help of the map, in the second step, a compass system is used to locate the direction that will lead it home. Over the past 60 years, it has been shown that several groups of animals have developed biological mechanism to extract map and compass information from the geomagnetic field (Wiltschko and Wiltschko, 1995). If animals can sense the geomagnetic field and extract from it directional and positional information, then the question arises: What parameters of the geomagnetic field can be used by the animal?

The geomagnetic field can be physically described at a given point on the Earth's surface as a vector (\mathbf{F}) resolved into three components in the X (north), Y (east) and Z (vertical) axes. The declination (D) is the angle between the horizontal component of the field (H_h) and the Geographic north (X axis), and is taken positive when H points to the east of north. The Inclination (I) is the angle between H and \mathbf{F} and is taken positive when \mathbf{F} is directed below the horizontal [Figure 5.1A]. At the geomagnetic equator, the magnetic field lines run parallel to the Earth's surface and $I = 0^\circ$, while at the north and south magnetic poles the geomagnetic field lines intersect the Earth's surface at 90° . The field is mainly derived from sources in the core and in the crust, with the dipole component in the core representing up to 90% of the observed field. The field derived from the crust is associated to magnetic anomalies, which arise from the strong magnetization of localized rocks and mineral bodies compared to the magnetization of the surrounding crustal rocks [Figure 5.1C].

The geomagnetic field is relatively stable over biological time scales and is axial, with the magnetic field lines roughly north-south directed and symmetric in both hemispheres, hence providing a reliable, static reference system for orientation and navigation. Alternatively, magnetic anomalies within the Earth's crust can also be recognized and used as reference features.

Taking advantage of these properties of the geomagnetic field, some groups of animals have developed a biological magnetic compass, similar to the magnetic compass used by

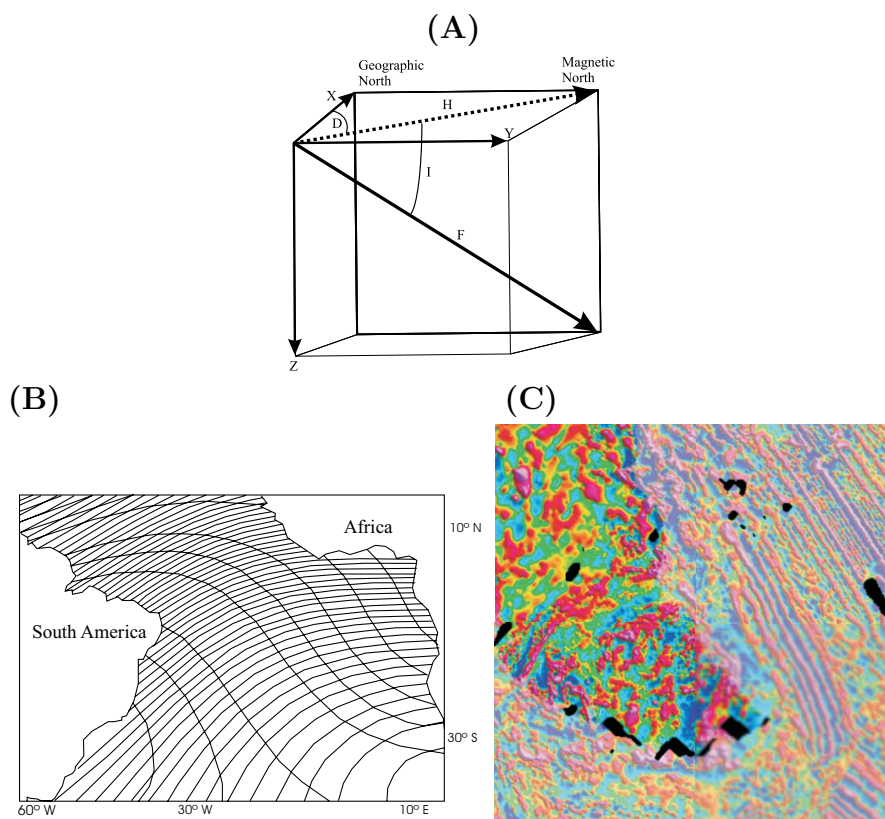


Figure 5.1: A) The geomagnetic field vector. B) variations of the intensity and inclination of the Earth's main field in the South Atlantic. The isodynamics are separated by 1000 nT and are aligned roughly NW-SE. The isoclines are separated by 2° and are aligned roughly NE-SW. These parameters form (nearly)orthogonal grids that could be potentially used by animals for position determination. C) total magnetic field in the area of Greenland. The regular north-south patterns observed in the ocean crust contrast with the chaotic features in land. The anomalies range from -300 nT (blue) to 400 nT (pink). B) from Lohmann et al. (1999); C) from U.S. Dep. of Interior and U.S. Geological Survey.

humans to locate the north magnetic pole. The magnetic compass has been described as an axial compass (or a so-called *Inclination compass*) for migratory birds and homing pigeons (Wiltschko and Wiltschko, 1972; Walcott and Green, 1974), and is based on the axial course of the geomagnetic field lines on the Earth's surface. The magnetic compass is used as a reference system and as a mechanism to maintain steady courses during homing and migrations. The functioning principles of the *Inclination-Compass* will be discussed in section 5.3.

As mentioned before, apart from a compass mechanism for orientation animals need to develop a system for position-determination. In this respect, the latitudinal variations of the geomagnetic field inclination (I) and intensity (H), can potentially provide stable

information about location [Figure 5.1B]. As mentioned before, the inclination angle of the geomagnetic field lines ranges from -90° at the South pole to $+90^\circ$ at the North pole, being 0° at the equator. On the other hand, the intensity of the geomagnetic field at the Earth's surface ranges from about $24\mu\text{T}$ to $68\mu\text{T}$.

Therefore animals able to discriminate the minute but steady changes of the inclination angle and the intensity of the geomagnetic field, can potentially establish their latitudinal position. To date, several models for position determination based on magnetic field parameters have been proposed. Lohmann et al. (1999) proposed that sea turtles use a combination of intensity and inclination, as independent coordinates for map information. Contours of equal magnetic intensity and inclination form a grid that can potentially be used as a bi-coordinate position-finding system over areas of the Atlantic ocean, where sea turtles spend most of their life cycle [Figure 5.1B]. This model cannot, however, be generalized since isolines of magnetic inclination and intensity intersect each other at high angles only over local regions of the Earth's surface. In regions where the isolines are near-parallel to each other, or where the magnetic landscape is dominated by crustal magnetic anomalies [Figure 5.1C], the bi-coordinate model is not viable for position determination (Walker et al., 2002).

A second model of position determination is based on systematic variations of the intensity and in the direction of intensity gradient of the Earth's main field. The idea that intensity may be a component of the navigational map system of animals, comes from the observation that homing pigeons are disoriented when released at magnetic anomalies (Walcott, 1978). On the other hand, region-wide distributions of clockwise and counter-clockwise orientation errors made by homing pigeons are symmetrical about the line of intensity slope through the loft (Gould, 1982) supporting the involvement of this field parameter in position determination (Walker, 1998; Walker et al., 2002).

Yet a third model takes into account the regular patterns of magnetic anomalies originating from rocks in the ocean crust, and produced during sea-floor spreading (Kirschvink et al., 1986). Although these anomalies are not present in the continental crust, they could potentially be used by marine animals to guide long-distance migrations [Figure 5.1C].

Despite the fact that these three models take into consideration different magnetic field parameters, they are not mutually exclusive. So far there exists no evidence that all animals capable of magnetic field perception use the same sources of information from the geomagnetic field for orientation and navigation. Furthermore, different groups of animals may have developed different magnetoreceptor systems, each of them designed to obtain

information from different field parameters according to their necessities and the local conditions of the geomagnetic field.

5.3 The *inclination* compass and map sense of animals

The magnetic compass of several bird species has been characterized as a so-called *inclination compass*, since it is based on the axial course of the field lines and their inclination in space. According to the inclination compass model, the polarity of the vector is irrelevant: reversing the horizontal component has the same effect as reversing the vertical component; and a reversal of both components, implying an inversion in the polarity of the field while maintaining the direction of the field lines, does not alter the behavior of the birds (Wiltschko and Wiltschko, 1972) [Figure 5.2].

The map-sense is a theoretical requirement for orientation and navigation as proposed by Kramer (1961) and can better be regarded as a spatial distribution of environmental factors that the animals are able to memorize and use later for navigation. The spatial pattern of environmental factors represents a directionally oriented mental image that the animals can extrapolate to unfamiliar sites and thus, requires learning processes that take place during the youngsters development (Wiltschko and Wiltschko, 1995); the map must be understood as a multifactorial system that gathers information from several environmental cues like odors, landmarks, infrasound or magnetic field parameters; information that is used after displacement to find positions relative to a goal or to a normal breeding area.

5.4 Hypotheses of mechanisms of magnetic field perception

Behavioral and electrophysiological experiments in migrating and homing birds, suggest that the inclination compass of birds may be related to the optic system (Wiltschko and Wiltschko, 1981). Following this ideas, Ritz et al. (2000) proposed a model for a photoreceptor-based magnetoreceptor, based on the observed effects of magnetic fields on

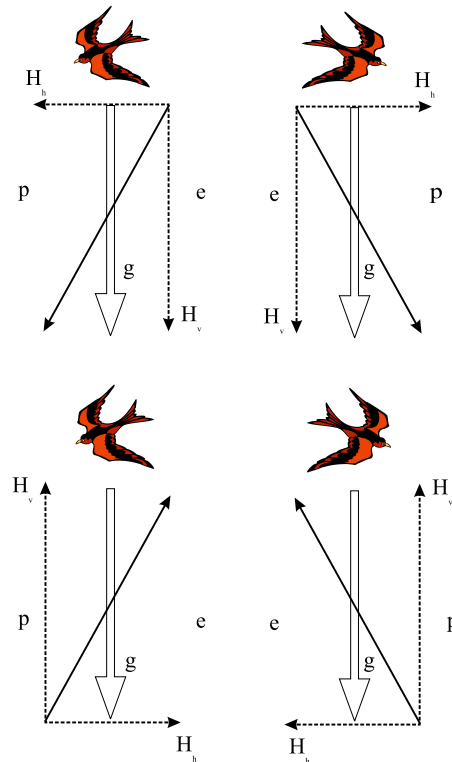


Figure 5.2: Principle of the *Inclination Compass* after Wiltschko and Wiltschko (1972). Here, the polarity of the vector is irrelevant since birds obtain directional information from the axial course of the lines. That way, birds cannot distinguish between northward and southward, but between poleward and equatorward. (g) gravity; (p) poleward; (e) equatorward; (H_v, H_h) vertical/horizontal components of the magnetic field. See text for further details.

radical-pair reactions. Exploiting the principles of magnetic resonance, Ritz et al. (2004), developed a diagnostic tool to identify a radical-pair process underlying magnetic compass orientation. The authors argued that an oscillating magnetic field (RF) that is in resonance with the splitting between radical-pair spin states, can perturb a radical-pair mechanism by directly driving singlet/triplet transitions. In typical biomolecules, many hyperfine splittings occur in the range of 0.110 MHz and a limited number may exist in the range of 1025 MHz. On the other hand, no change in magnetic alignment of magnetite receptors is expected for weak oscillating fields with frequencies larger than 100 kHz. To test this hypothesis, the orientation behavior of European robins was studied in oscillating magnetic fields. While in the control condition, the robins exhibited seasonally appropriate northerly orientation, in the presence of broadband (0.110 MHz, 0.085 mT) and single-frequency (7 MHz, 0.47 mT) oscillating fields, the birds were disoriented (Ritz

et al., 2004).

However, caution should be taken when interpreting these results. While RF fields in the range of 0.110 MHz do not affect SD magnetite particles, these frequencies do have an effect on SP particles, which show an absorption peak at frequencies ranging from 1-60 MHz (Malaescu and Marin, 2000). As a result, the magnetic susceptibility of the particles is reduced. As will be seen in the next chapter, clusters of SP magnetite particles have been identified in homing pigeons and are considered putative magnetoreceptor structures. Hence the effect of RF fields on the magnetic orientation behavior of birds can also be explained, albeit theoretically, assuming a magnetite based-magnetic sense.

The magnetite hypothesis assumes that biogenic magnetite particles are connected to nervous structures, and that the torque response exerted by the geomagnetic field on the magnetic particles is responsible for mechanical stresses on the surrounding cellular environment, which are transformed into nervous signals through the activation of membrane mechanoreceptors. Supporting the magnetite hypothesis is the fact that magnetic measurements on various animal tissues have revealed the presence of magnetite accumulations in the tissue (Gould et al., 1978; Walcott et al., 1979; Ueda et al., 1982, 1986; Edwards et al., 1992; Hanzlik et al., 2000). Magnetically stable SD magnetite particles have also been extracted from the head of the sockeye salmon, *Oncorhynchus nerka* (Mann et al., 1988) and the yellowfin tuna, *Thunnus albacares* (Walker et al., 1984). Accumulations of SP and SD magnetite particles have been reported in the abdomen of bees, *Apis mellifera*, apparently associated with nervous structures (Gould et al., 1978; Schiff, 1991). SP magnetite has also been extracted from the abdomen and thorax of two species of Australian termites, *Nasutitermes exitiosus* and *Amitermes meridionalis* (Maher, 1998), and from *Pachycondyla marginata*, a migratory ant (Avalos et al., 1999). The presence of SP magnetite in social insects has also been inferred from electron paramagnetic resonance (Esquivel et al., 1999; Wajnberg et al., 2000) and remanence measurements (Wajnberg et al., 2001). Yet, only in magnetic bacteria have accumulations of biogenic magnetite been clearly linked to orientation processes (see chapter 2). It is necessary to emphasize that the mere presence of magnetite in animal tissue does not demonstrate its involvement in magnetoreception. Accumulations of magnetite may well be contamination or waste, as for example in cancer tissue of mice (Kirschvink et al., 1982). Therefore, it is important to establish a clear connection between the magnetic particles and the nervous system when discussing magnetite-based magnetoreception.

The hypothesis that magnetite particles may underlie the animal magnetic sense, will

be the subject of this work in the following chapters. Since both SD and SP particles have been identified in organisms and proposed as components of putative magnetoreceptor structures, in the next chapter, the suitability of these particles for magnetic field perception will be considered.

Chapter 6

Biogenic magnetite and magnetic field perception

"The fact that an opinion has been widely held is no evidence whatever that it is not utterly absurd."

Bertrand Russell. (1872-1970)

6.1 Introduction

Since Lowenstam (1962) reported biogenic magnetite in the radular teeth of chitons, the idea that biologically synthesized magnetite particles may form the core of the animal magnetic sense became the working hypothesis of a number of behavioral, neurological and physiological studies. When discussing possible magnetic-field perception mechanisms based on magnetite particles, two approaches exist: magnetoreceptors based on SD particles and magnetoreceptors based on SP particles.

Traditionally, the SD models have been favored, since isolated SP particles are theoretically unsuitable for magnetic field perception. SD models fulfil the requirements for magnetic field perception, especially in terms of the required sensitivity. However, to date, no magnetoreceptor structure based on these particles has been clearly characterized in animal tissue, although a putative structure has been identified in fish (Walker et al., 1997; Diebel et al., 2000). On the other hand, a candidate magnetoreceptor structure based on clusters of SP particles has been identified and characterized in the upper beak skin of

homing pigeons. Contrary to single SP particles, clusters of SP particles possess magnetic properties which make them theoretically suitable for magnetic field perception.

The SD and SP models are, however, not mutually exclusive. There exists no reason to conclude that only one magnetoreceptor mechanism, whether based on SD or SP particles, exists among animals. Sensory mechanisms are developed according to environmental and genetic constraints, as well as to the specific purposes of the sensory mechanisms themselves. Therefore, it is not implausible that different groups of animals have developed different magnetite-based magnetoreceptor mechanisms, according to their necessities.

6.2 SD and SP particles as components of the animal magnetic sense

6.2.1 The SD model

The discovery of magnetotactic bacteria and magnetotaxis by Blakemore (1975), offered a possible model for the functioning of the animal magnetic sense. This model assumes the presence, within the animal tissue, of chains of SD particles in close connection to nerve structures. The magnetic torque that the geomagnetic field exerts on these chains, is transferred to the nerve cells and transformed into nervous impulses by means of mechanosensory structures in the cell's membrane [Figure 6.1] (Kirschvink and Gould, 1981; Walker et al., 2002). In the past 30 years, it has been shown that such a magnetoreceptor mechanism would fulfil the requirements for magnetosensory perception (Yorke, 1979), particularly its required sensitivity, albeit such a magnetoreceptor structure has not yet been unambiguously identified in animals.

Magnetically stable SD magnetite particles have been extracted from tissue of several fish species (Mann et al., 1988; Walker et al., 1984). These particles closely resemble the ones typically found in magnetotactic bacteria. However, these studies did not provide a characterization of the organic tissue in which the magnetic particles occurred, neither the exact location and arrangement of the particles within the tissue. Furthermore, the sole isolation of magnetite particles from animal tissue cannot be taken as evidence for their involvement in magnetoreception, since magnetite can also be formed as a by-product of metabolism. Only a direct characterization of the magnetite inclusions in the tissue, showing the ultrastructure of the candidate receptor and the nature of the cellular

surroundings, can be taken as indication for the presence of a magnetite-based magnetoreceptor. In that respect, Walker et al. (1997) and Diebel et al. (2000) imaged a candidate magnetoreceptor structure in the basal lamina of the olfactory epithelium in the rainbow trout, *Oncorhynchus mykiss*. The candidate magnetoreceptor was interpreted as a chain of SD particles of the same size and shape as bacterial magnetosomes. However, a detailed characterization of the fine-structure of the chain and its connection to the surrounding tissue was not possible. Furthermore, the authors could only identify one cell containing the candidate magnetoreceptor structure. This lack of information does not allow for a modelling of the functioning of the putative magnetoreceptor mechanism, hence the involvement of these particles in magnetic field perception in the rainbow trout remains as a working hypothesis.

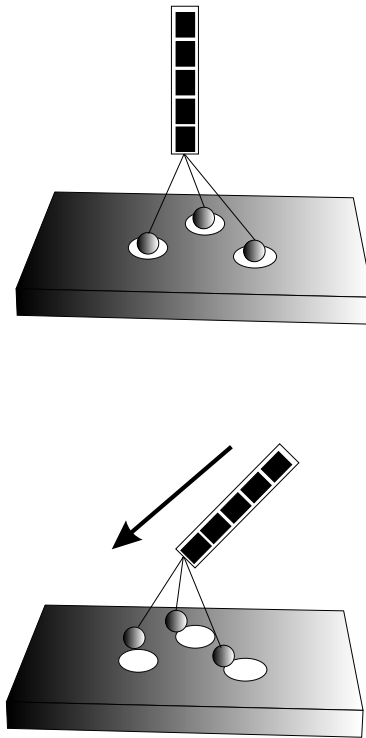


Figure 6.1: Possible magnetoreceptor elements based on a chain of SD particles. *Top*: The chain is linked by microtubule-like strands to mechanically gated ion channels in the membrane of the receptor cell. *Bottom*: The ion channels are activated due to the movement of the chain in response to the external magnetic field (arrow). From Walker et al. (2002)

6.2.2 The SP model

SP magnetite particles have been traditionally considered unsuitable for magnetic field perception. This is due to the fact that a small magnetite particle in a fluid medium moves randomly due to thermal fluctuations, derived from the movement of molecules around the particle. This "Brownian" motion causes the moment of the particle (μ) to deviate from the direction of the external magnetic field (B), with a directional probability given by the Boltzmann distribution ($\exp[\gamma \cdot \cos \phi]$), where $\gamma = \frac{(\mu \cdot B)}{kT}$ (ϕ is the angle between the external field and the particle's magnetic moment, k is the Boltzmann constant and T is the absolute temperature). At Earth's strength magnetic fields ($B=50\mu\text{T}$) SD particles as found in MTB have $\gamma > 1$, hence the magnetic energy (μB) overcomes the thermal energy (kT) allowing the particle to align with the external magnetic field. On the other hand, isolated SP particles have $\gamma < 0.1$, here Brownian motion dominates and the particles cannot track the directional changes of the external field. Therefore, contrary to stable SD particles, it is not possible to induce a torque response on a single SP particle.

However, clusters of SP particles show characteristic magnetic properties that can overcome thermal fluctuations and might be used for magnetic field perception (Shcherbakov and Winklhofer, 1999; Winklhofer, 1999). A cluster of SP particles acquires an induced magnetization in a magnetic field. Like a paramagnetic system, the SP collective loses its magnetization once the field is switched off. The pre-fix "super" refers to the fact that such a collective has a surprisingly large susceptibility¹, that is, even a magnetic field as weak as the geomagnetic field can induce a relatively large magnetization. Shcherbakov and Winklhofer (1999) were the first to propose a magnetoreceptor mechanism based on clusters of SP magnetite. Their *Osmotic magnetometer* is based on the fact that under the influence of a magnetic field, a spherical ferrovesicle (i.e. a ferrofluid droplet enclosed by a membrane) of SP magnetite particles will deform into a prolate ellipsoid with the long axis parallel to the magnetic field direction (Bacri et al., 1996) (see below, chapter 7). The reason for the deformation is the additional pressure the ferrovesicle produces in the direction of its magnetization to minimize the total energy by reducing the demagnetizing field (Shcherbakov and Winklhofer, 1999). This deformation is proportional to the intensity of the applied magnetic field and is axial with respect to the geomagnetic field direction [Figure 6.2].

¹The initial susceptibility $\chi = \frac{dM}{dH_0}$ for $0.03\mu\text{m}$ cubes of magnetite at room temperature is about 650, two order of magnitude higher than typical SD and MD susceptibilities (Dunlop and Özdemir, 1997)

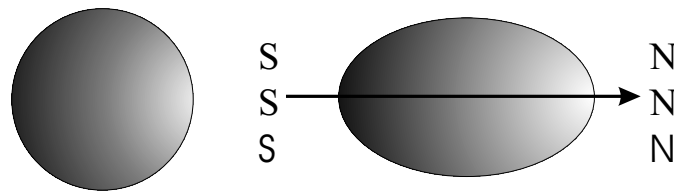


Figure 6.2: Sketched deformation of a ferrovesicle. In zero magnetic field the droplets have no net magnetization, and its initial shape is spherical (*left*). Under the influence of an external magnetic field (arrow), the ferrovesicle is magnetized parallel to the field and produces additional pressure in its direction, thereby deforming the sphere into an ellipsoid of revolution. From Shcherbakov and Winklhofer (1999)

6.3 A candidate magnetoreceptor structure in homing pigeons

Interestingly, clusters of SP magnetite particles have been identified in homing pigeons within nervous terminals of the ophthalmic nerve, and proposed as a putative magnetoreceptor structure (Hanzlik et al., 2000; Winklhofer et al., 2001; Fleissner et al., 2003).

Histological studies in skin sections from the upper beak of homing pigeons (*Columba livia*), bred and kept in the Zoological Institute of the University of Frankfurt, revealed the presence of up to six isolated sites of Fe^{3+} enrichments, which are bilaterally localized near the lateral rim of the beak: one pair next to the tip of the beak, another one next to the glandular base of the beak and a third one between the other two. These inclusions were found directly beneath the subcutis, the solid layer of the skin, between fat cells [Figure 6.3]. The Fe^{3+} enrichments were identified by means of the Prussian Blue (PB) reaction on fixed tissue. In the presence of Fe^{3+} and HCl, potassium hexacyanoferrate turns into dark blue ferric ferrocyanide (Hanzlik et al., 2000; Winklhofer et al., 2001; Fleissner et al., 2003)[Figure 6.4A].

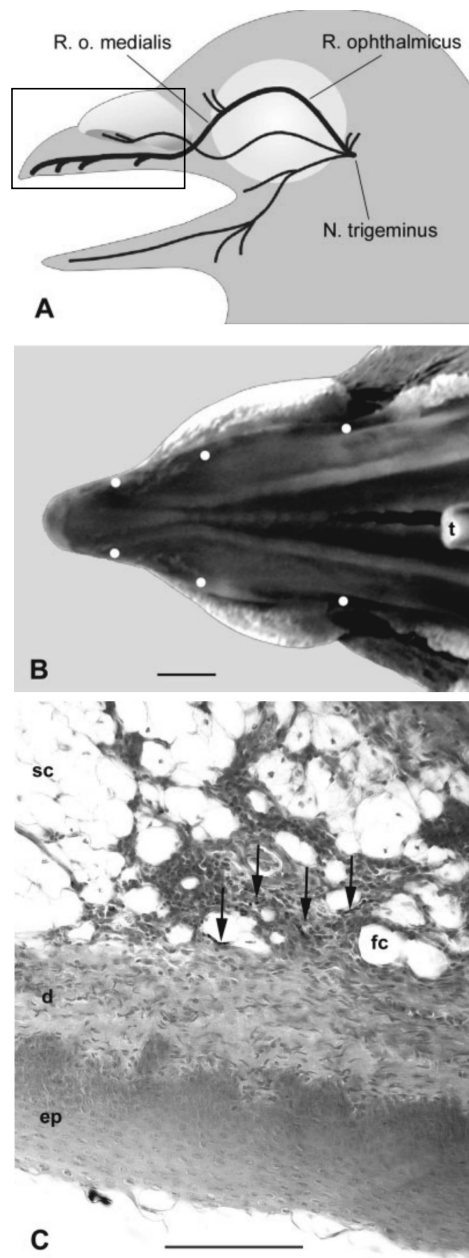


Figure 6.3: Localization of putative magnetoreceptors in the beak of homing pigeons. (A) Scheme of the pigeon skull with the peripheral course of the ophthalmic branch of the trigeminal nerve, which extends to form the entire somatosensory innervation of the tip of the upper beak. The rectangle shows the area where the iron rich inclusions were detected. (B) Macroscopic view of the inside of the upper beak. White dots indicate the sites of the candidate magnetoreceptor nerve endings (t, tongue). (C) Sagittal section through the inner skin of the upper beak. The PB-reactive terminals (arrows) are above the solid layers, epidermis (ep), and dermis (d), within the stratum laxum of the subcutis (sc); (fc = fat cells). Scale bars=2 mm in B, 100 μ m in C. From Fleissner et al. (2003).

At the highest magnification the Fe^{+3} enrichments were revealed as spherical inclusions 1-2 μm in diameter arranged in groups of 15-20 clusters in a chain-like configuration [Figure 6.4B] (Hanzlik et al., 2000; Fleissner et al., 2003). In the study by Fleissner et al. (2003), neurofilament immunohistology was used in order to elucidate whether the clusters occurred inside nervous cells of the ophthalmic nerve or not. The test was performed by a well-defined monoclonal antibody (MAB 1621, Chemicon, Temecula, CA), an antibody specific for avian tissue (Harris et al., 1993). Successfully immunostained sections were documented and then counterstained by PB as described above. This technique revealed the nervous origin of the cells containing the clusters [Figure 6.5].

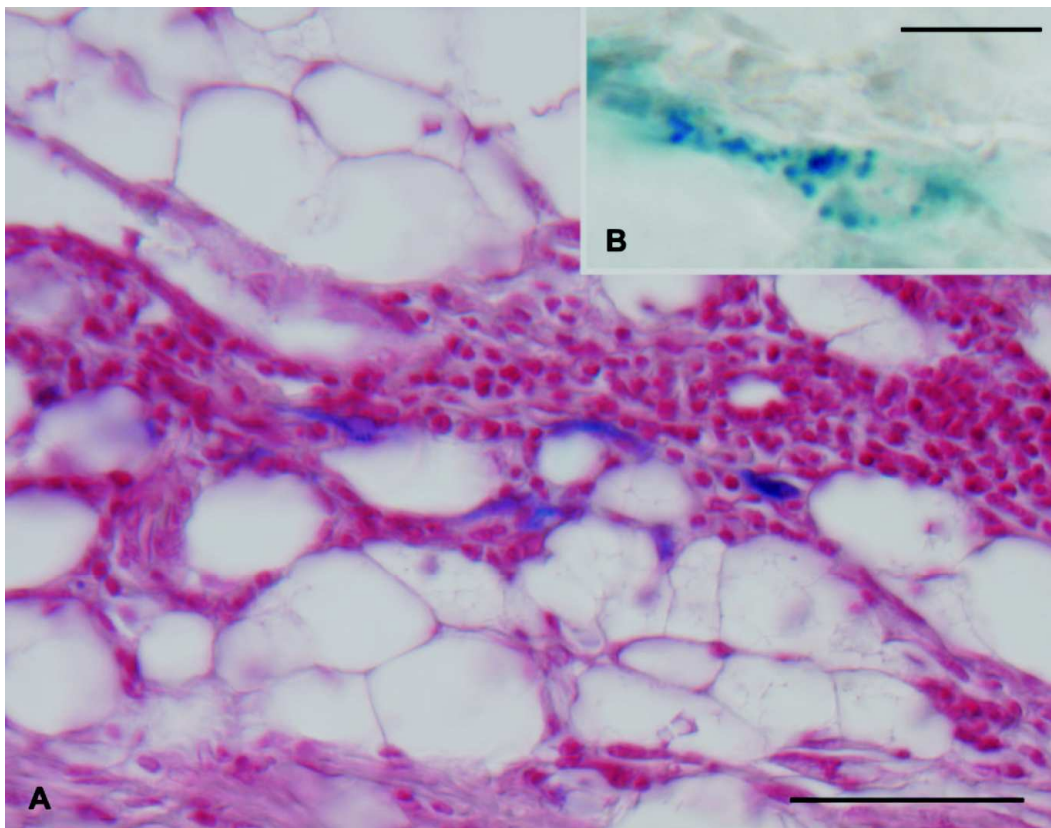


Figure 6.4: Prussian Blue (PB) reactive nerve endings in the skin of the upper beak of homing pigeons. PB-reactive products appear as small spherules and pale-blue background staining. (A) PB-stained section counterstained with Kernechtrot: an area of about 250 μm in diameter shows multiple marked nerve endings. (B) PB-stained section. The marked nerve ending contains a chain of dark-blue spherules (stack reconstruction of nine focal planes within a 10 μm -thick section). Scale bars=50 μm in (A), 10 μm in (B). From Fleissner et al. (2003).

The region of the upper beak of birds is innervated by the ophthalmic branch of the trigeminal nerve, which according to Semm and Beason (1990) is sensitive to Earth-strength magnetic fields. This suggests that the clusters are promising candidates as primary transducers of a magnetoreceptor system of homing pigeons. The Selected Area Electron Diffraction (SAED) pattern of the clusters showed a powder diffraction diagram characteristic of fine-grained crystalline material. The d-spacings and their corresponding intensities were diagnostic of magnetite and the grain-size histogram showed a range of particle size between 2-5 nm (Hanzlik et al., 2000). At this grain size, superparamagnetic behavior can be expected for the material at room temperature.

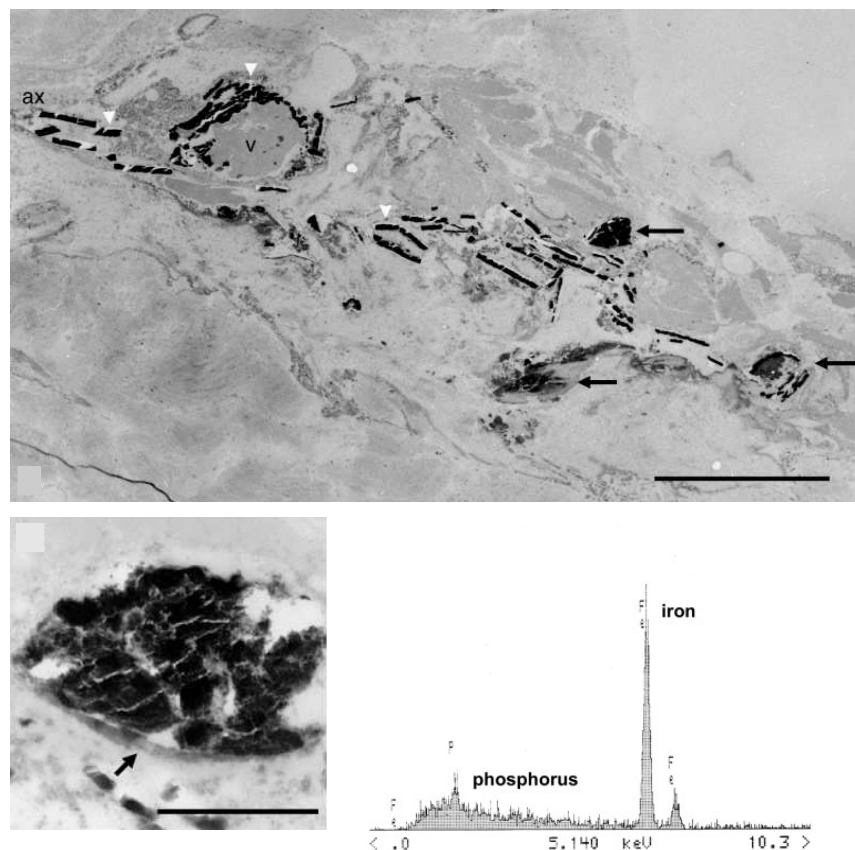


Figure 6.5: Fine-structural appearance of a terminal. (*Top*) The nerve endings contain two different varieties of iron compounds: several crystallographically identified SP clusters (black arrows) and iron platelets (white arrowheads) (sample from a series of 38 consecutive ultrathin sections). Scale bar=10 μm . (*Bottom left*) One of the identified SP clusters. Scale bar=1 μm . (*Bottom right*) X-ray analysis (EDX) of the SP clusters. Inside the SP cluster sites, mainly iron is evident. From Fleissner et al. (2003).

The spatial arrangement of the SP clusters within the tissue may be crucial for the

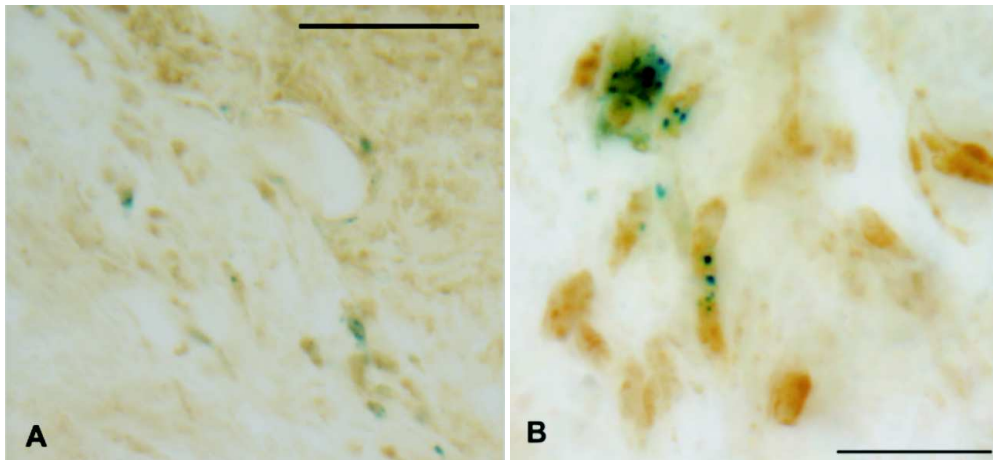


Figure 6.6: (A) Horizontal section of the upper beak skin doubly stained by an antibody with specificity against avian neurofilament (brown staining) and Prussian Blue (blue staining) to show high concentrations of iron-oxide. Dark-blue spherules can be found only inside neurofilament-immunoreactive terminals, but not all nerve terminals contain such PB-reaction products. (B) Stack reconstruction of 10 confocal planes within the same section as shown in (A). Scale bars= $50 \mu\text{m}$ in (A), $15 \mu\text{m}$ in (B). From Fleissner et al. (2003).

functioning of the candidate magnetoreceptor. Therefore further light-microscopy analysis of the biological samples were carried out in order to characterize the spatial distribution of the SP clusters within a nerve ending. The analysis of the tissue reveals an average cluster diameter of $0.8 \pm 0.2 \mu\text{m}$ [Figure 6.7*Top*]. The average distance between the center of two adjacent clusters was determined as $1.6 \pm 0.5 \mu\text{m}$ (typically two times the mean diameter of the clusters) [Figure 6.7*Bottom*]. Within a cell, the clusters are arranged in the form of chain-like aggregates (Davila et al., 2003).

It is important to note that the response of the SP clusters to magnetic fields depends on their magnetic susceptibility, which in turn is dependent on the size of the individual magnetite particles and their volume concentration in the clusters (Shcherbakov and Winklhofer, 1999). The susceptibility of SP particles increases with particle size until the SP/SD threshold ($\sim 50 \text{ nm}$), where the magnetization of the particles becomes blocked within the crystal lattice and the magnetic susceptibility of the particle drops by as much as two orders of magnitude (Dunlop and Özdemir, 1997). Magnetic interactions also decrease the magnetic susceptibility of SP particles.

The particle size distribution in the SP clusters identified by Hanzlik et al. (2000) in the upper beak skin of homing pigeons is $\sim 2 - 5 \text{ nm}$. From a theoretical point of view,

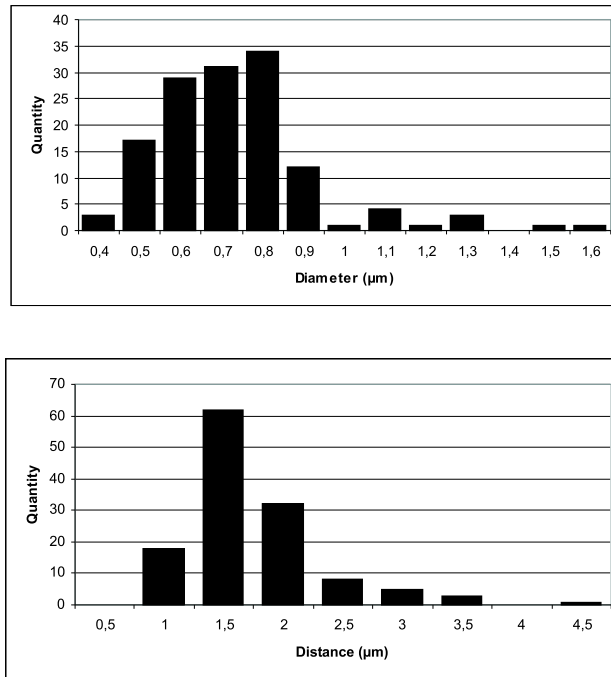


Figure 6.7: Size distribution of the SP clusters found in the upper-beak skin of homing pigeons (*Top*) and distance between adjacent clusters (*Bottom*). From Davila et al. (2003).

a particle size of 10 nm is optimal in terms of the magnetic susceptibility of the cluster. So far, it is unknown whether the measured particle size in the SP clusters is an artifact from the sample preparation procedure (i.e. partial dissolution of the particles due to the reactants employed for histology) or a real observation, in which case one would have to assume a close packing of the particles inside the clusters to increase their volume concentration and their magnetic susceptibility.

In addition, the clusters appear to be surrounded by a second type of amorphous iron-oxide inclusions, termed *platelets* by Fleissner et al. (2003). These inclusions are typically 0.2-0.5 μm in size and are rectangular in shape. The amount of phosphorous in the platelets is significantly larger than that in the clusters [Figure 6.8]. The chemical and physical properties of the platelets are completely different from the clusters and their possible role in magnetoreception remains unknown.

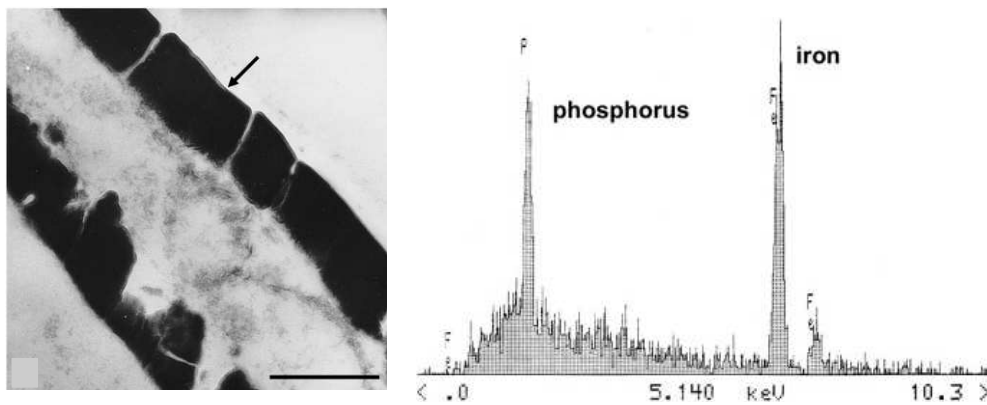


Figure 6.8: (*Left*) Iron platelets with their sheaths (arrow) anchored to the central fibrous core. (*Right*) EDX record of the noncrystalline platelets, where about the same amounts of iron and phosphorus can be detected. From Fleissner et al. (2003).

Chapter 7

Model experiments with ferrofluid spherules

"It doesn't matter how beautiful your theory is, it doesn't matter how smart you are. If it doesn't agree with experiment, it's wrong."

Richard Feynman. (1918-1988)

7.1 Introduction

So far it has not been possible to extract the SP clusters from the upper beak skin of pigeons, nor to study the response of the clusters to magnetic fields directly in the tissue. Therefore, a series of model experiments to simulate the magnetically driven motion of SP clusters in a liquid medium, were conducted with ferrofluid spherules, a technical analogue of SP clusters. By applying a magnetic field of controlled direction and intensity, it was possible to study the magnetic response of individual spherules and of groups of spherules. Experiments were also conducted with magnetic pulses to observe the response of groups of ferrofluid spherules to a strong, short magnetic pulse, a treatment used in the past to specifically effect a proposed magnetite-based magnetoreceptor mechanism (Wiltschko et al., 2002)

7.2 Ferrofluid spherules as technical analogues to the SP clusters

It is not clear up to this day, whether the SP particles found in the upper-beak skin of homing pigeons occur embedded in an elastic matrix or dispersed in a liquid (viscous matrix). Winklhofer et al. (2001) reflected on both scenarios when discussing the possible role of the SP clusters in magnetic field perception. The authors proposed an elastic-matrix scenario which assumes that the SP particles are attached to filaments of the cytoskeleton (CSK). As the CSK is connected to the cell's membrane any mechanical stress arising from the SP clusters would be transferred to membrane mechanoreceptors. On the other hand, the viscous-matrix scenario assumes that the SP particles occur suspended in a fluid (i.e. the cytoplasm) enclosed by a membrane. In that case the SP clusters might be better described as a magnetic colloid (or ferrofluid), that is, a liquid with superparamagnetic properties.

The physical properties of the matrix surrounding the magnetic nanoparticles, either solid-elastic or liquid-viscous, will be relevant in terms of the *amount* of response of the clusters to magnetic fields, however it will not be relevant in terms of the *nature* of this magnetic response. That is, the magnetic field induced deformations and magnetostatic interactions described below will occur in either scenario, although the amount of deformation and of magnetostatic interactions may differ when considering elastic or viscous forces.

In this chapter, the response of SP clusters to magnetic fields will not be estimated quantitatively (this will be the aim of the next chapter), but rather the nature of their magnetic responses will be discussed. Hence, the viscous-elastic scenario proposed by Winklhofer et al. (2001) was assumed, and a set of model experiments with a commercial ferrofluid, which possesses similar physical and chemical properties as the SP clusters, was designed.

The ferrofluid used in the model experiments (ferrofluid EFH1 provided by FerroTec, Unterensingen-Germany) is a colloidal suspension of magnetite nanoparticles in benzine [Figure 7.1]; the average size of the nanoparticles is 10 nm and they are coated with an oil soluble dispersant (surfactant) to prevent particle agglomeration. The composition and physical properties of the ferrofluid are summarized in Table 7.1. The surfactant around the crystals increases the distance between adjacent particles, thus reducing their

| | |
|---|---|
| Composition (by volume) | Magnetite: 3-15% Surfactant: 6-30% Carrier liquid: 55-91% |
| Grain size of the magnetic particles (nm) | 2-12 |
| Saturation magnetization at 25° (mT) | 90 |
| Magnetic susceptibility (SI) | ~ 0.1 |
| Carrier liquid | Benzin |

Table 7.1: Composition and physical properties of the ferrofluid used in the model experiments.

magnetic interaction. To prevent the agglomeration of the particles is of importance, since agglomeration causes the solid phase to separate from the carrier liquid and the ferrofluid loses its property of high magnetic susceptibility. For 10 nm particles, magnetic interactions are important and the use of a surfactant is necessary¹.

When brought into an aqueous environment the suspension forms separate spherical droplets of variable size, ranging from 20 to 100 μm in diameter. If the solution is then treated with ultrasonic, smaller spherules of sizes between 1-20 μm form².

The manipulation and observation of the spherules was conducted in the Bacteriodrome (see figure 3.3). A small amount of commercial ferrofluid was added to a water solution and stirred with ultrasonic for one minute, until spherules of the desired sizes were obtained. A sample containing several hundred spherules was then placed under the light microscope. The response of individual spherules and groups of spherules to magnetic fields ranging from 0.1 to 3 mT, was studied.

7.3 Response of individual ferrofluid spherules to weak magnetic fields

Shcherbakov and Winklhofer (1999) were the first to propose a magnetoreceptor mechanism based on clusters of SP magnetite. Their *Osmotic magnetometer* is based on the

¹Shcherbakov and Winklhofer (1999) estimated that for the magnetic particles forming the clusters found in the upper beak of homing pigeons (2-3 nm) no coating layer is needed, since thermal fluctuations alone will prevent agglomeration

²As will be seen in chapter 8, the characteristic time response of the interaction between adjacent SP clusters (and ferrofluid droplets) to magnetic field changes, does not depend on the size of the clusters/droplets. We can therefore study the magnetic interactions between groups of relatively large ferrofluid spherules and later extrapolate the results to the smaller clusters found in the upper beak skin of homing pigeons

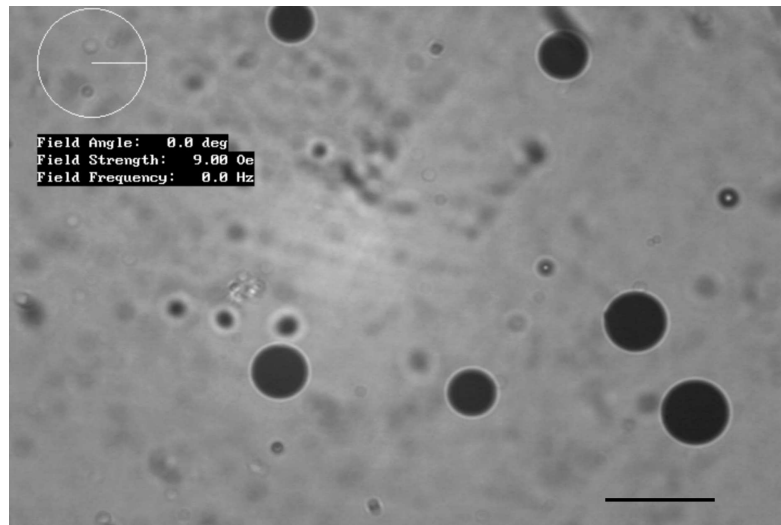


Figure 7.1: Spherules of ferrofluid. Each spherule consists of a carrier liquid (benzin), magnetic nanoparticles (magnetite) and a surfactant (long-chain hydrocarbon). These spherules were used to simulate the functioning of a putative magnetoreceptor mechanism in homing pigeons. Scale bar represents 100 μm

fact that under the influence of a magnetic field, a spherical ferrovesicle (i.e. a ferrofluid spherule enclosed by a membrane) of SP magnetite particles will deform into a prolate ellipsoid with the long axis parallel to the magnetic field direction [Figure 7.2]. This deformation is axial and proportional to the square of the intensity of the applied magnetic field (Bacri et al., 1996; Shcherbakov and Winklhofer, 1999; Winklhofer, 1999).

To confirm the predictions by Shcherbakov and Winklhofer (1999), the deformation of single ferrofluid spherules in a magnetic field was studied. First a glass receptacle was coated with commercial soap and filled with distilled water. The soap reduces the surface tension acting upon the droplets, thus facilitating their deformation. Later, the ferrofluid was added to obtain the spherules as described above. The elongation of the spherules at different magnetic field intensities (from 0 to 3 mT) was obtained by taking a snapshot of the deformed spherule at each field step and later analyzing the image with an imaging software. The deformation was measured as the axial elongation of the spherule, $\frac{a-R_0}{R_0}$ (where a is one half of the long axis of the deformed spherule and R_0 its initial radius), along the field direction [Figure 7.2]. Figure 7.3 shows plots for the deformation of 4 ferrofluid spherules in a magnetic field of increasing intensity.³As can be seen, the

³In order to obtain a linear fit, the axial deformation was plotted against the square of the magnetic field intensity, and both values were normalized to the initial radius of the spherule to facilitate the comparison of the results.

deformation of the spherules increases with increasing the field's intensity, following

$$\frac{a - R_0}{R_0} \propto \frac{\chi^2 H^2 R_0}{\gamma}, \quad (7.1)$$

where χ is the magnetic susceptibility of the ferrofluid, H is the applied magnetic field, R_0 is the initial radius of the spherule and γ is the surface tension (Shcherbakov and Winklhofer, 1999; Winklhofer, 1999). As mentioned before, the response of individual ferrofluid spherules to an external magnetic field is axial and the amount of deformation depends on the intensity of the applied field (all the results are summarized in Table 7.2 at the end of the chapter).

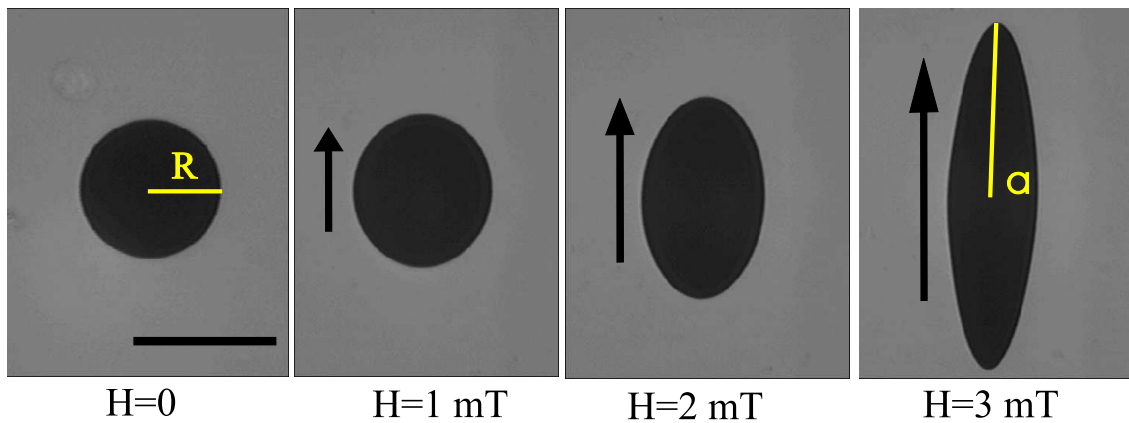


Figure 7.2: A ferrofluid spherule deforms into a prolate ellipsoid in a magnetic field, with its long axis (a) parallel to the applied field (arrows). The amount of deformation is proportional to the square of the field intensity (H). Scale bar = $50 \mu\text{m}$

The axial response fulfils the theoretical requirements of a magnetoreceptor mechanism involving the use of an *Inclination Compass*, as the axial deformation is the same in an antiparallel field. The intensity dependence of the deformation could potentially also be used to provide map information (see chapter 6).

However, caution is needed when extracting conclusions from these results. The magnetic field used in the experiments (from 0 to 3 mT) are an order of magnitude larger than the normal geomagnetic field, and a clear deformation could only be observed in relatively large spherules (diameter $\geq 20 \mu\text{m}$). Smaller spherules equivalent in size to the SP clusters would then require even higher fields to show a noticeable response. One needs to assume that the SP clusters in the upper beak skin of homing pigeons have a substantially larger magnetic susceptibility, or smaller surface tension, compared to that

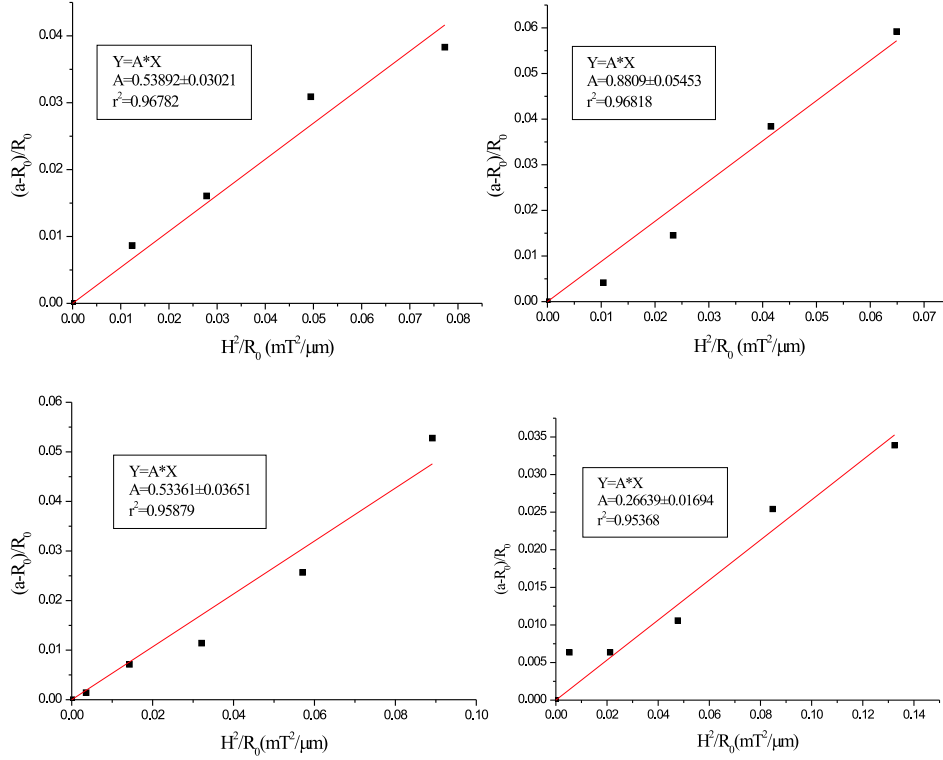


Figure 7.3: Axial elongation $[(a - R)/R]$ of ferrofluid spherules as a function of magnetic field intensity (H^2/R). The deformation of 17 spherules of different sizes was measured. In all cases $r^2 > 0.95$. Different slopes are due to different values of the surface tension (γ), see Eq. 7.1

of the ferrofluid spherules used in the experiments ($\chi \sim 7 \text{ SI} \approx 0.5 \text{ CGS}$), which allows for larger deformations. Hence, the suitability of individual SP clusters as transducers of the geomagnetic field, although theoretically possible, remains to be validated and for that, parameters such as γ and χ have to be determined.

7.4 Response of groups of ferrofluid spherules to weak magnetic fields

Here the observation that the SP clusters described in homing pigeons do not occur isolated from each other, but form structured aggregates of up to 20 clusters, is taken into account.

The close spacing between the clusters within an aggregate suggests that magnetic interactions between clusters may play an important role in the response of an aggregate to changes in the external magnetic field. Adjacent clusters of SP particles interact under a magnetic field, and this interaction is orders of magnitude stronger than in the case of single SP particles. Under certain conditions, the energy of the magnetic interactions of adjacent SP clusters can overcome the background thermal energy. These interactions depend on the intensity and the axial direction of the magnetic field and can potentially be transformed into directional information for orientation and navigation (Davila et al., 2003). Hence, the response of groups of ferrofluid spherules to magnetic fields was studied.

This response can be theoretically predicted. Ferrofluid spherules become polarized in the presence of a magnetic field due to their superparamagnetic behavior [Figure 7.5], therefore it is possible to use the dipole-dipole approximation to describe their magnetic interaction. The force between two adjacent spherules is

$$F_{attr} = \frac{-6m_1m_2}{d_{12}^4} \quad \text{and} \quad F_{rep} = \frac{3m_1m_2}{d_{12}^4}, \quad (7.2)$$

for the one-behind-another (F_{attr} , Figure 7.5*Top*) and the side-by-side position (F_{rep} , Figure 7.5*Bottom*) with respect to the field direction, where m_1 , m_2 are the induced magnetic moments of two spherules and d_{12} their center-to-center distance. The induced magnetic moment of a spherule, m is given by

$$m = \frac{\chi H_0 V}{1 + N\chi} \quad (7.3)$$

where V is its volume and χ its intrinsic susceptibility; H_0 denotes the applied magnetic field and N the demagnetization factor, which for a pair of ferrofluid spherules can be approximated by that of a suitably chosen prolate ellipsoid of revolution. In the case of magnetic attraction, N is smaller than the demagnetization factor of a single sphere, $4\pi/3$ (cgs units) and correspondingly larger than $4\pi/3$ in the case of repulsion. If a prolate ellipsoid with the same axial ratio as the pair of spheres and the same volume is chosen, one obtains for two-spheres in contact, $\frac{N_{attr}}{4\pi} = 0.17$ and $\frac{N_{rep}}{4\pi} = 1 - \frac{2N_{attr}}{4\pi} = 0.65$. For this example, the forces can be approximated by

$$F_{attr} \approx -6(\chi H_0 R)^2 \cos \phi, \quad \text{and} \quad F_{rep} \approx -3(\chi H_0 R)^2 \sin \phi, \quad (7.4)$$

where ϕ is the angle between the line connecting the centers of the spherules and the magnetic field lines. According to the model above, adjacent ferrofluid spherules will

interact in the presence of a magnetic field and as a result, the spherules will self assemble in groups responding to attractive or repulsive forces [Figure 7.4]. This interaction depends on the direction and intensity of the magnetic field but also on the original arrangement of the spherules and their freedom to move. The effective displacement of the spherules will also depend on the viscosity of the surrounding medium (see chapter 8).

The predicted behavior was indeed observed in the model experiments. When exposed to an external magnetic field, groups of ferrofluid spherules display a variety of interactions which ultimately result in the rearrangement of the spherules in chain like structures aligned with the ambient magnetic field [Figure 7.5B].

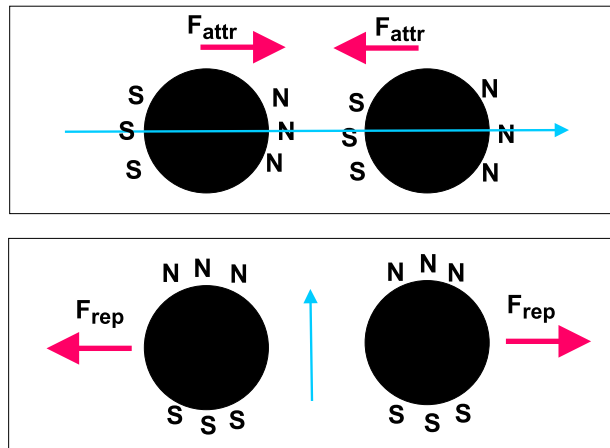


Figure 7.4: Dipole-dipole interaction between neighboring ferrofluid spherules. The blue arrows represent the magnetic field. *Top* One-behind-another configuration in which opposite poles result in attractive forces. *Bottom* Side-by-side configuration in which repulsive forces dominate. From Davila et al. (2003).

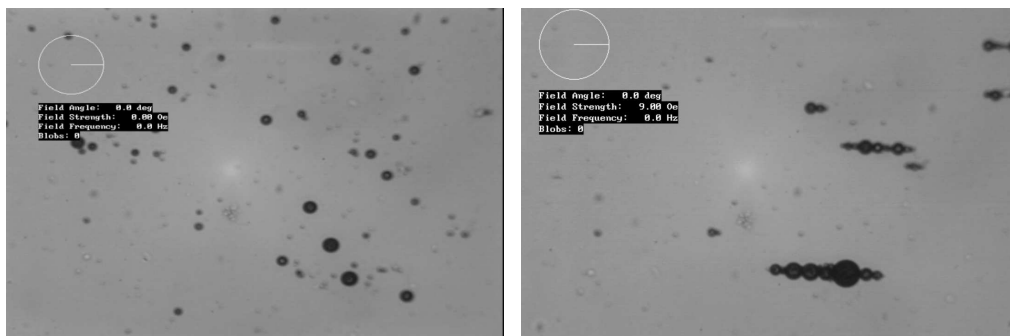


Figure 7.5: Formation of chains of ferrofluid spherules in the presence of a magnetic field. (*Left*) Zero field; (*Right*) after a field of 0.9 mT is applied.

The observation of magnetostatic interactions between ferrofluid spherules offers a series of novel mechanisms for the transformation of their magnetic field response into mechanical forces. Three different scenarios are studied here: (1) the attraction-repulsion responses that arise between adjacent ferrofluid spherules constrained to move only in one direction; (2) the pressure exerted between adjacent ferrofluid spherules on their surface of contact; and (3) the rotation response of a chain of spherules in a magnetic field whose direction changes in time.

7.4.1 The attraction-repulsion response of ferrofluid spherules

First the interaction between adjacent spherules was studied in a situation in which the spherules are constraint to move only in one direction. To simulate this in the model experiments, microgrooves similar in size to the spherules, were engraved into microscope slides (Plexiglas), and several spherules were placed there with a micropipette. The spherules could then move along one axis only. As expected, a magnetic field applied parallel to the free axis of movement, resulted in the attraction of the spherules, while a field applied perpendicular to the axis of movement, gave rise to repulsive forces [Figure 7.6].

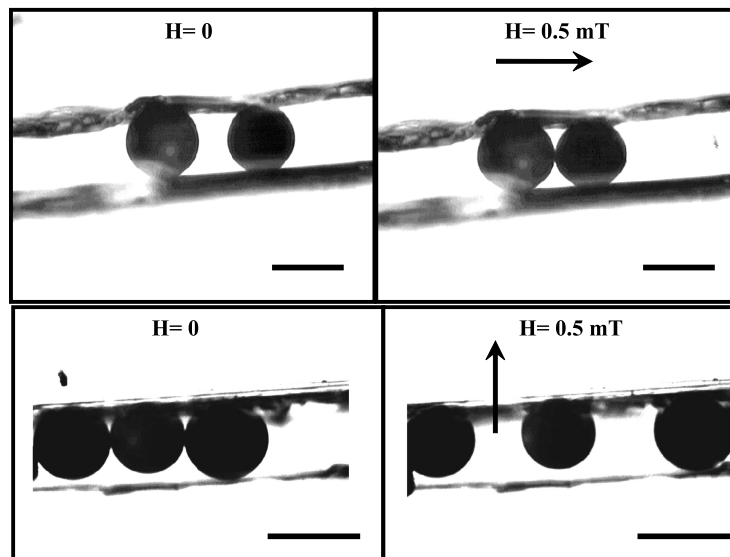


Figure 7.6: (*Top*) A pair of ferrofluid spherules oriented parallel to an applied magnetic field (arrow) attract each other. (*Bottom*) When aligned perpendicular to the magnetic field (arrow) the separate due to magnetostatic repulsion. The spherules are constrained to move in a direction parallel to the axis of the chain. Scale bar $50 \mu\text{m}$. From Davila et al. (2003)

Consequently, a chain of spherules constrained to move only in a direction parallel to its long axis, will shrink in a field applied parallel to the chain's axis and stretch in a field applied perpendicular to it (Davila et al., 2003). A direct consequence from this result is the existence of a critical angle between the chain of droplets and the magnetic field direction. While below this angle attractive forces dominate and the chain structure holds, above the critic angle repulsive forces will drive the spherules apart. According to Eq. 7.4, the critical angle at which repulsive forces overcome attractive forces is $\phi = 45^\circ$.

The attraction-repulsion response depends on both the direction and the intensity of the ambient field. This response offers therefore a mechanism for magnetic field perception sensitive to the parameters most likely being used by animals for orientation (see *The attraction-repulsion model* in chapter 9).

7.4.2 Pressure between two interacting ferrofluid spherules

Adjacent spherules attracting each other will exert a mutual pressure on their surfaces once they come into contact [Figure 7.7]. Following Hertz (1881), this pressure is given by

$$P_{int} \approx \frac{F_{attr}}{\pi s^2}, \quad (7.5)$$

including Eq. 7.4, we obtain

$$P_{int} \approx \frac{(\chi H_0 R)^2}{\pi s^2} \cos \phi, \quad (7.6)$$

Where s is the radius of the surface of contact, which is proportional to the elastic modulus of the spherules (E), following

$$s = \sqrt[3]{\frac{3\pi}{4} F_{attr} (k_1 + k_2) R}, \quad (7.7)$$

in which

$$k_1 = \frac{1 - \nu_1^2}{\pi E_1} \quad \text{and} \quad k_2 = \frac{1 - \nu_2^2}{\pi E_2}, \quad (7.8)$$

Where ν is the Poisson ratio and E is the Young modulus. Using Eq. (7.6 and 7.7) for two identical spherules, and assuming a low shear rigidity (ν_1 and $\nu_2 \sim 0$) we obtain

$$p_{int} \propto (\chi E H_0)^{2/3} \cos \phi, \quad (7.9)$$

From Eq. 7.6 it can be seen that since $R \gg s$, the pressure exerted between two attracting spherules will be relatively large, and at a maximum when $\phi = 0^\circ$. At $\phi = 90^\circ$, the spherules repel and the pressure disappears. As can be seen from Eq. 7.9 the pressure between adjacent spherules increases with increasing the magnetic field intensity.

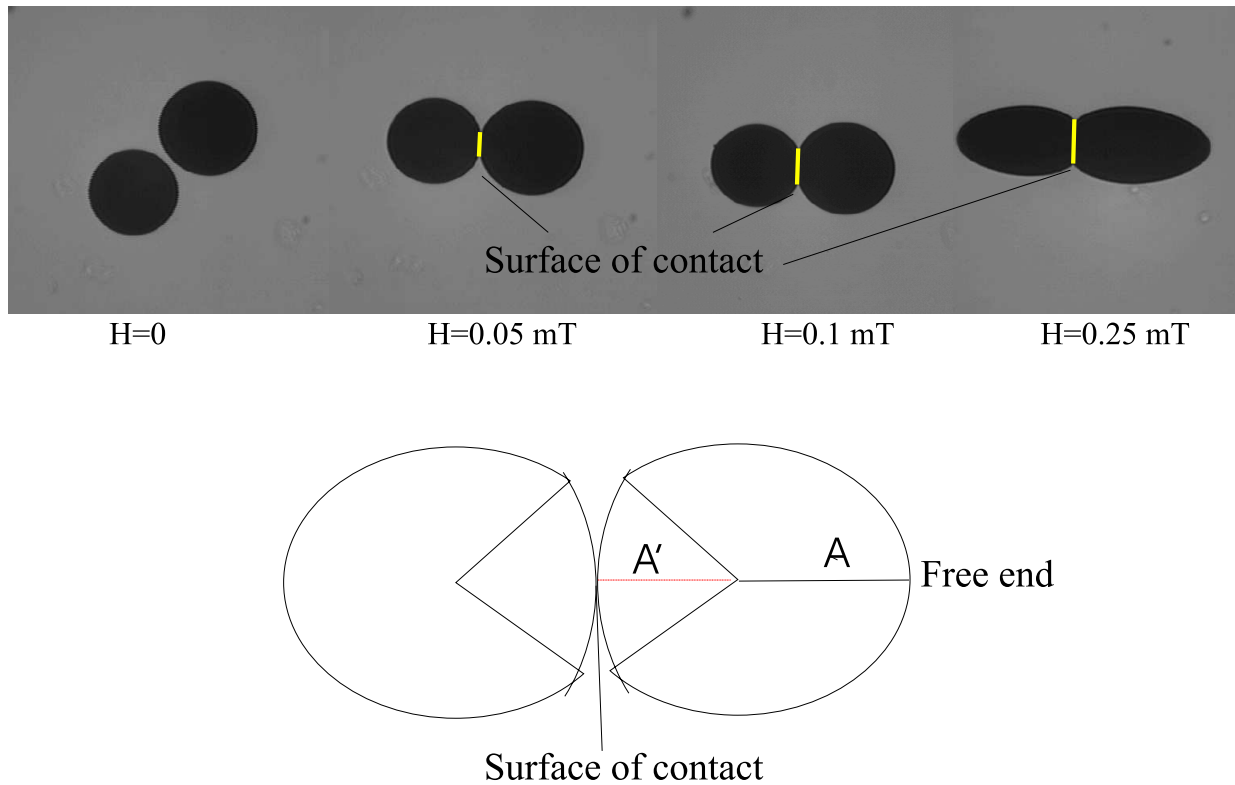


Figure 7.7: (*Top*) Two ferrofluid spherules ($\sim 50 \mu\text{m}$ in diameter) attract each other in the presence of a magnetic field. This attraction results in pressure at the surface of contact (yellow line) between the spherules. By increasing the magnetic field intensity the pressure increases as can be seen by the increment of the surface of contact. (*Bottom*) Scheme of two spherules showing the parameters used to estimate the dependence of the pressure exerted between them and the magnetic field intensity. See text for further details.

The pressure between adjacent ferrofluid spherules as a function of the ambient magnetic field intensity, was studied by forming pairs of spherules and measuring the amount of flattening in an increasing magnetic field. As can be seen in Figure 7.7*Top*, the surface of contact flattens as the spherules attract each other, and the amount of flattening is proportional to the magnetic field intensity. The free end of the spherules also shows the axial elongation described in the previous section.

The amount of flattening in an increasing magnetic field was measured as $(A-A')$, were

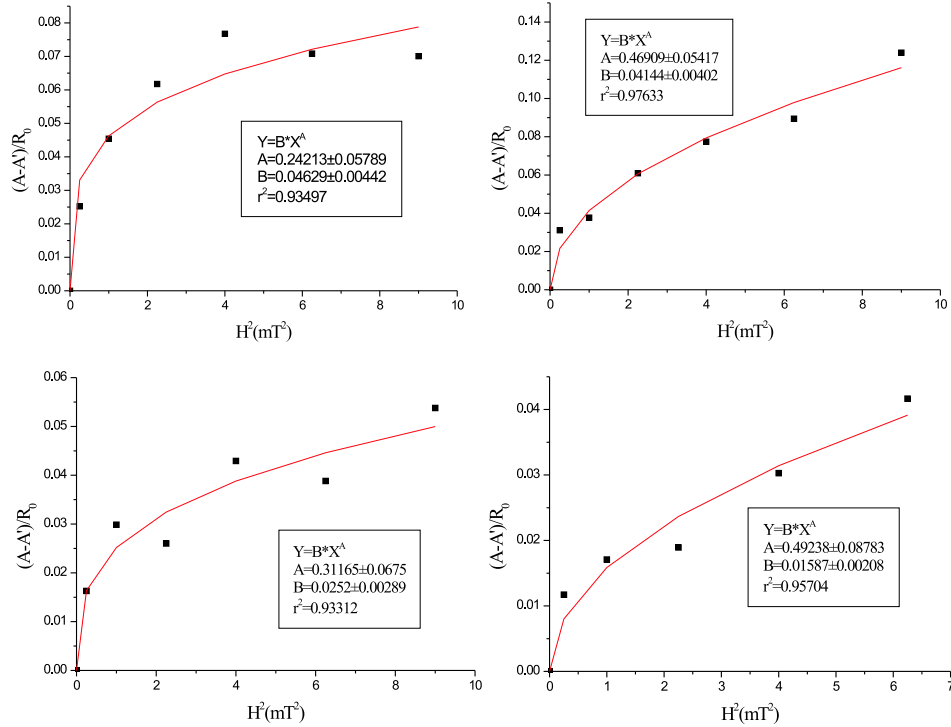


Figure 7.8: Amount of flattening of two ferrofluid spherules, $(A-A')/R$, as a function of the magnetic field intensity, H^2/R . As can be observed, the pressure shows a power law dependence with the external magnetic field.

A is the distance from the center of the ellipsoid to the pole of the free end, and A' is the distance from the center of the ellipsoid to the surface of contact [Figure 7.7 *Bottom*]. Figure 7.8 shows 4 measurements of the amount of flattening between two ferrofluid spherules as a function of the magnetic field intensity. The pressure exerted between two attracting ferrofluid spherules shows a power law dependence with the magnetic field intensity⁴ (all the results are summarized in Table 7.3 at the end of the chapter).

$$P \propto H^{0.71}, \quad (7.10)$$

Which is not far from the expected value (Eq. 7.9). There is a large uncertainty in Eq. 7.7 since the elastic properties of the ferrofluid spherules are not considered.

⁴The value for the exponent in the power law is based on measurements on 9 different pairs of spherules.

Comparison of the magnetostatic interactions between ferrofluid spherules and SD magnetosomes

It is interesting to compare here the internal forces due to magnetostatic interactions between ferrofluid spherules and bacterial magnetosomes. As shown in chapter 2, bacterial magnetosomes are arranged in chains and often surrounded by a lipid membrane ~ 4 nm thick. Hence adjacent magnetosomes will interact exerting a pressure on the lipid membrane that separates them. Shcherbakov et al. (1997) estimated a value for this pressure of 1.5 bar ($= 15 \times 10^5$ dyn/cm²). In contrast to the SP clusters, the pressure between two adjacent magnetosomes is independent of an external magnetic field. At Earth-strength magnetic fields and taking a typical value for the elastic modulus of biomaterials, $E \sim 10^2 - 10^5$ dyn/cm² (Duwe et al., 1990), the expected pressure between two adjacent ferrofluid spherules amounts to $\sim \chi \cdot 10^{-5} - 10^{-3}$ bar ($\sim \chi \cdot 10^1 - 10^3$ dyn/cm²). While the pressure between bacterial magnetosomes is orders of magnitude larger than that between ferrofluid droplets, the former is a constant at a given distance between the magnetosomes and independent of the strength of the external magnetic field, but the later increases with increasing the field's intensity (Eq. 7.7)[Figure 7.9]. Hence, the results presented here provide another mechanism to transform the magnetic interaction between adjacent SP clusters into mechanical stresses, which is sensitive to the magnetic field intensity. This observation allows to propose a novel mechanism for magnetic field perception (see the *pressure model* in chapter 9).

7.4.3 The Pseudo-torque response of chains of ferrofluid spherules

Finally, the dynamics of chains of ferrofluid spherules which are completely free to move, was studied in a magnetic field constantly changing its direction. As expected from the results above, a chain of spherules oriented parallel to the magnetic field direction, holds together due to the dominating attractive forces between adjacent spherules. However, if the magnetic field is applied at oblique angles with respect to the chain axis, it rotates into alignment with the axis of the field, as long as the angle between field and long axis is smaller than 45° [Figure 7.10]. The chain in Figure 7.10 is deformed during its rotation due to the viscosity of water, which opposes the movement of the chain resulting in a slower motion of the spherules at the chain endings.

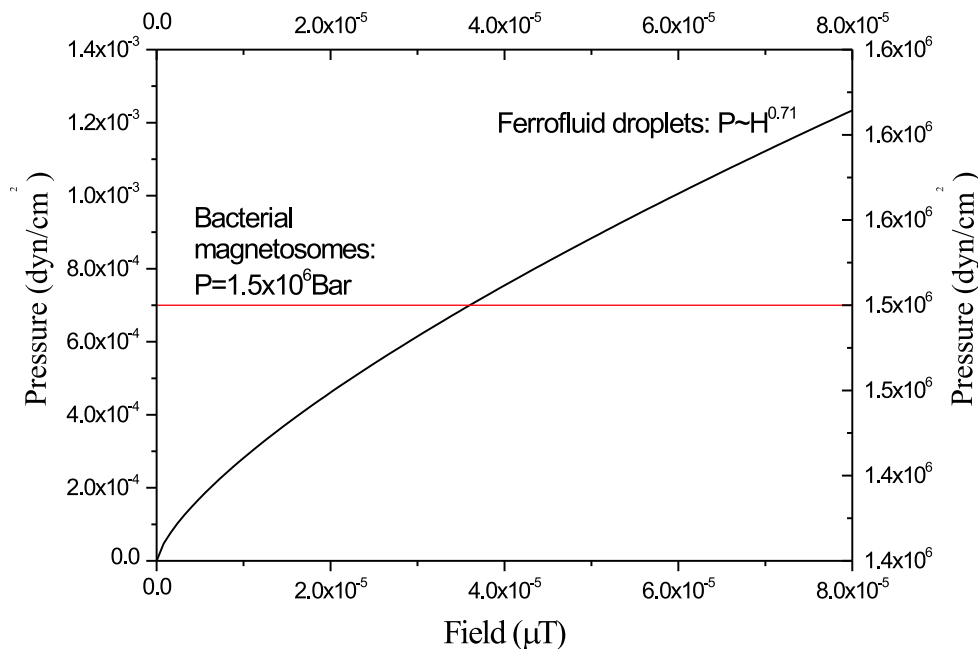


Figure 7.9: Plot comparing the pressure exerted between two adjacent magnetosomes (red line and right hand vertical scale) and two ferrofluid spherules (black line and left hand vertical scale) in a magnetic field (the plotted values for the magnetic field intensity are in the range of the Earth's magnetic field). While the pressure between magnetosomes is orders of magnitude larger than that of ferrofluid spherules, the former is constant at any field intensity and the later increases with increasing the magnetic field.

The resulting chain rotation is due to the magnetostatic interactions between neighboring spherules, and although it macroscopically resembles the torque-response of a chains of SD particles, as found in magnetotactic bacteria, the physical principles underlying the rotation of a chain of ferrofluid spherules are different (Davila et al., 2005). This torque-like response is therefore referred to as *pseudo-torque*. Figure 7.11 shows the microscopic mechanism governing the pseudo-torque response. The magnetic field induces the polarization of the spherules. If the field is not perpendicular to the chain, the polarization of each spherule results in an unstable configuration in which similar poles are close to each other [Figure 7.11 A (*left*)]. This will induce the displacement of the spherules until opposite poles face each other [Figure 7.12 A (*right*)]. Hence, the displacement of each individual spherule results in the realignment of the chain parallel to the magnetic field [Figure 7.11 B], contrary to the torque response of a chain of SD particles, in which the

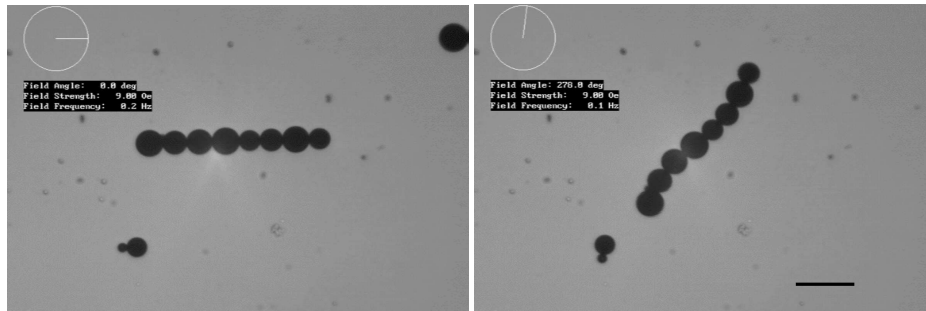


Figure 7.10: (*Left*) Chain oriented parallel to the ambient field lines. (*Right*) a rotation of the field induces the rotation of the chain. The direction of the ambient field is represented on the top-left corner of the pictures. Scale bar=50 μm

whole chain rotates as a solid unit. Another important property of the pseudo-torque response is its axial response, contrary to chains of SD particles, where the direction of the rotation depends on the direction of the external magnetic field [Figure 7.12]. The pseudo-torque only occurs if the angle between the long axis of the chain and the magnetic field vector does not exceed the critical value. Above this critical angle magnetostatic repulsion lead to a disruption of the chain and the formation of smaller sub-chains. The concept of pseudo-torque will be further developed in the next chapter.

7.5 Response of groups of ferrofluid spherules to strong, pulsed magnetic fields

As will be described in chapter 10, a short, strong magnetic pulse applied to the head of homing pigeons and migratory birds affects their orientation behavior. Such treatment is designed to affect a magnetoreceptor system based on ferrimagnetic particles (Beason et al., 1995, 1997; Wiltschko et al., 1998, 2002). A positive response is then regarded as a proof that magnetically stable SD particles are the essential component of the magnetic sensory system. However, despite the positive results obtained in these behavioral experiments, it has not been possible so far to link the observed response of the birds to a specific magnetite-based magnetoreceptor mechanism. Model experiments were therefore conducted to simulate the response of chains of ferrofluid spherules to a treatment with a short, strong magnetic pulse, similar to that applied in the behavioral tests.

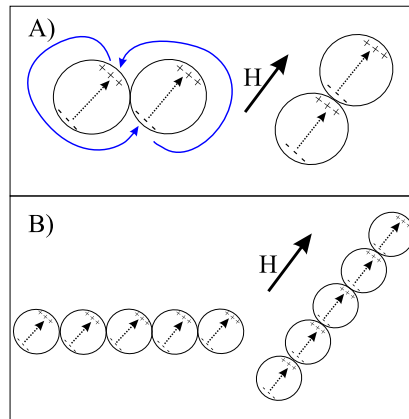


Figure 7.11: The Pseudo-torque response. A) a magnetic field (H) applied with an angle with respect to the chain's axis, induces the polarization of adjacent spherules (+ and - symbols) resulting in a side-by-side configuration. In that situation the spherules are displaced (blue lines) until they acquire a stable one-behind-another configuration. B) This microscopic response results in the rotation of the whole chain.

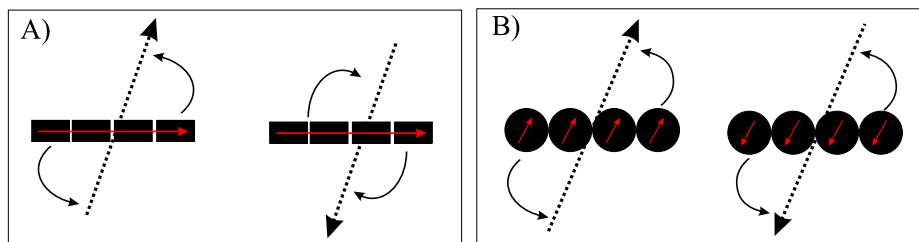


Figure 7.12: A) (*left*) a chain of SD particles with a net magnetic moment (red arrow) rotates counterclockwise into alignment with the external field (dashed arrow), and (*right*) clockwise if the field is applied in the opposite direction. In contrast, B) the pseudo-torque response is invariant with respect to the field polarity.

The intensity of the magnetic pulse was 0.5 T and its duration 2 msec. As can be seen in Figure 7.13, for a single chain of ferrofluid spherules the magnetic pulse leads to a disruption of the chain, due to the magnetostatic interactions between the spherules. It can also be seen that the spherules elongate as the field is applied. This is only a transient feature preceding the disruption of the chain (Davila et al., 2005). The chain disruption is interpreted as a result of the repulsive force arising between adjacent spherules, as occurs in the repulsion-attraction response presented above. Although the pulse is applied for a short time, its intensity is large enough to drive the spherules apart. It should be noted that a pulse applied parallel to the chain's axis will have the effect of high pressure between adjacent spherules (see Figure 7.9). If applied below the critical angle of 45° , it induces the chain's rotation. Above the critic angle, the pulse results in the chain's

disruption. In other words, the a brief but strong magnetic pulse has, in principle, the same effects as a weak magnetic field applied for sufficient long time. This is due to the fact that the dynamics of ferrofluid spherules (and of SP clusters) in a magnetic field are controlled by magnetostatic forces.

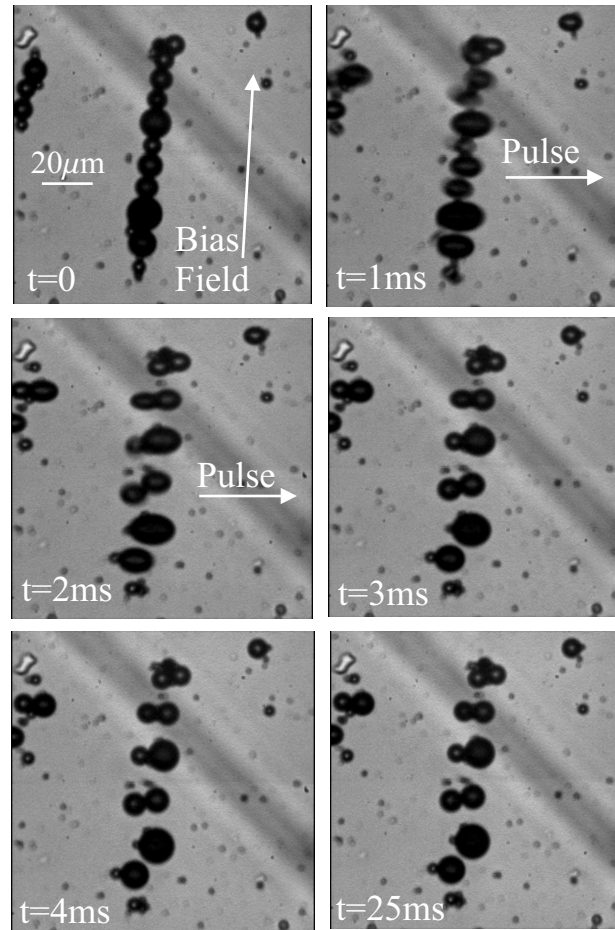


Figure 7.13: Response of a chain of ferrofluid spherules to a short, strong magnetic pulse (movie available as online supplement). $t = 0$ Initial configuration of the chain of ferrofluid spherules, aligned in a bias field of 0.1 mT. ($t = 1 - 3$ msec.) application of a 0.5 T pulse for 2 msec. perpendicular to the chain axis. The spherules elongate into the pulse field direction and subsequently form pairs, thereby disrupting the chain configuration. ($t = 4$ msec.) arrangement immediately after the pulse treatment and ($t = 25$ msec.) thereafter. From Davila et al. (2005).

| Sample | H (mT) | a (μm) | b (μm) | Sample | H (mT) | a (μm) | b (μm) |
|--------|--------|---------------------|---------------------|---------|--------|---------------------|---------------------|
| Elong1 | 0 | 80.9 | 81.4 | Elong10 | 0 | 64.7 | 64.2 |
| | 0.5 | 80.8 | 81.4 | | 0.5 | 64.9 | 64.0 |
| | 1 | 81.6 | 81.5 | | 1 | 65.2 | 64.2 |
| | 1.5 | 82.2 | 81.4 | | 1.5 | 65.2 | 64.3 |
| | 2 | 83.4 | 81 | | 2 | 65.5 | 64.3 |
| | 2.5 | 84 | 80.5 | | 2.5 | 66.4 | 63.8 |
| Elong2 | 0 | 96.3 | 97.2 | Elong11 | 0 | 63.7 | 63.7 |
| | 0.5 | 96 | 97.5 | | 0.5 | 63.9 | 63.9 |
| | 1 | 96.7 | 97.3 | | 1 | 63.9 | 63.6 |
| | 1.5 | 97.7 | 97 | | 1.5 | 64.6 | 63.7 |
| | 2 | 100 | 97 | | 2 | 65.3 | 63.7 |
| | 2.5 | 102 | 95.8 | | 2.5 | 66.2 | 63.4 |
| Elong3 | 0 | 70.1 | 71.9 | Elong12 | 0 | 47.4 | 48.9 |
| | 0.5 | 70.2 | 71.5 | | 0.5 | 47.6 | 49.1 |
| | 1 | 70.6 | 71.4 | | 1 | 47.9 | 48.9 |
| | 1.5 | 70.9 | 71.4 | | 1.5 | 48.3 | 48.6 |
| | 2 | 71.9 | 70.9 | | 2 | 48.9 | 48.3 |
| | 2.5 | 7.93 | 7.63 | | 2.5 | 48.9 | 48.3 |
| | 3 | 73.8 | 70.3 | | 3 | 49.3 | 47.8 |
| Elong4 | 0 | 75.7 | 76.2 | Elong13 | 0 | 47.2 | 47.7 |
| | 0.5 | 75.7 | 76.6 | | 0.5 | 47.5 | 47.6 |
| | 1 | 76.2 | 76.2 | | 1 | 47.5 | 47.7 |
| | 1.5 | 77.1 | 76.2 | | 1.5 | 47.7 | 47.4 |
| | 2 | 77.4 | 75.2 | | 2 | 48.4 | 47.7 |
| | 2.5 | 78.6 | 75.2 | | 2.5 | 48.8 | 47.0 |
| Elong5 | 0 | 70.4 | 71.9 | Elong14 | 0 | 81.4 | 81.4 |
| | 0.5 | 70.6 | 71.8 | | 0.5 | 81.3 | 81.6 |
| | 1 | 71.2 | 71.6 | | 1 | 81.5 | 81.7 |
| | 1.5 | 71.5 | 71.5 | | 1.5 | 82.4 | 81.2 |
| | 2 | 72.8 | 71.1 | | 2 | 83.5 | 80.7 |
| | 2.5 | 78.6 | 70.7 | | 2.5 | 84.1 | 80.5 |
| Elong6 | 0 | 94.0 | 94.0 | Elong15 | 0 | 64.8 | 64.3 |
| | 0.5 | 94.0 | 94.0 | | 0.5 | 64.5 | 64.4 |
| | 1 | 94.5 | 93.7 | | 1 | 64.7 | 64.0 |
| | 1.5 | 95.6 | 93.7 | | 1.5 | 65.0 | 64.2 |
| | 2 | 96.4 | 93.2 | | 2 | 65.4 | 63.8 |
| | 2.5 | 97.0 | 92.6 | | 2.5 | 66.0 | 63.2 |
| Elong7 | 0 | 113.7 | 114.3 | Elong16 | 0 | 92.2 | 93.4 |
| | 0.5 | 113.7 | 114.3 | | 0.5 | 92.8 | 92.7 |
| | 1 | 113.8 | 114.3 | | 1 | 92.5 | 92.7 |
| | 1.5 | 114.2 | 113.4 | | 1.5 | 93.5 | 92.3 |
| | 2 | 116.6 | 112.7 | | 2 | 94.6 | 91.7 |
| | 2.5 | 118.1 | 112.1 | | 2.5 | 94.6 | 90.8 |
| Elong8 | 0 | 128.7 | 129.3 | Elong17 | 0 | 92.2 | 93.4 |
| | 0.5 | 128.7 | 129.3 | | 0.5 | 92.8 | 92.7 |
| | 1 | 129.7 | 128.6 | | 0.5 | 92.8 | 92.7 |
| | 1.5 | 130.9 | 128.1 | | 0.5 | 92.8 | 92.7 |
| | 2 | 132.8 | 127.7 | | 0.5 | 92.8 | 92.7 |
| | 2.5 | 134.7 | 126.7 | | 0.5 | 92.8 | 92.7 |
| Elong9 | 0 | 73.3 | 73.8 | | | | |
| | 0.5 | 73.6 | 73.88 | | | | |
| | 1 | 73.6 | 73.3 | | | | |
| | 1.5 | 74.4 | 73.3 | | | | |
| | 2 | 75.6 | 72.9 | | | | |
| | 2.5 | 76.5 | 72.2 | | | | |

Table 7.2: Results of the measurements conducted to estimate the axial deformation of ferrofluid spherules as a function of the field intensity (H). a = long axis of the ellipsoid; b = short axis of the ellipsoid.

| Sample | H (mT) | A (relative units) | A' (relative units) | Sample | H (mT) | A (relative units) | A' (relative units) |
|--------|--------|--------------------|---------------------|--------|--------|--------------------|---------------------|
| Feero1 | 0 | 14.5 | 14.5 | Ferro6 | 0 | 19.36 | 19.36 |
| | 0.5 | 14.4 | 14.03 | | 0.5 | 19.36 | 18.64 |
| | 1 | 14.63 | 13.97 | | 1 | 19.46 | 18.57 |
| | 1.5 | 14.59 | 13.69 | | 1.5 | 19.69 | 18.21 |
| | 2 | 14.70 | 13.59 | | 2 | 19.97 | 17.82 |
| | 2.5 | 14.63 | 13.60 | | 2.5 | 20.18 | 17.72 |
| | 3 | 14.39 | 13.38 | 3 | 20.59 | 17.62 | |
| Feero2 | 0 | 25.2 | 25.2 | Ferro7 | 0 | 26.93 | 26.93 |
| | 0.5 | 25.11 | 24.33 | | 0.5 | 27.25 | 26.58 |
| | 1 | 25.16 | 24.21 | | 1 | 27.04 | 26.32 |
| | 1.5 | 25.51 | 23.97 | | 1.5 | 27.14 | 26.02 |
| | 2 | 25.88 | 23.92 | | 2 | 27.35 | 26.07 |
| | 2.5 | 26.33 | 24.07 | | 2.5 | 27.45 | 25.97 |
| | 3 | 27.04 | 23.92 | 3 | 27.66 | 26.12 | |
| Feero3 | 0 | 7.92 | 7.92 | Ferro8 | 0 | 25.25 | 25.25 |
| | 0.5 | 7.89 | 7.76 | | 0.5 | 25.44 | 24.76 |
| | 1 | 7.93 | 7.69 | | 1 | 25.52 | 24.72 |
| | 1.5 | 8.01 | 7.80 | | 1.5 | 25.40 | 24.33 |
| | 2 | 7.96 | 7.62 | | 2 | 25.46 | 24.24 |
| | 2.5 | 7.93 | 7.63 | | 2.5 | 25.61 | 24.43 |
| | 3 | 8.03 | 7.60 | 3 | 25.71 | 24.32 | |
| Feero4 | 0 | 8.35 | 8.35 | Ferro9 | 0 | 24.77 | 24.77 |
| | 0.5 | 8.42 | 8.22 | | 0.5 | 24.55 | 24.28 |
| | 1 | 8.44 | 8.10 | | 1 | 24.61 | 24.17 |
| | 1.5 | 8.49 | 8.12 | | 1.5 | 24.66 | 23.98 |
| | 2 | 8.58 | 8.11 | | 2 | 24.79 | 23.92 |
| | 2.5 | 8.56 | 8.21 | | 2.5 | 24.89 | 23.71 |
| | 3 | 8.58 | 8.12 | | | | |
| Feero5 | 0 | 27.05 | 27.05 | | | | |
| | 0.5 | 27.19 | 26.87 | | | | |
| | 1 | 27.11 | 26.65 | | | | |
| | 1.5 | 27.04 | 26.53 | | | | |
| | 2 | 27.14 | 26.33 | | | | |
| | 2.5 | 27.35 | 26.22 | | | | |

Table 7.3: Results of the measurements conducted to estimate the amount of flattening of pairs of ferrofluid spherules as a function of the field intensity (H). A is the distance from the center of the ellipsoid to the pole of the free end, and A' is the distance from the center of the ellipsoid to the surface of contact.

Chapter 8

Dynamics of SP clusters in a liquid medium

"Do not quench your inspiration and your imagination; do not become the slave of your model."

Vincent van Gogh. (1853-1890)

8.1 Introduction

Despite their usefulness for model experiments, the use of ferrofluid spherules to simulate the response of SP clusters to magnetic fields is no more than a theoretical approximation. When modelling the functioning of a putative magnetite-based magnetoreceptor mechanism, one also has to take into consideration the physical and chemical properties of the cellular environment surrounding the magnetic particles. For that purpose, a numerical model that predicts the dynamics of interacting SP clusters under both weak and strong magnetic fields, was developed. In this model the spatial constraint that arises from the fact that the SP clusters occur within narrow nerve terminals, which limits their motion, was considered. The numerical model also considers the visco-elastic properties of the cell plasma, which are significantly different from that of water. Finally, the model provides an estimate of the characteristic time for the magnetostatically driven response of the SP clusters. The validity of the model is again tested in model experiments with ferrofluid spherules.

8.2 Interacting clusters of SP magnetite particles

The following quantitative consideration of interacting clusters of SP particles in magnetic fields has been elaborated under the guidance of Prof. Valera Shcherbakov, while Prof. Shcherbakov was visiting the Institute of Geophysics in Munich. The physical model is based on the physics of SP systems. As shown above, in a uniform external magnetic field \mathbf{H}_0 , a cluster of SP particles is polarized and will have a macroscopic magnetic moment \mathbf{m} . Assuming that the field inside a cluster is homogeneous, the free energy F of a group of N clusters is given by

$$F = -\frac{1}{2} \sum_{i=1}^N \mathbf{m}_i \cdot \mathbf{H}_0, \quad (8.1)$$

where

$$\begin{aligned} \mathbf{m}_i &= \nu_i \chi_i \left(\mathbf{H}_0 + \sum_{j \neq i} \mathbf{H}_j(\mathbf{r}_i) \right) \\ &= \chi_i \nu_i \left(\mathbf{H}_0 + \sum_{\substack{j=1 \\ j \neq i}}^N \left(\frac{3 \mathbf{R}_{ij} (\mathbf{m}_j \cdot \mathbf{R}_{ij})}{R_{ij}^5} - \frac{\mathbf{m}_j}{R_{ij}^3} \right) \right) \end{aligned} \quad (8.2)$$

is the magnetic moment of cluster i , ν_i denotes its volume, χ_i is its effective susceptibility, and \mathbf{H}_j is the interaction field, that is, the magnetic field produced by cluster j situated at \mathbf{r}_j acting on cluster i at \mathbf{r}_i . \mathbf{R}_{ij} is the distance vector joining the centers of cluster i and j . The effective susceptibility, χ_i depends on both the particle-size distribution and particle concentration in the cluster, and also includes corrections for both the demagnetizing field $\mathbf{H}_D = -N_D \mathbf{M}$ and the Lorentz field $\mathbf{H}_L = 4\pi \mathbf{M}/3$ (approximation for $\chi < 1$), where \mathbf{M} is the magnetization of the cluster and N_D its geometrical demagnetizing factor. For a spherical cluster, with $N_D = 4\pi/3$, these corrections mutually cancel each other and the effective susceptibility amounts to the microscopic susceptibility.

To calculate the free energy F for a particular configuration, $\mathbf{m}(\mathbf{r})_{1\dots N}$ from Eq. (9.1), a set of N linear equations Eq. (8.2) has to be solved first in order to find the magnetic moments $\mathbf{m}_{1\dots N}$. Using an iterative approach, the zero-order expression $\mathbf{m}_j \simeq \chi_j \nu_j \mathbf{H}_0$ for \mathbf{m}_j is substituted on the right-hand side of Eq. (8.2) to obtain a first-order approximation, that is,

$$\mathbf{m}_i \simeq \chi_i \nu_i \mathbf{H}_0 + \chi_i \nu_i \sum_{\substack{j=1 \\ j \neq i}}^N \chi_j \nu_j \left(\frac{3 \mathbf{R}_{ij} (\mathbf{H}_0 \cdot \mathbf{R}_{ij})}{R_{ij}^5} - \frac{\mathbf{H}_0}{R_{ij}^3} \right), \quad (8.3)$$

Inserting (8.3) into (8.1) and omitting the constant term $-\frac{1}{2} H_0^2 \sum \chi_i \nu_i$, the following expression for the free energy F , is obtained

$$F = \frac{1}{2} H_0^2 \sum_{i,j=1}^N \sum_{i \neq j} \chi_i \chi_j \nu_i \nu_j \left(\frac{1}{R_{ij}^3} - \frac{3(\mathbf{h}_0 \cdot \mathbf{R}_{ij})^2}{R_{ij}^5} \right), \quad (8.4)$$

with the unit vector $\mathbf{h}_0 = \mathbf{H}_0/H_0$. Now it is possible to compute the trajectory of each SP cluster in a system of N clusters due to the magnetic interactions with the neighboring clusters. Eq. (8.4) can be further simplified: The SP clusters observed in the pigeon-beak skin are roughly similar in size (Davila et al., 2003) and so only groups of equally sized ferrofluid spherules are considered in the model experiments in chapter 7. Following this reasoning, henceforth a group of identical clusters (same radius R , volume $\nu = 4\pi R^3/3$, and microscopic susceptibility χ) constrained to move in a plane (imposed by experimental set-up), will be considered. Let (X_i, Y_i) be the Cartesian co-ordinates of the center of cluster i . Introducing the normalized co-ordinates $x_i = X_i/R$ and $y_i = Y_i/R$ and the dimensionless expression for the free energy $f = F R^3/(\chi^2 \nu^2 H_0^2) = F 9/(16 \pi^2 \chi^2 R^3 H_0^2)$, Eq. (8.4) becomes

$$f = \sum_{i=1}^N \sum_{j>i}^N \left(\cos^2 \phi \frac{(y_i - y_j)^2 - 2(x - x_j)^2}{r_{ij}^5} + \sin^2 \phi \frac{(x_i - x_j)^2 - 2(y - y_j)^2}{r_{ij}^5} - 3 \sin 2\phi \frac{(y_i - y_j)(x - x_j)}{r_{ij}^5} \right), \quad (8.5)$$

where $r_{ij} = R_{ij}/R$. To prevent the clusters from overlapping each other (rigid-spheres approximation), the repulsive potential

$$V_{cc}(x_i, x_j, y_i, y_j) = V_0 \exp \left(\frac{2 - \sqrt{(x_i - x_j)^2 + (y_i - y_j)^2}}{\gamma} \right) \quad (8.6)$$

is used, where V_0 and $\gamma \ll 1$. To constrain the positions of the clusters within the dendrite, the potential

$$V_m(y_i) = V_0 \exp \left(\frac{y_i^2 - (\rho - 1)}{\gamma} \right) \quad (8.7)$$

is included, where the axis of the dendrite defines the x -coordinate and $\rho = R_d/R$ is the scaled radius of the dendrite ($R_d = 2.5 \mu\text{m}$).

To compute each trajectory $\mathbf{r}_{1\dots N}(t)$ in a system of N SP clusters interacting under a magnetic field, the following set of Stokes equations has to be solved:

$$\frac{dx_i}{d\tau} = -\frac{\partial(f + V_{cc} + V_m)}{\partial x_i} \quad \text{and} \quad \frac{dy_i}{d\tau} = -\frac{\partial(f + V_{cc} + V_m)}{\partial y_i}, \quad (8.8)$$

where $\tau = t/t_0$ denotes the dimensionless time, with

$$t_0 = 27 \eta / (8 \pi \chi^2 H_0^2). \quad (8.9)$$

t_0 is the characteristic time scale, a measure of the time required to change the configuration of a group of SP clusters surrounded by a medium with a dynamic viscosity η , under a magnetic field H_0 . The smaller the characteristic time scale, the faster the SP clusters in a group will be displaced from their positions by the magnetic interactions that arise among the clusters under a magnetic field. It is important to note that the characteristic time, t_0 , does not depend on the size of the interacting SP clusters. It is therefore possible to study the magnetic interactions between groups of relatively big SP clusters (such as the ferrofluid spherules of the model experiments) and later extrapolate the results to smaller SP clusters such as the ones found in the upper beak skin of homing pigeons. Eqs. (8.5)–(8.8) allow to trace the magnetostatically-driven movements of every single SP cluster within a group of N clusters for a given configuration.

To illustrate the physical meaning of Eq. (8.5), it is recasted it in a more compact form,

$$f = -A \cos^2 \phi - B \sin^2 \phi - 3C \sin 2\phi, \quad (8.10)$$

where

$$\begin{aligned} A &= \sum_{i=1}^N \sum_{j>i}^N \frac{2(x-x_j)^2 - (y_i-y_j)^2}{r_{ij}^5}, \quad B = \sum_{i=1}^N \sum_{j>i}^N \frac{2(y_i-y_j)^2 - (x-x_j)^2}{r_{ij}^5} \\ C &= \sum_{i=1}^N \sum_{j>i}^N \frac{(x_i-x_j)(y_i-y_j)}{r_{ij}^5}. \end{aligned} \quad (8.11)$$

The expression (8.10) for the free energy is anisotropic with respect to the angle ϕ . If a co-ordinate system is chosen such that $C = 0$, the energy spectrum of the system shows a well-known uniaxial shape with a minimum value at $\phi = 0$, i.e.,

$$f = (A - B) \sin^2 \phi. \quad (8.12)$$

This anisotropy produces a macroscopic torque

$$T = -\frac{\partial F}{\partial \phi} = \frac{16 \pi^2 \chi^2 H_0^2 R^3}{9} (B - A) \sin 2\phi. \quad (8.13)$$

A chain of clusters will therefore behave as an "axial" compass needle in a rotating magnetic field (Davila et al., 2005), as was otherwise observed in the model experiments with ferrofluid droplets.

8.2.1 Dynamics of SP clusters in a weak magnetic field

Figure 8.1 shows the dynamics of ferrofluid droplets under a magnetic field ($H_0 = 0.9$ mT) in comparison with the numerical simulation. It can be seen that the model realistically mimics the dynamics of a group of SP clusters. The model also shows the strong tendency of SP clusters to self-organize into elongated macro-structures aligned with the magnetic field (i.e. single chains, double chains, etc) as observed in the model experiments with ferrofluid spherules. Wilhelm et al. (2003) also reported the tendency of cellular endosomes possessing an SP lumen to arrange into chaplets in a magnetic field.

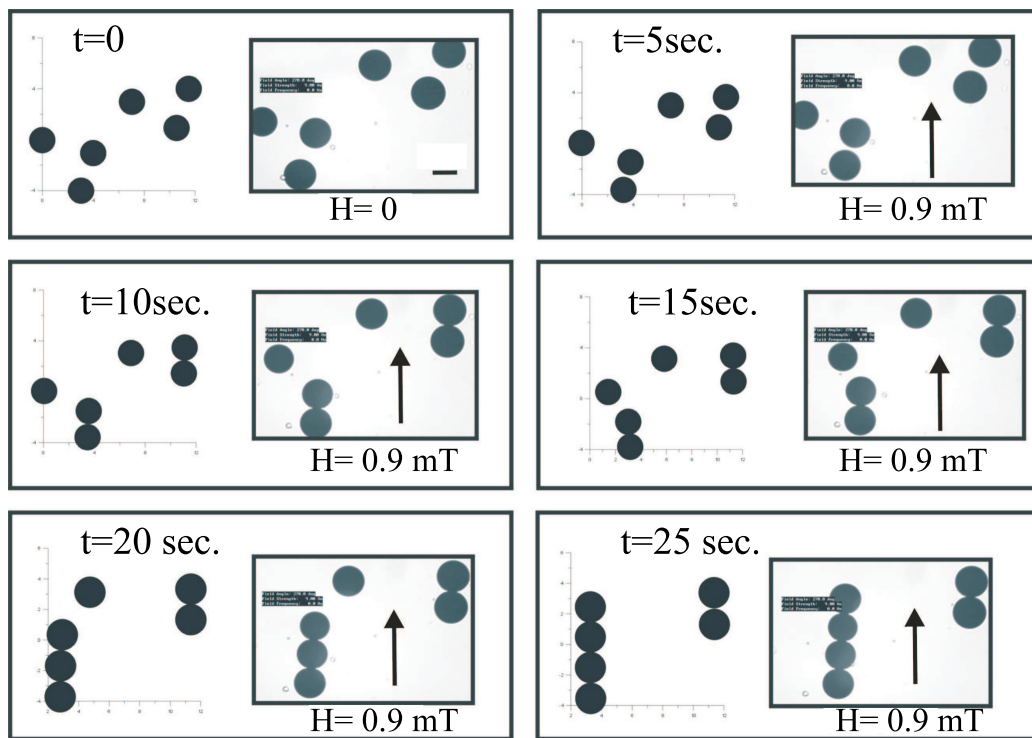


Figure 8.1: Comparison between numerical simulations and experiments (insets) on magnetically interacting ferrofluid spherules, which self-assemble into a linear configuration under the influence of a magnetic field of 0.9 mT (arrow). The scale bar represents 50 μm . From Davila et al. (2005)

The dynamics of chains of ferrofluid spherules were discussed in chapter 7. With the numerical simulations it is also possible to study the dynamics of chain-like configurations of SP clusters in a magnetic field. The numerical model allowed to control the initial configuration of the interacting clusters as well as to choose the number of clusters for a given configuration (up to 10 clusters). The model predicts that if the chain is parallel to

the field direction, it will hold together due to the dominating attractive forces; however, if the magnetic field is applied at oblique angles with respect to the chain axis, it will rotate into alignment with the axis of the field. These results confirm the previously observed pseudo-torque response of chains of ferrofluid spherules to magnetic fields (chapter 7). Interestingly, this pseudo-torque only occurs if the angle between the long axis of the chain and the magnetic field direction does not exceed a critical value (45° for a single chain). Above this critical angle, repulsive interactions between adjacent clusters will arise and chain disruption occurs, as also observed in the model experiments with ferrofluid spherules presented in the previous chapter. The same response was observed in the case of an arrangement of SP clusters in which single chains are stacked above one another with an offset of $\frac{1}{2}$ the cluster's diameter between layers.

To illustrate this magnetic behavior the dynamics of chains of SP clusters in a rotating magnetic field, was modelled. An scenario in which the chains occur in an elongated dendrite $5\mu\text{m}$ thick, was simulated, and therefore the chains could only rotate until they met the dendrite's membrane. In such a scenario, the single chain proves mechanically less stable than a stacked arrangement of chains [Figures 8.2, 8.3]. The numerical model was also applied to a situation in which chain-like structures of SP clusters are placed in a magnetic field that randomly changes its direction with respect to the chain axis. In that situation, a single chain of SP clusters is soon disrupted, while a stacked structure again shows a higher degree of stability in the same fluctuating magnetic field [Figures 8.4, 8.5].

8.2.2 Characteristic time response of interacting SP clusters

From Eq. (8.9) the characteristic time scale for the magnetostatically-driven motion of SP clusters in a magnetic field can be estimated. For $H_0 = 50 \text{ T}$, $\chi \sim 0.1$ (cgs), a value typical of ferrofluids based on magnetite, and $\eta = 0.1 \text{ Pa}\cdot\text{sec}$. the viscosity of the cellular cytoplasm, roughly 100 times that of water (Valberg and Feldman, 1987), the characteristic time is obtained as, $t_0 \sim 400 \text{ sec}$. The numerical value of χ is not well constrained as the magnetic susceptibility of the SP clusters in the pigeon has not yet been measured (Davila et al., 2005). This result applies both to the pseudo-torque response and the attraction-repulsion response.

When discussing sensory transduction in a more general sense, one can postulate that the stimulus be converted into a receptor potential or nervous signal within a fraction of a second and, consequently, the characteristic time scale obtained for the dynamics

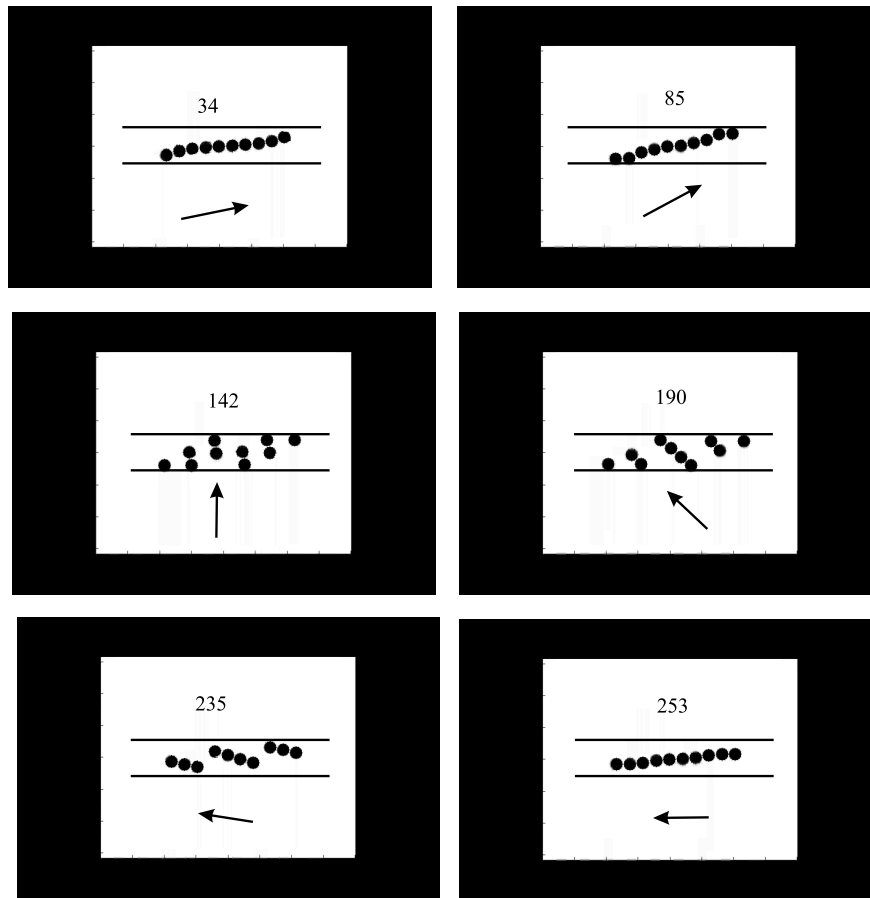


Figure 8.2: Simulation of the dynamics of a single chain in a rotating field (arrow). The chains rotates in the field until it meets the dendrite's membrane (thick lines), at which point it breaks. The chain reassembles again when the field is parallel to the dendrite's axis. Numbers represent model time steps. From Davila et al. (2005)

of chains of SP clusters in cellular environments seems to stand in contradiction with that general tenet. The result of the numerical model on the dynamics of SP clusters, therefore, has implications for the working principle of this putative receptor. A group of SP clusters inside a nerve terminal, will not track a relative change in the direction of the geomagnetic field on time scales of seconds to minutes. However, the stresses due to the magnetostatic interaction between the SP clusters (i.e. stress and strain in the attraction-repulsion and mechanical torques in the chain rotation) will be transferred *immediately* onto the cytoskeleton and the bounding membrane. In other words, we cannot expect a macroscopic displacement of the SP clusters during the postulated magnetoreception process, yet varying stress acting on the membrane of the free nerve endings. Because

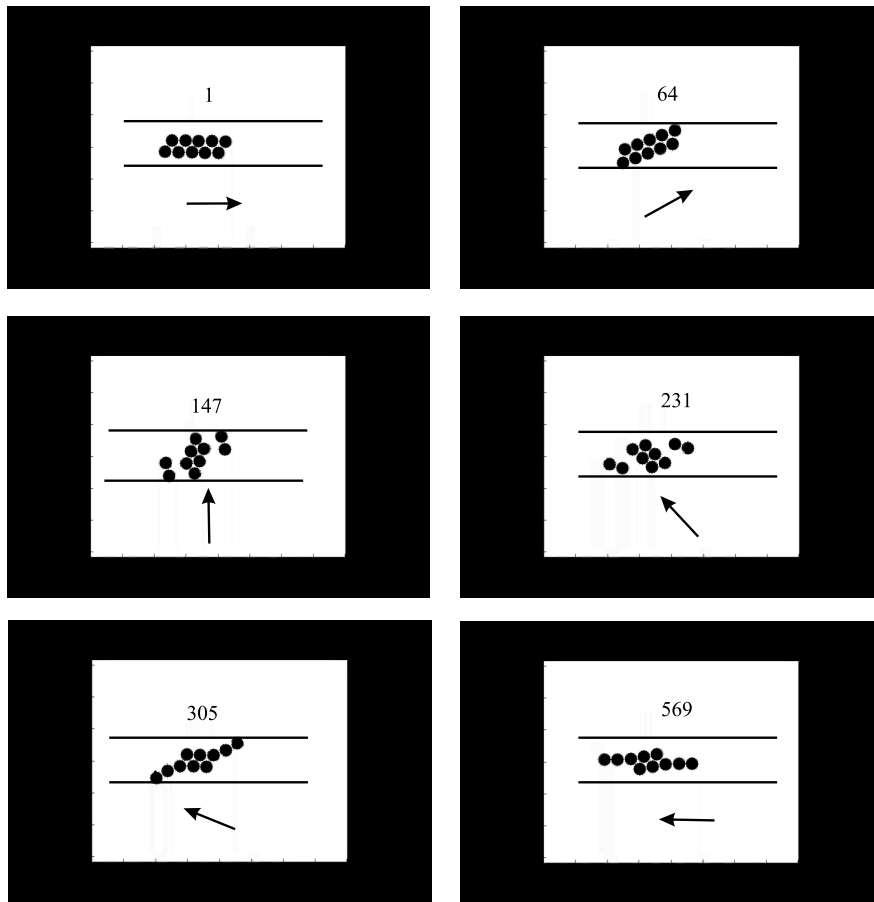


Figure 8.3: Simulation of the dynamics of a double chain in a rotating field (arrow). As occurs with the single chain, the double chain breaks when it meets the dendrite's membrane (thick lines). The chain reassembles again when the field is parallel to the dendrite's axis. Numbers represent model time steps. From Davila et al. (2005)

free nerve endings are mechanoreceptors, the stress due to the magneto-mechanical torque could generate a nerve signal. It can be concluded that a transducing mechanism in the form of chain-like structures of SP clusters is temporally stable and reversible, which is required for the animal to compare given parameters of the geomagnetic field at two different points in order to orient and navigate.

8.2.3 Dynamics of SP clusters in a strong pulsed field

As in chapter 7, the effects of a magnetic pulse on a chain of SP clusters was studied. The model predicts that a brief (1 msec) but strong pulse (0.5 T) applied exactly parallel to

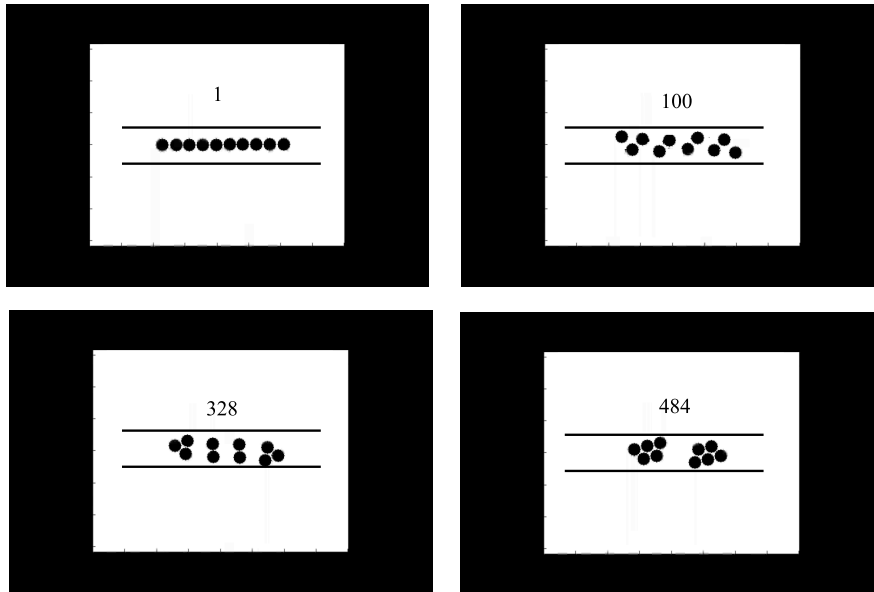


Figure 8.4: Simulation of the dynamics of a single chain in a field that changes randomly its direction with respect to the chains axis. The chain breaks at 100 model steps (top right picture), and reassembles into two double chains that eventually join (not shown). Thick lines represent the dendrite's membrane. Numbers represent model time steps. From Davila et al. (2005)

the chain axis will cause only a momentary compression between adjacent clusters [Figure 8.6A]. However, when applied at high oblique angles or perpendicular to the chain axis, the chain breaks into several sub-chains of varying lengths, which align into the axis of the pulse field [Figure 8.6C]. While for the single chain the critical angle at which chain disruption occurs is $\phi \sim 45^\circ$, for the stacked-chain this value is $\phi \sim 70^\circ$. At smaller angles, the chains will rotate into alignment with the field as a unit [Figure 8.6B]. The value of the critical angle also varies with the number of clusters within the chains, with higher critical angles for smaller chains. It should be emphasized that the response of the chain of clusters depends on the axial direction, but not on the polarity of the pulsed field.

In the next chapter, three magnetoreceptor mechanisms based on interacting clusters of SP magnetite will be proposed. These models take into account the results obtained from the experiments with ferrofluid spherules and from the numerical simulations. The proposed model mechanism allow to explain most of the observed responses of homing pigeons and migratory birds to magnetic fields, hence providing a strong case for the involvement of SP clusters in magnetic field perception, in these groups of animals.

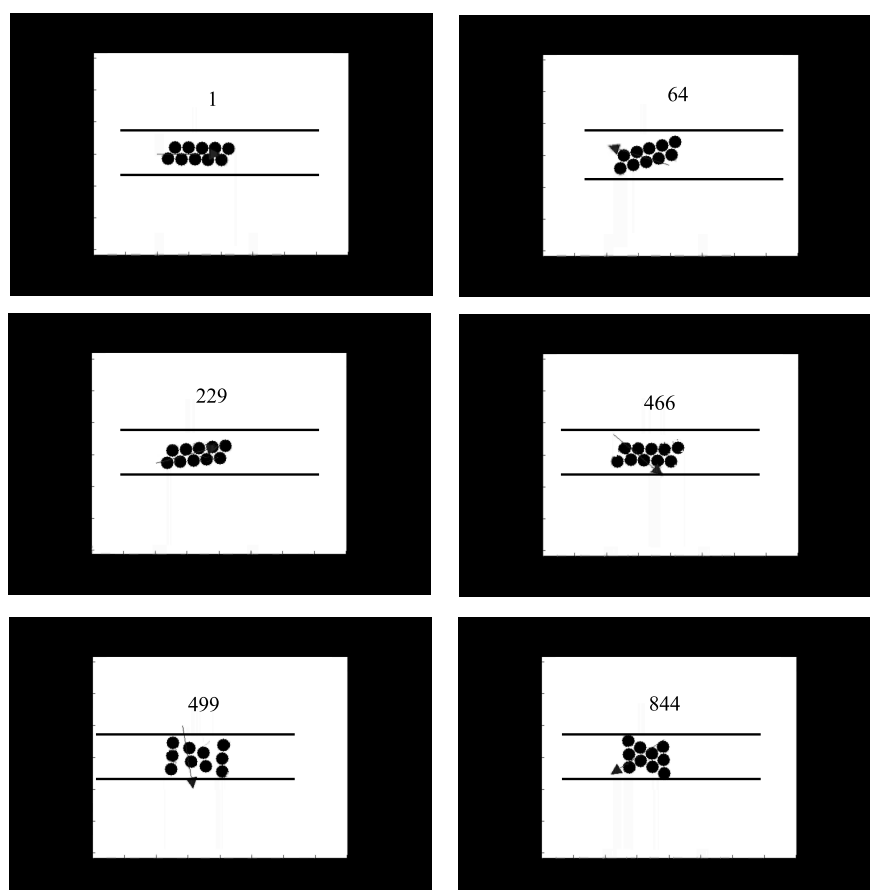


Figure 8.5: Simulation of the dynamics of a double chain in a field that changes randomly its direction with respect to the chains axis (arrow). In that case the double chain breaks after 500 model steps, thus proving more stable than the single chain. Thick lines represent the dendrite's membrane. Numbers represent model time steps. From Davila et al. (2005)

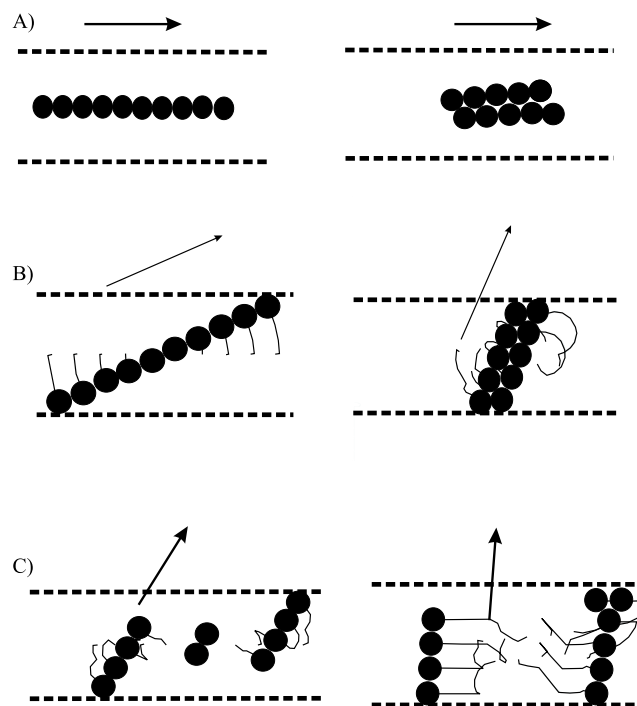


Figure 8.6: Effect of a brief magnetic pulse on a single chain (*left*) and a double chain (*right*) of SP clusters as predicted from the numerical simulations. The trajectories of the clusters are represented by the thin line wiggles. The dashed lines depict the membrane of the dendrite containing the clusters. A) A pulse applied parallel to the chain axis leaves the chain intact. B) If applied at an oblique angle, the pulse brings the chain into alignment with the field. This so-called pseudo-torque response occurs only until a critical angle, while at higher angles C) the chain breaks up into sub-chains of variable sizes. From Davila et al. (2005)

Chapter 9

Magnetoreceptor mechanisms based on interacting clusters of SP magnetite

”The proof of evolution lies in those adaptations that arise from improbable foundations”

Stephen Jay Gould. *The Panda’s Thumb* (1992)

9.1 Introduction

The study by Fleissner et al. (2003) on the ultrastructure of the candidate magnetoreceptor identified in the upper beak skin of homing pigeons, has substantially widened the spectrum of possible magnetoreceptor mechanisms in animals. In this chapter three different models for a transducer mechanism of the geomagnetic field based on interacting SP cluster, will be presented.

The models respond to two different scenarios:

The *Attraction-Repulsion* model (Davila et al., 2003) assumes that the SP clusters are constrained to move only in a direction parallel to the membrane of the nerve ending.

The *Pressure* model, is a direct consequence of the former, and assumes that the SP clusters are located between pressure receptors which transform the attraction-repulsion forces between adjacent clusters into a nerve impulse.

The *Pseudo-torque transducer* model (Davila et al., 2005), on the other hand, assumes that the clusters are free to move within the nerve ending, as a result, torque-like responses arise similar to that of chains of SD particles, that can potentially be transformed into nerve signals. On first sight this model seems to be identical in response to a chain of magnetosomes as found in magnetotactic bacteria. There is however a decisive difference as explained in figure 7.12. Also this model fulfils the requirements of an inclination compass.

9.2 The Attraction-Repulsion model

This model is based on the magnetic interactions that arise in the presence of a magnetic field between adjacent clusters arranged in a chain. The clusters occur within a nerve terminal as described by Fleissner et al. (2003) and are assumed to be anchored to the nerve membrane by means of the cell cytoskeleton, that way the clusters are constrained to move only along the cell membrane. The cytoskeleton filaments are in turn connected to mechanosensitive ion channels in the cell membrane, which are activated by stresses exerted on the membrane [Figure 9.1].

If the SP clusters in the chain are constrained to move in only one direction, the magnetostatic interactions between adjacent clusters lead to attraction and repulsion forces, depending on the direction of the field relative to the axis of the chain [Figure 7.8]. Consequently, mechanical stresses are exerted on the surrounding tissue. Similar to most of the magnetite-based receptor models, this model requires mechano-receptors to transform the field-induced deformation into nerve impulses.

For a cluster size of radius $R \sim 0.5\mu\text{m}$, the attraction force is $F_{attr} \sim \chi^2 \times 10^{-8}$ dyne (Eq. 7.4) in the geomagnetic field ($H_0 = 50 \mu\text{T}$). It is not possible yet to give a better estimate as the actual value of the susceptibility remains to be determined. Although 10^{-8} dyne (0.1 pN) may appear small, one should bear in mind that this force acts on microscopic structures on the cellular or subcellular level. For instance, this force is comparable to the weight of a cell's nucleus ($\sim 2 \times 10^{-8}$ dyne) in water according to Sachs and Morris (1998), which suggests that the attraction or repulsion forces between the clusters are able to cause local deformations on the cellular level (Davila et al., 2003).

The attraction-repulsion forces depend on both the intensity and the axial direction of the magnetic field, and therefore this model fulfils the requirements for the *Inclination*

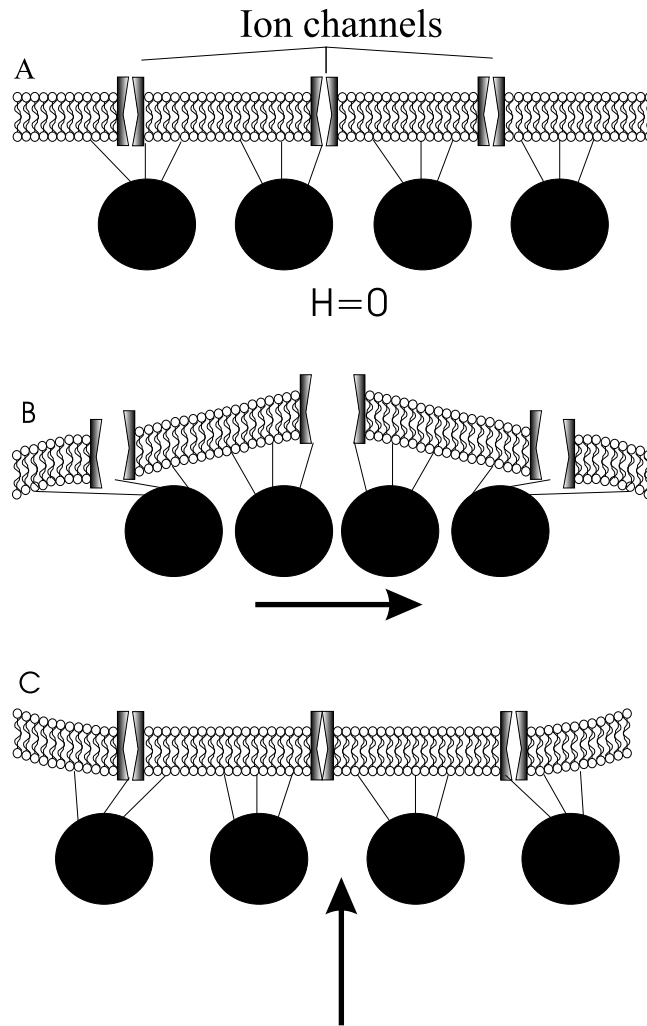


Figure 9.1: The attraction-repulsion model: the chain of SP clusters is attached to the membrane of a nerve cell by tiny fibers, which allow the magnetic interaction force to be transferred to the nerve system. (a) No deformation occurs in zero magnetic field. (b) The clusters attract each other when the chain axis is oriented parallel to the magnetic field, (c) but repel each other when the magnetic field is perpendicular to the chain axis. As the clusters are linked with the nervous membrane, stress due to magnetic interactions can be transferred to the membrane. Depending on its magnitude, that stress may induce opening (or closing) of mechano-sensitive ion channels in the membrane. From Davila et al. (2003)

Compass and the magnetic map systems.

9.3 The Pressure Model

As shown in the model experiments with ferrofluid spherules, adjacent SP clusters will interact, in the presence of a magnetic field, resulting in stresses on the surface of contact between the clusters. In a cellular environment, two clusters attracting each other will exert pressure on the surrounding cellular cytoskeleton, following Eq. 7.6. [Figure 9.2] illustrates the functioning of a putative magnetoreceptor mechanism based on this principle.

The SP clusters are assumed to be in nerve endings, constrained to move in only one direction, and separated by a pressure receptor (i.e. a Pacinian corpuscle¹). In the presence of a magnetic field, the clusters attract each other when the field is parallel to the line connecting the cluster's centers. The attraction exerts stress on the pressure receptor, which results in its activation and the transformation of the mechanical stress into a nerve impulse.

The attraction force will be maximum when the SP clusters are aligned with the geomagnetic field. For a cluster size of radius $R \sim 0.5\mu\text{m}$, the pressure between two clusters is $P_{int} \sim \chi^2 \times 10^0 - 10^1 \text{ dyne/cm}^2$ (Eq. 7.6) in the geomagnetic field ($H_0 = 50 \mu\text{T}$). Again it is not possible yet to give a better estimate, as the actual value of the susceptibility remains to be determined. For comparison, the human ear has a threshold of $2 \times 10^{-4} \text{ dyne/cm}^2$ at the ear drum (Stephens and Davis, 1938). As the angle (ϕ) between the pair of clusters and the magnetic field lines increases, the pressure exerted on the mechanoreceptor becomes negative; when the field is perpendicular to the pair of clusters, the clusters repel each other and do not exert compressional forces on the mechanoreceptor but extensional. The response of the clusters to the field is axial, and therefore the mechanism fulfils the requirements of the *Inclination Compass*. Furthermore, the stress exerted on the pressure receptor is proportional to the magnetic field intensity (see equation 9.5), and therefore the same mechanism can also provide map-information.

For this model an important question is the sensitivity of the postulated mechanism, which is define here as relative pressure change due to a change in magnetic field intensity. From Eq. 7.7

¹See <http://users.rcn.com/jkimball.ma.ultranet/BiologyPages/M/Mechanoreceptors.html> for further information on mechanoreceptors

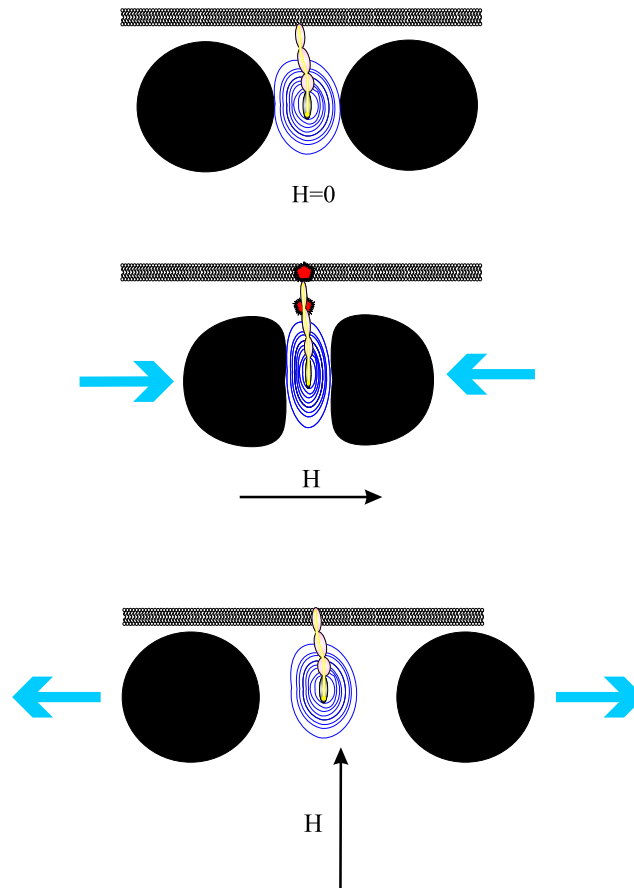


Figure 9.2: The pressure model. (*Top*) A mechanoreceptor structure (Pacini corpuscle) is located between two neighbor clusters. (*Center*) In the presence of a magnetic field, the clusters show a maximum mutual attraction when they are aligned with the geomagnetic field lines (i.e. in the north-south direction), thus exerting a maximum pressure on the mechanoreceptor. (*Bottom*) if the the clusters are aligned perpendicular to the magnetic field (i.e. in the east-west direction), they repel and the pressure on the mechanoreceptor ceases. At intermediate angles, the pressure depends on the angle between the clusters and the magnetic field lines.

$$\frac{\delta P_{int}}{\delta H} \sim \frac{7}{10} \cdot H^{1/3}, \quad (9.1)$$

hence the mechanism shows higher sensitivities at weak fields [Figure 9.3].

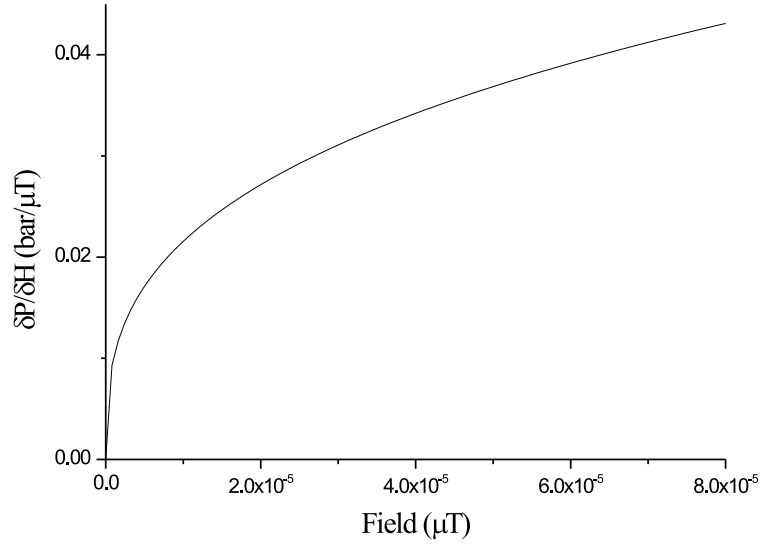


Figure 9.3: Sensitivity of the pressure model, here defined as relative pressure changes due to a change in magnetic field intensity. As can be seen, at fields close to zero, the relative change in pressure due to an increment of the magnetic field intensity is maximum.

The mechanism described here is only partially based on the histological work by Fleissner et al. (2003). In their work, the authors did not report on the presence of pressure receptors connected to the SP clusters, and therefore this mechanism has to be understood as a theoretical conception, that takes into account the basic response of SP clusters to magnetic fields and places it in a hypothetical biological system.

9.4 The Pseudo-Torque Transducer Model

Contrary to the models presented above, this model assumes that the SP clusters are free to move within the nervous terminal, and only constrained by the physical limits of the nerve ending (i.e. the cell membrane). In this scenario, the numerical model presented in chapter 8 predicts that under a magnetic field of constant direction, the SP clusters will

self-organize in chains aligned with the external field in order to achieve the energetically most favorable configuration. The chain is held together by magnetic interactions between nearest neighbors. For a change in the direction of the applied field, the model predicts a rotation of the chain of clusters into the new field direction (Eq. 8.13). What looks like a torque-mechanism on a macroscopic scale, can also be regarded as a rearrangement within the chain of clusters, driven by magnetic interactions between nearest neighbors [Figure 8.2].

The observed pseudo-torque response is particularly interesting since it resembles, at first sight, the well known mechanism for passive magnetotactic orientation displayed by magnetic bacteria. The actual structure of the postulated transducer mechanism within a nervous terminal will be a result of two competing factors: (1) the shape anisotropy of the structure, which will determine the amount of torque and hence, its theoretical suitability, and (2) the structural stability, which will determine its practical suitability as a sensory mechanism.

A group of N SP clusters arranged in a single chain shows a maximum shape anisotropy and hence induces a maximum torque, while it is easily disrupted under a fluctuating magnetic field. On the other hand, a double chain arrangement of the same number of clusters, has a smaller shape anisotropy and displays a smaller torque response, but is much more stable to any fluctuations of the ambient field (see chapter 8). While a loss in the amount of pseudo-torque can be compensated by increasing the number of cellular receptors, the transducing mechanism needs to have a certain degree of structural stability for sensory purposes. Therefore, a double chain structure of SP clusters stands as a more efficient and likely configuration of the transducing mechanism.

The pseudo-torque can induce a bending stress in the membrane of the nerve terminal that contains the clusters [Figure 9.4]. The membrane of the lower part of the terminal is being stretched, which increases the ion flow through stress-activated ion channels in the membrane. Similarly, compression in the membrane of the upper part diminishes the ion flow. The resulting changes in the electric potential of the membrane can then be considered primary receptor potentials. Stress is produced not only in the membrane, which changes its permeability to ions, but also within the terminal, and consequently, the cytoskeleton may be involved in transduction of the magneto-mechanical stimulus.

It is important to note that in contrast to the compass of magnetotactic bacteria, the response of the SP pseudo-torque model is again invariant with respect to the field polarity as explained in figure 7.12. The torque responds to the axis of the geomagnetic field lines,

but not to their polarity, which is in accord with the *magnetic inclination compass*. On the other hand, since the amount of deformation induced by the torque on the nerve terminal, is also dependent on the intensity of the magnetic field, the proposed mechanism could also provide the magnetic components of the navigational map.

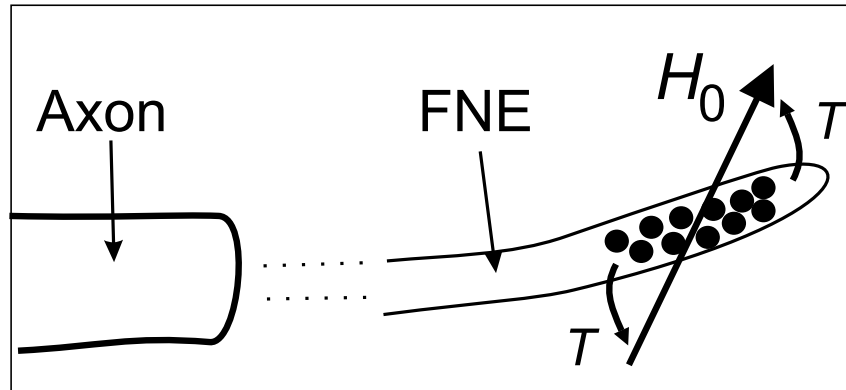


Figure 9.4: Proposed mechanism of magnetic-field transduction. The clusters of SP magnetite are ensheathed by the membrane of the free nerve ending (FNE). Without the membrane, the chain of clusters would rotate into the field axis, therefore, the membrane experiences a bending torque T . Because FNE are sensitive to mechanical stimulation, the torque could be transduced into a nervous signal. From Davila et al. (2005)

Although it is assumed in the Pseudo-torque Transducer Model the SP clusters to move freely, the same torque will be acting on a chain of SP clusters if they are locally fixed. In the next chapter the proposed mechanisms will be tested in the light of the results from behavioral experiments conducted with short magnetic pulses on homing pigeons, aiming to affect a magnetite-based magnetoreceptor system.

Chapter 10

Testing the SP models with behavioral experiments

"There's two possible outcomes: if the result confirms the hypothesis, then you've made a discovery. If the result is contrary to the hypothesis, then you've made a discovery."

Enrico Fermi. (1901-1954)

10.1 Introduction

One way of testing the magnetite hypothesis for magnetic field perception is to conduct behavioral experiments in animals using a brief but strong magnetic pulse (Wiltschko et al., 1994). Because of its short duration (a few milliseconds), a magnetic-pulse treatment should, in principle, selectively affect ferrimagnetic material.

In a series of experiments, migratory birds and homing pigeons subjected to a magnetic pulse treatment, showed deviations from their normal orientation behavior (Wiltschko et al., 1994; Beason et al., 1995; Wiltschko et al., 1998, 2002). The results obtained in these experiments have defied explanation so far, when considering magnetoreceptor mechanisms based on chains of SD magnetite. In this chapter a possible explanation for the results observed in the pulse experiments will be proposed, based on the SP cluster transducer mechanisms.

10.2 Pulse experiments in birds

After treatment with a brief magnetic pulse of intensity 0.5 T, Australian silvereyes, deviated from their natural migratory direction by as much as 90°. A clear effect of the pulse was only observed for a few days after treatment, and the migrants returned to their normal migratory direction within one week (Wiltschko et al., 1994, 1998, 2002). Similar results were obtained on other different species of migratory birds (Beason et al., 1995; Wiltschko and Wiltschko, 1995a; Beason and Semm, 1996). In homing pigeons an identical magnetic pulse induced deflections of flying direction on the treated birds ranging from 1° to 60°. The direction and extent of the deflections depended in that case on the field direction of the pulse with respect to the head of the birds. A clear effect was only observed during the first three days (Beason et al., 1997). The fact that migratory birds and homing pigeons display changes in their orientation behavior after a magnetic-pulse treatment may be taken as evidence of a magnetoreceptor system based on ferrimagnetic material.

When interpreting results, one needs to know how the magnetite particles are arranged in the tissue and the nature of the connection in the nervous system. Predictions can then be made about the effects a magnetic pulse will have on the magnetic sense at the (sub)cellular level.

10.3 Interpretation of the pulse experiments

As shown in chapter 6, when discussing magnetite-based magnetic field perception, two models have been proposed: one based on chains of SD particles as found in MTB (Kirschvink and Gould, 1981; Kirschvink et al., 2001; Walker et al., 2002), the other based on clusters of SP magnetite particles (Shcherbakov and Winklhofer, 1999; Winklhofer, 1999; Davila et al., 2003, 2005). A pulse magnetic field such as the one applied in the behavioral experiments, will have a different response depending if the material is SD particles or SP clusters: if the pulse field is strong enough, SD particles will partially be remagnetized in a different direction with lasting effects in the animal orientation behavior. SP clusters, on the other hand, will undergo only a transient magnetic push.

In the behavioral experiments, the pulse treatment had temporary effects on the behavior of the studied animals, which can be taken as an argument against a sensory system based on SD particles as found in MTB. In the following, the consequences of the pulse

treatment for a SP system as presented in the models of chapter 9, will be discussed.

A slightly different response to the pulses is expected, depending if the SP clusters are elastically fixed in the tissue, as assumed in the pressure model, or if the clusters are relatively free to move as in the attraction-repulsion model and in the pseudo-torque model.

In the case of elastically fixed SP clusters, the pulse will exert a push to the system when it is parallel to the axis connecting the center of the clusters. Unless exceeding a critical field strength, this push will not permanently change the spatial arrangement of the clusters and the effects of the pulse on the SP clusters will only be transient.

For freely moving SP clusters, the pulse may cause the disruption of the original cluster arrangement as experimentally shown in the experiments with ferrofluid droplets [Figure 7.12]. The structural stability of the chains is lost when a strong magnetic pulse is applied at an angle perpendicular or oblique to the chain axis [Figure 8.2]. In this case, the original configuration of the SP clusters will dramatically change, impairing the transducer mechanism. The disruption of the chains and subsequent deterioration of the transduction mechanism may be responsible for the behavioral response observed after a magnetic pulse treatment, as reported for migratory birds and homing pigeons.

In the studies of Beason et al. (1995), Beason et al. (1997), Wiltschko et al. (1998) and Wiltschko et al. (2002), each bird was treated with only one magnetic pulse, either parallel to the long axis of the beak or perpendicular to it. Such a pulse treatment would only have disrupted a population of chains whose long axes were at angles larger than the critic angle for chain disruption with respect to the direction of the pulse ($\sim 70^\circ$ for a double-chain of 10 clusters), while chains at lower angles would have only been rotated by the magnetic pulse as a unit, the extent of rotation being dependent on the physical constraints of the cellular space; finally, chains aligned with the applied pulse would just feel a push without altering their original arrangement [Figure 10.1]. That way, the magnetoreceptor mechanism would only be partially damaged. The studies by Beason et al. (1997) and Wiltschko et al. (2002) suggest that the pulse treatment did not entirely disrupt the magnetoreceptor system of the birds, but rather produced a partial impairment of the system, thus inducing the observed deflections instead of disorientation.

To explain the effects of the pulse treatments, one can assume that the magnetoreceptor system of these birds consists of a large number of cellular receptors in the form of chains of SP clusters, and that the cellular receptors form different populations, each of which is calibrated to sense one particular component of the geomagnetic field. In order for

this to work, the bird has to have developed an independent reference system defined, for example, by the sun compass, which obviously is not affected by the pulse. In this case, the disruption of only one population of receptors would bias the sensory mechanism towards the other two components of the geomagnetic field, while the disruption of two or the three populations would produce a complete loss of the sensory mechanism [Figure 10.2]. Furthermore, since the x component of the geomagnetic field has a larger contribution to the total intensity than the y component, it is expected that the disruption of the population of receptors sensitive to the former component will have more dramatic effects. However, it is difficult to predict what the outcome of a partially damaged magnetoreceptor might be.

Interestingly, in the study by Beason et al. (1997) a group of homing pigeons was treated with a south-anterior pulse and another group with a south-left pulse, therefore each group of birds was treated with a perpendicular field with respect to the other. Following the line of reasoning stated above, such a pulse treatment would have affected different populations of cellular receptors in the south-anterior and the south-left groups, and directional differences in the orientation response would be expected. Indeed, the two groups showed deflections with respect to the controls, although the deflections in the south-left group were greater (median 37°) than that of the south-anterior group (median 12°). When released from the same place the direction of the deflection also differed from one group to the other. In the studies by Wiltschko et al. (1998) and Wiltschko et al. (2002) all the birds were treated with the same pulse (south-anterior), and were deflected unimodally or bimodally roughly $\pm 90^\circ$ with respect to the controls. This might indicate that a population of cell receptors sensitive to one of the horizontal components of the geomagnetic field was almost completely impaired, while the other remained almost unaffected, thus biasing the outcome signal.

This assumption can be tested by treating the birds with two perpendicular pulses (i.e. a south-anterior pulse followed by a south-left pulse), in that way the two populations of cell receptors will be affected, since the chains not disrupted by the first pulse should be disrupted by the second. Such a treatment should yield more dramatic behavioral responses.

10.3.1 Chain recovery process

Beason et al. (1997) and Wiltschko et al. (2002) reported that the above described effects

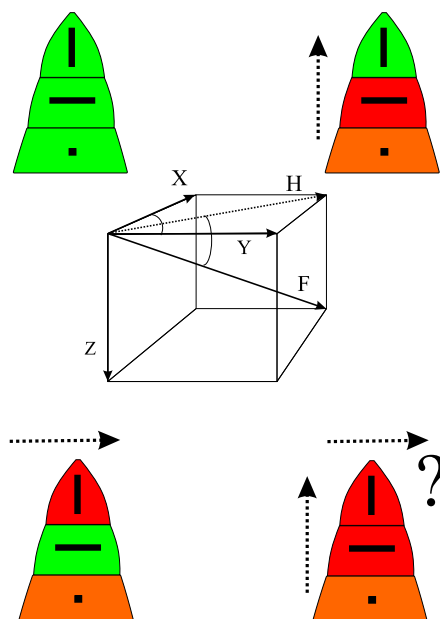


Figure 10.1: Predicted effects of a single-pulse and a double-pulse treatment on a putative magnetoreceptor mechanism based on chain-like structures of SP clusters. It is assumed the presence of three independent populations of receptors in the upper beak (thick solid lines), each of them sensitive to one of the components of the geomagnetic field. While a single pulse (dashed arrow) would partially impair the magnetoreceptor mechanism (red/orange areas in the beak), a double-pulse would completely impair the magnetoreceptor system.

of a magnetic pulse treatment in birds are transient and last between 1 and 10 days. The numerical model presented in chapter 8, was applied to estimate the time required for a double-chain of $N = 10$ clusters as shown in Figure 8.2c, disrupted by a pulse field, to recover the initial configuration under an Earth-strength magnetic field ($H_0 = 50\mu\text{T}$). Applying Eq. 8.9 a best-case estimate of some 15 hours for the recovery time (between 150 and 200 dimensionless time steps), is obtained. This time scale applies to the case where the dendrite containing the SP clusters remains oriented parallel to the magnetic field for the whole duration of the recovery process. In reality, however, a test bird will hop around in a rather erratic manner, which is equivalent to a magnetic field constantly changing in direction with respect to the bird's head. Therefore the recovery process under a randomly changing magnetic field axis was simulated. It turns out that the recovery time is now much longer (between 2 and 3 days, or between 600 and 700 dimensionless time steps). This result is in good agreement with the recovery time observed in experiments on homing pigeons and Australian silvereyes. Interestingly, the free space available for the chain of SP clusters, as defined by the diameter of the nerve terminal, influences both the

way a chain breaks up and eventually recovers. Assuming a double chain arrangement of the SP clusters and an inner diameter of the terminal $R_d = 2.1\mu\text{m}$, the recovery is dramatically accelerated (by one order of magnitude) in a steady field applied parallel to the dendrite axis, albeit yielding a single chain instead of a stacked chain. This also holds for a steady magnetic field applied at a slightly oblique angle (up to 30°) with respect to the dendrite axis. At higher angles, however, the (linear) chain structure is not completely recovered and, instead, several sub-chains form. In the case of a fluctuating field, the original double chain configuration is indeed recovered, although the recovery process is sped up by $\sim 50\%$. In terms of absolute time, this still translates into 1-2 days of recovery time. Thus, a fluctuating field (as realized by the bird hopping about in an erratic manner) is required to recover the stable double chain configuration. It is important to mention that here only physical forces driving the recovery process are taken into account. Neural healing mechanisms though important, are not considered.

10.3.2 Effects of a bias field

Wiltchko et al. (2002) used a biasing field of 1 mT prior to the pulse treatment, in an attempt to align the magnetite system in a preferred direction, to test the assumption that the magnetoreceptor mechanism consists of mobile, magnetically stable, SD magnetosomes chains. While both groups received the same pulse treatment, for one group the biasing field was parallel to the pulse direction (PAR-birds), and for the other group it was antiparallel (ANTI-birds). While the exposure for 5 sec. of the biasing field alone had no noticeable effect on the orientation behavior, the pulse treatment had the same effect on both PAR-birds and ANTI-birds. The result of this experiment is evidence against the model of a magnetoreceptor based on SD particles as proposed by Kirschvink et al. (2001) and Walker et al. (2002), as the pulse should reverse the magnetic moment of either the PAR- or ANTI-birds, and clear differences between both groups should be observed.

In the case of groups of SP clusters, the biasing field would neither disrupt the clusters nor effectively displace them in a preferred direction. The model would explain the null effect of the biasing field on the orientation of the birds [Figure 10.2]. Consequently, both PAR-birds and ANTI-birds would have been subjected to the same pulse treatment, hence displaying the reported identical behavioral response.

The numerical model presented here predicts that the long time effects of a magnetic pulse are equivalent to those of a magnetic bias field applied for a sufficiently long time.

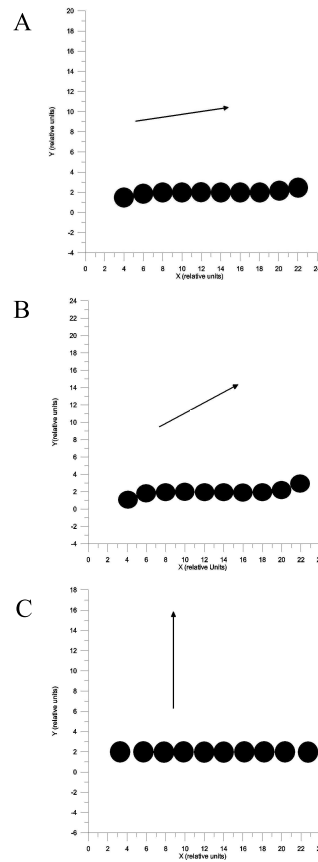


Figure 10.2: Simulation of the effects of a bias field (arrow), equivalent to the field used by Wiltschko et al. (2002), on a chain of SP clusters. A) A field applied at a low angle, above the critic angle B) and perpendicular to the chain C) has no noticeable effect on the initial configuration. This result is in agreement with the lack of response reported in homing pigeons after application of the bias field.

One can estimate the time t_{bias} required for a given bias field H_{bias} to cause effects similar to a strong pulse. By applying Eq. 8.9, the following scaling relation is obtained:

$$t_{pulse} H_{pulse}^2 = t_{bias} H_{bias}^2 \quad (10.1).$$

From (Equ. 10.1) it can be seen that a bias field of 10 mT applied for 5 seconds is needed in order to produce a behavioral response similar to that of the pulse field treatment. It is possible that a pulse field of lower intensity than those used in the behavioral experiments already causes chain disruption. Therefore it would be interesting to design a behavioral experiment to determine the minimum pulse strength required to cause statistically significant disorientation. This way, the characteristic time scale of the

receptor system can be experimentally determined.

Finally, from (Eq. 10.1) it is possible to predict that a magnetic pulse of intensity $H_{pulse} = 50$ mT will yield no effect. Since a 50 mT pulse field should largely affect magnetically blocked SD magnetite, the absence of a behavioral response to the pulse would also argue strongly against the involvement of SD particles.

Conclusions

"A conclusion is the place where you got tired of thinking."

Arthur Bloch. (1948-)

In the first part of this work, the magnetic properties of magnetotactic bacteria were characterized and the suitability of rock magnetic techniques to identify biogenic magnetite in natural samples was tested.

Among other methods, particularly the *delta-delta* test was applied for testing concentrated samples of naturally occurring magnetotactic bacteria, harvested and extracted from sediments of lake Chiemsee. The samples yielded δ -ratios (δ_{FC}/δ_{ZFC}) > 2 . This result supports the use of the *delta-delta* test for the detection of chains of SD magnetite particles.

However, the sensitivity of the *delta-delta* test to detect biogenic magnetite drastically decreases when applying this criteria to natural samples such as lake sediments containing magnetotactic bacteria. In such environments, magnetite occurs in mixtures of both biogenic and non-biogenic components, which blur the distinct magnetic properties of the former. Due to their small volume, biogenic magnetite particles are also prone to undergo chemical alterations that can largely affect their magnetic properties.

For that reason, magnetic techniques have proved useful yet insufficient, to detect and characterize biogenic magnetite particles in natural samples, and a multidisciplinary approach using both magnetic and non-magnetic techniques is required to unambiguously identify biogenic magnetite in natural samples.

The second part of this work focused on the possible role of biogenic magnetite as part of the magnetoreceptor system in higher organisms. Although still a working hypothesis, the idea that biogenic magnetite particles constitute the transducer mechanism of the

animal magnetic sense is supported by the detection and isolation of SD and SP biogenic magnetite particles in tissue of different species.

The suitability of chains of SD particles, as found in magnetotactic bacteria, for magnetic field perception has been proved in the past. Here the hypothesis that SP particles can also be used for magnetic field perception is tested, in the light of histological findings in the upper beak skin of homing pigeons, identifying clusters of SP magnetite within nervous terminals of the ophthalmic nerve.

Model experiments with spherules of ferrofluid, a technical analogue to the SP clusters, were conducted to assess the suitability of these structures for magnetic field perception. In the presence of a magnetic field, adjacent spherules interact magnetostatically, resulting in attraction-repulsion and torque-like responses. The same behavior was observed in a numerical model developed to simulate the dynamics of SP clusters in a liquid medium.

Based on these results, three models for a magnetoreceptor mechanism based on SP clusters have been proposed: the attraction-repulsion model, the pressure model and the pseudo-torque transducer model. These models meet the requirements of both the inclination compass and the navigational map system as described for birds.

The pseudo-torque transducer mechanism is of particular interest since it resembles that of a biological compass needle and has been already realized in nature in the form of intracellular chains of SD magnetite, responsible for the magnetotaxis of magnetotactic bacteria.

Based on the functioning principles of the proposed magnetoreceptor mechanisms, it is possible to explain some of the observed orientation responses of birds after a treatment with a short, strong magnetic pulse, a result that supports the hypothesis that clusters of SP magnetite form part of the magnetoreceptor mechanism of homing pigeons.

When comparing the magnetic properties of SD particles and clusters of SP particles in view of possible transducer mechanisms of magnetic stimuli in animals, it is important to keep in mind the characteristics of the inclination compass -perception of the magnetic field axis, not the polarity- and the navigational map -perception of intensity changes-.

A magnetoreceptor based on chains of stable SD particles will always perceive the vector of the magnetic field as in the case of magnetotactic bacteria. On the other hand, intensity changes can only be detected with a chain of SD particles by a torque measurement, which depends on the orientation of the chain with respect to the field. The distinct magnetic properties of SD particles, which make them suitable for magnetic field perception, also depend on the particle size. Larger particles behave as magnetic multi-domains,

thus reducing their remanent magnetization, while smaller particles are superparamagnetic, and are largely affected by thermal fluctuations.

SP clusters, on the contrary, respond to the axis but not the polarity of the magnetic field, and the magnetostatic interactions between SP clusters scale with the magnetic field intensity. This behavior does not depend on the size of the clusters, hence allowing for the use of large clusters, less affected by thermal buffering.

On the light of these results, the tenet that only chains of SD particles are suitable for magnetic field perception ought to be reconsidered.

Acknowledgements

The work presented here is not the product of one person, but of many people who, present or absent, helped in making it happen. Many of them may not be aware of the great help they provided.

First of all I would like to gratefully thank my Doktorvater Herrn Prof. Dr. Nikolai Petersen. His support and his knowledge have always been a great inspiration. From him I have learnt not only the value of science but also the values needed for science to advance.

I feel especially indebted to my co-supervisor Dr. Michael Winklhofer. He has been always there to help me in the moments of doubt and has been an example of companionship. Without his knowledge and expertise on biomagnetism I would not have been able to find my way.

An important part of this work would not have been possible without the guidance of Prof. Valera Shcherbakov. It has been a privilege to work next to him.

I thank Dr. Michael E. Evans for carefully reading this manuscript and for his valuable comments and corrections of the original text.

Especial thanks to Prof. Dr. Valerian Bachtadse for his helpful revision and comments of the final manuscript.

The work presented here on the magnetic properties of magnetotactic bacteria and lake sediments would not have been possible without the leadership of Dr. Yongxin Pan.

I thank Dr. Marianne Hanzlik for having patiently introduced me into the Electron microscopy techniques and for the many answers she gave to my many questions about magnetotactic bacteria.

To Frau Manuela Weiss, thanks for your help and support in and from Niederlippach.

To my colleges and friends at the Dpt. of Earth and Environmental Sciences in Munich, thank you for sharing the good and the bad moments.

A mi familia, por su constante apoyo. A Mari y Alfonso. Por todo y por siempre.

Bibliography

- R. Aragon, D. Buttrey, J.P. Shepherd, and J.M. Honig. Influence of nonstoichiometry on the verwey transition. *Phys. Rev. B*, 31:430–436, 1985.
- D. A. Avalos, E. Wajnberg, P. S. Oliviera, I. Leal, M. Farina, and D. M. S. Esquivel. Isolation of magnetic nanoparticles from *pachycondyla marginata* ants. *J. Exp. Biol.*, 202:2687–2692, 1999.
- J. C. Bacri, V. Cabuil, A. Cebers, C. Menager, and R. Perzynski. Flattening of ferro-vesicle undulations under a magnetic field. *Europhys. Lett.*, 33:235 – 240, 1996.
- S. K. Banerjee and B. M. Moskowitz. Ferrimagnetic properties of magnetite. In J. L. Kirschvink, D. S. Jones, and B. J. MacFadden, editors, *Magnetite biomineralization and magnetoreception in organisms*, pages 17–41. Plenum, New York, 1985.
- R. C. Beason, N. Dussourd, and M. E. Deutschlander. Behavioural evidence for the use of magnetic material in magnetoreception by a migratory bird. *J. Exp. Biol.*, 198:141–145, 1995.
- R. C. Beason and P. Semm. Does the avian ophthalmic nerve carry magnetic navigational information. *J. Exp. Biol.*, 199:1241–1244, 1996.
- R. C. Beason, R. Wiltschko, and W. Wiltschko. Pigeon homing: effects of magnetic pulses on initial orientation. *The Auk*, 114:405–415, 1997.
- R. P. Blakemore. Magnetotactic bacteria. *Science*, 19:377–379, 1975.

- B. Carter-Stiglitz, B. Moskowitz, and M. Jackson. More on the low-temperature magnetism of stable single domain magnetite: Reversibility and non-stoichiometry. *Geophys. Res. Lett.*, 31:L06606 doi:10.1029/2003GL019155, 2004.
- S. Cisowski. Interacting vs. non-interacting single-domain behavior in natural and synthetic samples. *Phys. Earth Planet. Inter.*, 26:56–62, 1981.
- A. F. Davila, G. Fleissner, M. Winklhofer, and N. Petersen. A new model for a magnetoreceptor in homing pigeons based on interacting clusters of superparamagnetic magnetite. *Phys. Chem. Earth*, 28:647–652, 2003.
- A. F. Davila, M. Winklhofer, V.P. Shcherbakov, and N. Petersen. Magnetic pulse affects a putative magnetoreceptor mechanism. *Biophys. J.*, 89:56–63, 2005.
- R. Day, M. Fuller, and V.A. Schmidt. Hysteresis properties of titanomagnetites: Grain-size and compositional dependence. *Phys. Earth Planet. Int.*, 13:260–267, 1977.
- M.J. Dekkers, J.L. Matti, G. Fillion, and P. Rochette. Grain-size dependence of the magnetic behaviour of pyrrhotite during its low-temperature transition at 34 k. *Geophys. Res. Lett.*, 18:855–858, 1993.
- E.F. DeLong, R.B. Frankel, and D.A. Bazylinski. Multiple evolutionary origins of magnetotaxis in bacteria. *Science*, 259:803–806, 1993.
- C. E. Diebel, R. Proksch, C. R. Green, P. Neilson, and M. M. Walker. Magnetite defines a vertebrate magnetoreceptor. *Nature*, 406:299–302, 2000.
- D. J. Dunlop. Coercive forces and coercivity spectra of submicron magnetite. *Earth Planet. Sci. Lett.*, 78:288–295, 1986.
- D. Dunlop and İ. Özdemir. *Rock Magnetism : Fundamentals and Frontiers*. Cambridge University Press, 1997.

- H. P. Duwe, J. Käs, and E. Sackmann. Bending elastic moduli of lipid bilayers: Modulation by solutes. *J. Phys. France*, 51:945–962, 1990.
- H. Edwards, G. Schnell, R. DuBois, and V. Htchison. Natural and induced remanent magnetism in birds. *The Auk*, 109:43–56, 1992.
- D. M. S. Esquivel, D. Acosta-Avalos, L. J. El-Jaick, A. D. M. Cunha, M. G. Malheiros, E. Wajnberg, and M. P. Linhares. Evidence for magnetic material in the fire ant *solenopsis* sp. by electron paramagnetic resonance. *Naturwissenschaften*, 86:30–32, 1999.
- M. E. Evans and F. Heller. *Environmental Magnetism: Principles and applications of enviromagnetics*. Academic Press, Oxford, 2003.
- K. Fabian, A. Kirchner, W. Williams, F. Heider, T. Leibl, and A. Hubert. Three-dimensional micromagnetic calculations for magnetite using fft. *Geophys. J. Int.*, 124: 89–104, 1996.
- K. Fabian. Some additional parameters to estimate domain state from isothermal magnetization measurements. *Earth Planet. Sci. Lett.*, 213:337–345, 2003.
- J. W. E. Fassbinder, H. Stanjek, and H. Vali. Ocurrance of magnetic bacteria in soil. *Nature*, 343:181–183, 1990.
- G. Fleissner, E. Holtkamp-Rötzler, M. Hanzlik, M. Winklhofer, G. Fleissner, N. Petersen, and W. Wiltschko. Ultrastructural analysis of a magnetoreceptor in the beak of homing pigeons. *J. Comp. Neurol.*, 458:350–360, 2003.
- R. B. Frankel and R. P. Blakemore. *Iron Biominerals*. Plenum Press, New York, 1991.
- R. B. Frankel, G.G. Papaefthymiou, R.P. Blakemore, and W. O’Brien. Magnetic guidance of organisms. *Biochim. Biophys. Acta.*, 763:147–159, 1983.
- T. Frederichs, T. von Dobeneck, U. Bleil, and M.J. Dekkers. Towards the identification of siderite, rhodochrosite, and vivianite in sediments by their low-temperature magnetic properties. *Phys. Chem. Earth*, 28(669-679), 2003.

- E. I. Friedmann, J. Wierzchos, C. Ascaso, and M. Winklhofer. Elementary mechanics of the endothelium in blood vessels. *Proc. Natl. Acad. Sci. USA*, 98(2176-2181), 2001.
- C. Gleitzer. Electrical properties of anhydrous iron oxides. *Key Eng. Mat.*, 125-126:355418, 1997.
- J. L. Gould, J. L. Kirschvink, and K. S. Deffeyes. Bees have magnetic remanence. *Science*, 201:1026–1028, 1978.
- J. L. Gould. The map sense of pigeons. *Nature*, 296:205–211, 1982.
- M. Hanzlik, C. Heunemann, E. Holtkamp-Rötzler, M. Winklhofer, N. Petersen, and G. Fleissner. Superparamagnetic magnetite in the upper-beak tissue of homing pigeons. *Biometals*, 13:325–331, 2000.
- M. Hanzlik. *Elektronenmikroskopische und magnetomineralische Untersuchungen an magnetischen Bakterien des Chiemsees und bakteriellem Magnetit*. Dissertation, Ludwig-Maximilians-Universitaet, Muenchen, 1999.
- J. Harris, S. Moreno, G. Shaw, and E. Muguaini. Unusual neurofilament composition in cerebella unipolar brush neurons. *J. Neurocytol.*, 22:1039–1059, 1993.
- H. Hertz. Uber die berührung fester elastischer korper (on the contact of elastic solids). *J. Reine Angew. Math.*, 92:156–171, 1881.
- K. Hilgenfeldt. Diagenetic dissolution of biogenic magnetite in surface sediments of the benguela upwelling system. *Int. J. Earth Sci.*, 88:630–640, 2000.
- B.A. Housen, S.K. Banerjee, and B.M. Moskowitz. Low-temperature magnetic properties of siderite and magnetite in marine sediments. *Geophys. Res. Lett.*, 23:2843–2846, 1996.
- H.P. Johnson, W. Lowrie, and D.V. Kent. Stability of anhysteretic remanent magnetization in fine and coarser magnetite and maghemite particles. *J. Roy. Astron. Soc.*, 41:1–10, 1975.

- J. L. Kirschvink, A.E. Dizon, and J.A. Westpahl. Evidence from strandings for geomagnetic sensitivity in cetaceans. *J. Exp. Biol.*, 120:1–24, 1986.
- J. L. Kirschvink and J. L. Gould. Biogenic magnetite as a basis for magnetic field detection in animals. *BioSystems*, 13:181–201, 1981.
- J. L. Kirschvink, D. S. Jones, and B. J. MacFadden, editors. *Magnetite biomineralization and magnetoreception in organisms; a new biomagnetism*, volume 5 of *Topics in geobiology*. Plenum Publ., New York, NY, United States, 1985.
- J. L. Kirschvink, F. L. Tabrah, and S. Batkin. Ferromagnetism in two mouse tumors. *J. Exp. Biol.*, 101:321–326, 1982.
- J. L. Kirschvink, M.M. Walker, and C.E. Diebel. Magnetite-based magnetoreception. *Curr. Opin. Neurobiol.*, 11:462–467, 2001.
- E. Kneller. Fine particle theory. In A. E. Berkowitz and E. Kneller, editors, *Magnetism and metallurgy, vol I*, pages 365–471. Academic Press, London and New York, 1969.
- G. Kramer. Long-distance orientation. In A.J. Marshall, editor, *In: Biology and comparative physiology of birds*, pages 341–371. London: Academic Press, 1961.
- K. J. Lohmann, J.T. Hester, and C.M.F. Lohmann. Long distance navigation in sea turtles. *Ethol. Ecol. Evol.*, 11:1–23, 1999.
- H. A. Lowenstam. Magnetite in denticle capping in recent chitons (polyplacophora). *Geol. Soc. Am. Bull.*, 73:435–438, 1962.
- H. A. Lowenstam. Minerals formed by organisms. *Science*, 211:1126–1131, 1981.
- W. Lowrie and M. Fuller. On the alternating field demagnetisation characteristics of multidomain thermoremanent magnetization. *J. Geophys. Res.*, 76:6339–6349, 1971.
- B. A. Maher. Magnetite biomineralization in termites. *Proc. Roy. Soc. (London), Ser B*, 265:733–737, 1998.

- I. Malaescu and C. N. Marin. Deviation from the superparamagnetic behaviour of fine-particle systems. *J. Magn. Magn. Mater.*, 218:91–96, 2000.
- S. Mann, N. H. Sparks, M. M. Walker, and J. L. Kirschvink. Ultrastructure, morphology and organization of biogenic magnetite from sockeye salmon, *oncorhynchus nerka*: Implications for magnetoreception. *J. Exp. Biol.*, 140:35–49, 1988.
- S. Mann. *Biomineralization: Principles and Concepts in Bioinorganic Materials Chemistry*. Oxford University Press, 2001.
- I. D. Mayergoyz. Mathematical models of hysteresis. *IEEE Transactions on Magnetics*, 22:603–608, 1986.
- D.S. McKay, E.K. Gibson, K.L. Thomas-Keprta, H. Vali, C.S. Romanek, S.J. Clemett, X.D.F. Chillier, C.R. Maechling, and R.N. Zare. Search for past life on mars: Possible relic biogenic activity in martian meteorite alh84001,. *Science*, 273:924–930, 1996.
- Y. Miyamoto and S. Chikazumi. Crystal symmetry of magnetite in low temperature phase deduced from magnetoelectric measurement. *J. Phys. Soc. Japan*, 57:20402050, 1988.
- B.M. Moskowitz, M. Bruce, R. Frankel, and D.A. Bazylinski. Rock magnetic criteria for the detection of biogenic magnetite. *Earth Planet. Sci. Lett.*, 120:283–300, 1993.
- B. M. Moskowitz, R. B. Frankel, P. J. Flanders, R. P. Blakemore, and B. B. Schwartz. Magnetic properties of magnetotactic bacteria. *J. Mag. Mag. Mat.*, 73:273–288, 1988.
- A.R. Muxworthy, D. Heslop, and W. Williams. , influence of magnetostatic interactions on first-order-reversal-curve (forc) diagrams: a micromagnetic approach. *Geophys. J. Int.*, 158:888–897, 2004.
- L. Néel. Théorie du trainage magnétique des ferromagnétiques en grains fins avec applications aux terres cuites. 5:99–136, 1949.

- Ö Özdemir, D.J. Dunlop, and B.M. Moskowitz. The effect of oxidation on the verwey transition in magnetite. *Geophys. Res. Lett.*, 20:1671–1674, 1993.
- Ø Paasche, R. Løvlie, S.O. Dahl, J. Bakke, and A. Nesje. Bacterial magnetite in lake sediments: late glacial to holocene climate and sedimentary changes in northern norway. *Earth Planet. Sci. Lett.*, 223:319–333, 2004.
- Y.X. Pan, N Petersen, A. F. Davila, L. M. Zhang, M. Winklhofer, Q.S. Liu, M. Hanzlik, and R.X. Zhu. The detection of bacterial magnetite in recent sediments of lake chiemsee (southern germany). *Earth Planet. Sci. Lett.*, 232:109–123, 2005.
- Y.X. Pan, R.X. Zhu, Q.S. Liu, and M. Jackson. Low-temperature magnetic behavior related to thermal alteration of siderite. *Geophys. Res. Lett.*, 29:DOI: 10.1029/2002GL016021, 2002.
- N. Petersen, T. von Dobeneck, and H. Vali. Fossil bacterial magnetite in deep-sea sediments from the south atlantic ocean. *Nature*, 320(6064):611–615, 1986.
- N. Petersen, D. G. Weiss, and H. Vali. Magnetic bacteria in lake sediments. In *Proceedings of the NATO Advanced Study Institute on Geomagnetism and paleomagnetism*. D. Reidel Publishing Company, 1989. Proceedings of the NATO Advanced Study Institute on Geomagnetism and paleomagnetism. Newcastle upon Tyne, United Kingdom. Apr. 11–22, 1988.
- M. Posfai, P. R. Buseck, D. A. Bazylinski, and R. B. Frankel. Iron sulfides from magnetotactic bacteria: Structure, composition, and phase transitions. *American Mineralogist*, 83:1469–1481, 1998.
- C. Radhakrishnamurthy, Sastry N. P., and E. R. Deutsch. Ferromagnetic behaviour of interacting superparamagnetic particles aggregates in basaltic rocks. *Pramana*, 1:61–65, 1973.

- T. Ritz, S. Adem, and K. Schulten. A model for vision-based magnetoreception in birds. *Biophys. J.*, 78:707–718, 2000.
- T. Ritz, P. Thalau, J.B. Phillips, R. Wiltschko, and W. Wiltschko. Resonance effects indicate a radical-pair mechanism for avian magnetic compass. *Nature*, 429:177–180, 2004.
- A.P. Roberts, C.R. Pike, and K.L. Verosub. First-order reversal curves: A new tool for characterizing the magnetic properties of natural samples. *J. Geophys. Res.*, 105:28461–28475, 2000.
- H. J. Roesler, editor. *Lehrbuch der Mineralogie*. Deutscher Verlag fuer Grundstoffindustrie, Leipzig, 1979.
- F. Sachs and C. E. Morris. Mechanosensitive ion channels in nonspecialized cells. *Rev. Physiol. Bioch. P.*, 132:1–77, 1998.
- H. Schiff. Modulation of spike frequencies by varying the ambient magnetic field and magnetite candidates in bees (*apis mellifera*). *Comp. Biochem. Physiol.*, 100:975–978, 1991.
- P. Semm and R. C. Beason. Responses to small magnetic variations by the trigeminal system of the bobolink. *Brain Res. Bull.*, 25:735–740, 1990.
- V. P. Shcherbakov, M. Winklhofer, M. Hanzlik, and N. Petersen. Elastic stability of chains of magnetosomes in magnetotactic bacteria. *Eur. Biophys. J.*, 26(4):319–326, 1997.
- V. P. Shcherbakov and M. Winklhofer. The osmotic magnetometer: A new model of a magnetite-based magnetoreceptor in animals. *Eur. Biophys. J.*, 28:380–392, 1999.
- A.V. Smirnov and J.A. Tarduno. Detection of ferromagnetism in the red imported fire ant (*solenopsis invicta*) using magnetic resonance imaging. *J. Geophys. Res.*, 105:16457–16471, 2000.

- S. Spring, R. Amann, W. Ludwig, K. Schleifer, H. van Gernerden, and N. Petersen. Dominating role of an unusual magnetotactic bacterium in the microaerobic zone of a freshwater sediment. *Appl. Environ. Microbiol.*, 59:2397–2403, 1993.
- F. D. Stacey and S. K. Banerjee. *The physical principles of rock magnetism*. Elsevier, Amsterdam, 1974.
- S. S. Stephens and H. Davis. *Hearing, its Psychology and Physiology*. J. Wiley, New York, 1938.
- K.L. Thomas-Keprta, S.J. Clemett, D.A. Bazylinski, J.L. Kirschvink, D.S. McKay, S.J. Wentworth, H. Vali, E.K. Jr. Gibson, and C.S. Romanek. Magnetofossils from ancient mars: a robust biosignature in the martian meteorite alh84001. *Appl. Env. Microbiol.*, 68:36633672, 2002.
- R. Thompson, J. Bloemendal, J. A. Dearing, F. Oldfield, T. A. Rummery, J. C. Stober, and G. M. Turner. Environmental applications of magntic measurements. *Science*, 207: 481–486, 1980.
- K. Ueda, M. Kusunoki, M. Kato, R. Kakizawa, T. Nakamura, K. Yaskawa, M. Koyama, and Y. Maeda. Magnetic remanences in migratory birds. *J. Yamashina Inst. Ornithol.*, 14:166–170, 1982.
- K. Ueda, Y. Maeda, M. Koyama, K. Yaskawa, and T. Tokui. Magnetic remanences in salmonid fish. *Bull. Jpn. Soc. Sci. Fish*, 52:166–170, 1986.
- P. A. Valberg and H. A. Feldman. Magnetic particle motions within living cells. measurement of cytoplasmic viscosity and motile activity. *Biophys. J.*, 52:551–561, 1987.
- H. Vali, B. Weiss, Y.L. Li, S.K. Sears, S.S. Kim, J.L. Kirschvink, and C. Zhang. Formation of tabular single-domain magnetite induced by geobacter metallireducens gs-15. *Proc. Natl. Acad. Sci. USA*, 101:16121–16126, 2004.

- E.J.W. Verwey. Electronic conduction of magnetite (Fe_3O_4) and its transition point at low-temperature. *Nature*, 44:327–328, 1939.
- E. Wajnberg, D. Acosta-Avalos, L. J. El-Jaick, L. Abraçado, J. L. A. Coelho, A. F. Bakuzis, P. C. Morais, and D. M. S. Esquivel. Electron paramagnetic resonance study of the migratory ant *pachycondyla marginata* abdomens. *Biophys. J.*, 78:1018–1023, 2000.
- E. Wajnberg, G. Cernicchiaro, D. Acosta-Avalos, L.J. El-Jaick, and D. M. S. Esquivel. Induced magnetization of social insects. *J. Magn. Magn. Mater.*, 226-30:2040–2041, 2001.
- C. Walcott, J. L. Gould, and J. L. Kirschvink. Pigeons have magnets. *Science*, 205:1027–1029, 1979.
- C. Walcott and R.P. Green. Orientation of homing pigeons altered by a change in the direction of the applied magnetic field. *Science*, 184:180–182, 1974.
- C. Walcott. Anomalies in the earth’s magnetic field increase the scatter of pigeon’s vanishing bearings. In K. Schmidt-König and W. T. Keeton, editors, *Animal Migration, Navigation, and Homing*, pages 99–108. Springer, Berlin, 1978.
- M.M. Walker, T.E. Dennis, and J. L. Kirschvink. The magnetic sense and its use in long-distance navigation by animals. *Curr. Opin. Neurobiol.*, 12:735–744, 2002.
- M.M. Walker, J. L. Kirschvink, S.-B. R. Chang, and A. E. Dizon. A candidate magnetic sense organ in the yellowfin tuna, *thunnus albacares*. *Science*, 224:751–753, 1984.
- M.M. Walker. On a wing and a vector: a model for magnetic field navigation by homing pigeons. *J. Theor. Biol.*, 192:341–349, 1998.
- M. M. Walker, C. E. Diebel, C. V. Haugh, P. M. Pankhurst, and J. C. Montgomery. Structure and function of the vertebrate magnetic sense. *Nature*, 390:371–376, 1997.

- P. J. Wasilewski. Magnetic hysteresis in natural materials. *Earth Planet. Sci. Lett.*, 20: 67–72, 1973.
- B.P. Weiss, S.S. Kim, J.L. Kirschvink, R.E. Kopp, M. Sankaran, A. Kobayashi, and A. Komeili. Ferromagnetic resonance and low-temperature magnetic tests for biogenic magnetite. *Earth Planet. Sci. Lett.*, 224:73–89, 2004a.
- B.P. Weiss, S.S. Kim, J.L. Kirschvink, R.E. Kopp, M. Sankaran, A. Kobayashi, and A. Komeili. Magnetic tests for magnetosome chains in martian meteorite alh84001. *Proc. Natl. Acad. Sci. USA*, 101:8281–8284, 2004b.
- C. Wilhelm, A. Cebers, Bacri J. C., and F. Gazeau. Deformation of intracellular endosomes under a magnetic field. *Eur. Biophys. J.*, 32:655–660, 2003.
- R. Wiltschko, U. Munro, H. Ford, and W. Wiltschko. Effect of a magnetic pulse on the orientation of silvereyes, *zosterops l. lateralis*, during spring migration. *J. Exp. Biol.*, 201:3257–3261, 1998.
- R. Wiltschko, U. Munro, Beason R.C., H. Ford, and W. Wiltschko. A magnetic pulse leads to a temporary deflection in the orientation of migratory birds. *Experientia*, 50: 697–700, 1994.
- R. Wiltschko and W. Wiltschko. *Magnetic orientation in animals*. Zoophysiology (vol 33). Springer, Berlin, 1995.
- W. Wiltschko, U. Munro, R. Wiltschko, and J.L. Kirschvink. Magnetite-based magnetoreception in birds: the effect of a biasing field and a pulse on migratory behaviour. *J. Exp. Biol.*, 205:3031–3037, 2002.
- W. Wiltschko and R. Wiltschko. Magnetic compass of european robins. *Science*, 205: 1027–1029, 1972.
- W. Wiltschko and R. Wiltschko. Disorientation of inexperienced young pigeons after transportation in total darkness. *Nature*, 291:433–434, 1981.

- W. Wiltschko and R. Wiltschko. Migratory orientation of european robins is affected by the wavelength of light as well as by a magnetic pulse. *J. Comp. Physiol. A*, 177: 363–369, 1995a.
- M. Winklhofer, K. Fabian, and F. Heider. Magnetic blocking temperatures of magnetite calculated with a three-dimensional micromagnetic model. *J. Geophys. Res.*, 102(B 10): 24695–22709, 1997.
- M. Winklhofer, E. Holtkamp-Rötzler, M. Hanzlik, G. Fleissner, and N. Petersen. Clusters of superparamagnetic magnetite particles in the upper-beak skin of homing pigeons: evidence of a magnetoreceptor? *Eur. J. Mineral.*, 13:659–669, 2001.
- M. Winklhofer. *Theoretische Modelle der Magnetfeldrezeption auf der Grundlage biologischer Magnetit-Teilchen*. Dissertation, Ludwig-Maximilians-Universitaet, Muenchen, 1999.
- E. P. Wohlfarth. Relation between different modes of acquisition of the remanent magnetization of ferromagnetic particles. *J. Appl. Phys.*, 35:595–596, 1958.
- E. D. Yorke. A possible magnetic transducer in birds. *J. Theor. Biol.*, 77:101–105, 1979.

Lebenslauf

Name: Alfonso Fernandez Davila
Geburtsdatum: 28 März 1978
Geburtsort: Manresa, Spanien
Familienstand: Ledig
Staatsangehörigkeit: Spanisch

Schulbildung

1984-1992 Grundschule in Manresa, Spanien
1993-1996 Gymnasium "La Salle" in Manresa, Spanien
1996 C.O.U. "Escola Joviat" (Abitur)

Ausbildung

1996-2001 Studium der Marinewissenschaften an der Universidade de Vigo, Spanien.
2002-2005 Wissenschaftlicher Angestellter an der Ludwig-Maximilians-Universität München, Fakultät für Geowissenschaften, Sektion Geophysik, im Rahmen des Projektes "Biogenische Magnetit" gefördert von der VW-Stiftung Titel der Doktorarbeit: *Detection and function of biogenic magnetite*; Betreuer Prof. Dr. Nikolai Petersen (LMU München).

Publikationen

A.F. Davila, G. Fleissner, M. Winklhofer, N. Petersen, (2003). "A new model for a magnetoreceptor in homing pigeons based on interacting clusters of superparamagnetic magnetite", *Phys. Chem. Earth*, 28: 647-652

Muxworthy, A., Matzka, J., Fernandez-Davila, A., Petersen, N. (2003). "Magnetic signature of daily sampled urban atmospheric particles", *Atmospheric Environment*, 37: 4163-4169.

Y. Pan, N. Petersen, A. F. Davila, L. Zhang, M. Winklhofer, Q. Liu, M. Hanzlik, R. Zhu (2005). "The detection of bacterial magnetite in recent lake sediments of lake Chiemsee (southern Germany)". *EPSL*. 232: 109-123.

A.F. Davila, M. Winklhofer, V. Shcherbakov, N. Petersen, (2005). "Magnetic pulse affects a putative magnetoreceptor", *Biophys. J.*, 89: 56-63.

Y. Pan, N. Petersen, M. Winklhofer, A. F. Davila, Q. Liu, T. Frederichs, M. Hanzlik, R. Zhu (2005). "Rock magnetic properties of uncultured magnetotactic bacteria". *EPSL*. Accepted.